Rheological Behavior of Dense Granular Matter

by

Mehrdad Kheiripour Langroudi

A dissertation submitted to the Graduate Faculty in Engineering in partial

Fulfillment of the requirements for the degree of Doctor of Philosophy

The City University of New York

2011

This manuscript has been read and accepted for the Graduate Faculty in Engineering in satisfaction of the dissertation requirement for the degree of Doctor of Philosophy.

Date

Prof. Gabriel I. Tardos
Professor of Chemical Engineering
Chair of Examining Committee

Date

Dean Mumtaz K. Kassir
Executive Officer

Supervisory Committee

Dr. James N. Michaels

Dr. Paul R. Mort

Prof. Morton Denn

Prof. Jeffrey Morris

Prof. Charles Maldarelli

THE CITY UNIVERSITY OF NEW YORK

ABSTRACT

Rheological Behavior of Dense Granular Matter

by

Mehrdad Kheiripour Langroudi

Advisor: Professor Gabriel I. Tardos

Research in powder flows is motivated by numerous applications in industrial processes and in geophysics. The division of granular flows into slow or quasi-static and fast or rapid regimes is well documented. The existence of a "transitional regime" where particle mobilization and/or shear are strong enough to dissipate significant energy through particle collisions, but do not completely eliminate the continuous particle enduring contacts, was demonstrated more recently. The basic motivation for our work was to supply relevant experiments that allow the particle bed to dilate freely as shearing is increased and for inter-particle collisions to occur in a dense bed where particle–particle friction is also prevalent and, to more thoroughly study the transitional or intermediate regime of powder flow.

A major objective was to modify a traditional Couette device and using it as a "powder rheometer" by providing continuous powder feed and discharge with a very small flow rate that allows for decrease in bed solid fraction. This decrease enabled the continuously sheared powder bed to translate from the slow, quasi-static regime at low shear rates to the intermediate regime at higher shear rates. Upon reaching steady state, we measured the local normal (with a remote sensor) and shear stresses (back-calculated from the

measured torque) inside the shearing zone and generated a reliable continuum model by generalizing the Schaeffer model for quasi-static flow and by introducing additional terms to characterize the transitional regime. The change in solid fraction was then recorded by using a capacitance probe and its influence on the rheology was also studied.

The set of Visco-plastic constitutive equations for a wide variety of particles with different shapes, sizes, surface structure and elasticity (plasticity) obtained from the axial-flow Couette device, were then validated by several theoretical models. Some were in collaboration with DEM simulations from the group of Professor Sundar Sundarasen of Princeton University for flow in a Jenike-type shear cell and more recently with the group of Professor Shankar Subramaniam at the University of Iowa in the Couette geometry. Further comparisons were made with a computational fluid dynamics (CFD) approach developed at the University of Dortmund (FeatFlow) by the group of Professor Stefan Turek. Finally, a continuous model was developed "in house" using commercially available software (FLUENT) that was transformed and adapted to a relatively dense bed and used to model the free surface flow of dry granular matter. We designed a lab scale spheronizer and results from experiments in terms of surface height and shape, solid volume fraction and wall normal stress as a function of rotational speed were compared with those obtained from computations.

Furthermore, we developed a new indirect technique of estimating the thickness of the shear band (number of particles that exist in the active shearing zone) by measuring solid fraction as a function of position and shear rate in the shear gap. Using tracer (colored) particles we found that the flow pattern inside a Couette cell with axial flow is dispersive and mixing increases by increasing the shearing rate. It was also found that the particles

inside the shear band move faster axially than those trapped outside of the active shearing zone.

The above studies, performed in different geometries such as plane shear in the Jenike and Couette cells and free surface flows in the centripetal geometry (of the spheronizer) revealed that, using adequate software (even commercially available codes such as FLUENT), reasonably model quite complicated flows with acceptable accuracy as long as the powders are reasonably free flowing. The material in this thesis was partially published in Powder Technology (two papers, denoted Kheiripour Langroudi at al., 2010a and 2010b, in the references) and AIP conference proceeding (one paper, denoted Kheiripour Langroudi at al., 2009) and was partially submitted for publication to two other prestigious journals (also denoted Kheiripour Langroudi et. al., 2010c and Kheiripour Langroudi and Tardos, 2010 in the references). The last part of the thesis (Chapter 7) contains the experiments and modeling of the spheronize. To extend the findings to a further geometry, experiments were carried out (and described in the thesis) in emptying a flat-bottom hopper where the discharge orifice is moving across the base at some given velocity. This geometry is the basis for functioning of a tablet filling machine, which is widely used in pharmaceutical industries.

To my beloved parents, for their invaluable and everlasting love, encouragement and support throughout my life.

Acknowledgement

This dissertation would not have been possible without the guidance and help of several individuals who in one way or another contributed to, and extended their valuable assistance in the preparation and completion of this study.

First and foremost, I would like to express my deep and utmost gratitude to my advisor, Professor Gabriel I. Tardos, for his constant support, patience and encouragement. His perpetual energy and enthusiasm in research has motivated me a lot during the course of this study. In addition, he was always accessible and willing to help. As a result, research life became smooth and rewarding for me. Not only did I learn the fundamentals of powder technology from him but also he taught me tremendous lessons for my life. He was always there if I needed any help and he was treating me as if I were his own son. I was so fortunate to have the opportunity to work with him and I am indebted to him for the rest of my life for all the knowledge of powder technology and life advices that he passed on to me.

I am also grateful to my co-advisors, Dr. James Michaels of Merck & Co., Inc. and Dr. Paul Mort of Procter & Gamble Co. for their guidance, encouragement, and support. They generously provided their fruitful ideas, which were always helpful for completing this dissertation. Since both of my co-advisors are distinguished scientist from well-known companies, I could do applied-research and I was all along familiar with industrial needs. I am thankful for their carefully following of my work, their useful comments and corrections, and for the time they spent on this research.

I also would like to thank Professor Morton Denn, Professor Jeffrey Morris, and Professor Charles Maldarelli for their remarkable comments and for serving in my Ph.D. committee. Special thanks to our collaborators at Princeton University, Professor Sankaran Sundaresan and Dr. Jin Sun, who did the DEM simulation of the Jenike shearing cell (Chapter 3) and to Professor-Dr. Stephan Turek and Dr. Abderrahim Ouazzi (Dortmund University, Germany) for simulating the Couette shearing cell with our Visco-plastic constitutive law (Chapter 4).

In addition, I acknowledge Dr. Mehrdad Shahnam of the National Energy Technology Laboratory (NETL) for his tremendous help and support during the computational part of Chapter 7. I appreciate his patience for step-by-step guidance that was very helpful to me to overcome the numerical challenges. I am also thankful to Professor Michel Louge of Cornell University for valuable advice regarding the installation, calibration and use of the Capacitance probe (Chapters 5 and 6).

Many thanks go in particular to Mr. John Bailey of Nova Chemicals Inc. for generously donating all types of Polyethylene granules for this study and to Mr. Jeffrey Crowder of P&G, for performing the colorimetry experiments and sharing the results with me (Chapter 5). I would also like to thank the technicians of CCNY, Mr. Zhen-Rong Xu and Mr. Andy Eng for helping me construct the different experimental devices of this research study.

I also like to specifically acknowledge the following institutions and industries for financial support during the course of this dissertation: Merck & Co., Inc., The National Science Foundation (NSF), Procter & Gamble Co., The Department of Energy (DOE), International Fine Particles Research Institute (IFPRI) and Graduate Center of The City University of New York.

My deepest gratitude goes to my family members for their unflagging love and support throughout my life. To my beloved grandfather, Sadegh Jahanshahi, who departed me physically a long time ago but existed in me virtually and encouraged me to go far and to be successful and strong in spite of all hardships of life. Special thanks to my uncles, Iraj and Mohammad Jahanshahi, who encouraged me a lot and were always willing to help and support me. I would also like to thank my sister, Maryam, and my brother, Masood who always cheered me on and had their best wishes for me. Last and most important, my parents deserve special mention for their ultimate support, sacrifices, encouragement and prayers and I would like to dedicate this dissertation to them. My father, Hojatollah Kheiripour Langroudi, in the first place is the person installed in me the fundamental of my learning character, showing me the joy of intellectual pursuit ever since I was a child. He taught me to rely only on my own self-confidence and capabilities and to be proud of who I am. He gave me the freedom to think and decide independently and to find my own

way that was suited best for me. I am indebted to my father for his care and love and for providing the best possible environment for me to grow and attend school. Words fail me to express my appreciation and feelings toward my mother, Mahin Jahanshahi, whose unlimited and continuous sacrifices, love, encouragement and support made me the person I am today. I have no suitable word that can fully describe her everlasting love toward me. She always motivated me to elevate myself, to live with my dreams and to never give up. She taught me to follow my heart until my dreams come true and to be hard working and persistent until I reach my goals.

Table of Content

List of Figures

List of Tables

1 Introduction

As an accepted general definition, *Powders* are materials composed of particles up to 100 μm in diameter with further sub-division into ultra fine (0.1 to 1 μm), superfine (1 to 10 μm), or granular (10 to 100 μm). A *granular solid* consists of particles ranging from about 100 to 3000 μm (Brown & Richard, 1970) while a *granular material* covers the combined range of powders and granular solids with components ranging in size from about 10 μm up to 3 mm. This definition includes most materials used in industry and is employed in the present study.

Those who have observed dry sand on the beach know that a collection of solid grains can behave macroscopically like a fluid and flow. They can also behave as solids and may exhibit characteristics of both phases, sometimes within the same flow. Understanding and modeling these observations is difficult (Hermann & Luding, 1998; Behringer et al., 1999) and granular flows have been the subject of intense scrutiny in fluid mechanics, soil mechanics, rheology, and statistical physics. Research is motivated by numerous applications encountered in industrial processes such as the design of hoppers, bins and mixers and in geophysics for the description and prediction of landslides and avalanches.

Previously, granular flows were divided into slow or Quasi-static (frictional), where the deformations are very slow and the effective friction coefficient is taken to be a material property and thus constant. Inter-particle force chains dominate this regime of flow and the local shear stress is proportional to pressure and is independent of shear rate. On the

other end of the spectrum, the fast or rapid (collisional) flow regime was identified, where particles interact through collisions and the flow is very rapid and dilute, but scales in such a way that the effective friction coefficient is again independent of the shear rate. It was found that in this regime the local shear stress is a quadratic function of shear rate. This flow is traditionally described by molecular kinetic theories (Campbell, 1990).

Since the powder is a physical system, in order for it to move from the Quasi-static to rapid granular flow, there must be a transition containing the properties of the two edges. As a result, granular flows have more recently been classified into three regimes adding the *Intermediate regime* of flow where the material is dense but still flows. Particle mobilization and/or shear are strong enough to dissipate significant energy through particle collisions, but do not completely eliminate the continuous particle enduring contacts typical of quasi-static flows (GDR MiDi, 2004). Many practically important flows in nature and in a wide range of technical applications occur in this regime and the lack of validated rheological models limits predictive modeling of such flows.

The primary intent of this study is to supply relevant experiments that allow the bed of powder to dilate freely as shearing is increased and for inter-particle collisions to occur in a dense bed where particle–particle friction is also prevalent. We achieve these conditions in a Couette geometry where the inner cylinder is rotating and the outer cylinder is stationary. We over-impose a very slow axial flow over the radial shearing of the powder thereby assuring a slight decrease in the solid fraction of the bed (Kheiripour Langroudi et al., 2010a). This procedure also ensures that the particle bed reaches a steady state in which the solid fraction is somewhat lower than that corresponding to maximum packing and hence collisions and relative movement between particles can

take place. The change in solid fraction can be recorded using a capacitance probe and the effect of the axial flow on the mixing/segregation of particles can be studied in detail using tracers. This combination of techniques allows for detailed observation of flow patterns and is essential in understanding the micro-behavior of powder flows. Measurement of solid fraction distributions as a function of radial position in the Couette geometry allows the measurement of the shear band thickness: using this method, we found that the modified Couette cell (with the imposed axial flow) results in an increase in the number of particles undergoing radial shearing compared to the traditional Couette (Kheiripour Langroudi et al., 2010c).

At the present time, there is no unified theory for granular materials. The main goal of this research is to study experimentally and theoretically the intermediate or transitional regime of flow. Specifically, we intend to measure local stresses in the flow using novel techniques and to extract from these measurements constitutive equations to be used in modeling (Kheiripour Langroudi et al., 2009). Furthermore the stress inhomogeneity in granular layers was captured by measuring the transmitted stress in a Jenike shear cell (commonly used to measure internal and wall friction coefficients), where we added normal force (stress) transducers on the shearing bottom wall and applied known normal stresses to the upper surface of the granular layer. We found that normal stresses are transmitted through horizontal layers only if the particles are in continuous shear (Kheiripour Langroudi et al., 2010b).

To investigate the impact of solid fraction on the rheology of compressible powders and to find a relationship between dilatancy, rheology and flowability, a new experimental set up (similar to a tablet press) was designed and constructed. Using this instrument, the

rheological properties of compressible powders could be compared with their ability for dilation (by measuring the solid fraction using the capacitance probe) and flow through an orifice (Kheiripour Langroudi and Tardos, 2010).

Finally in order to validate and generalize the constitutive equation obtained in the Couette geometry (Kheiripour Langroudi et al. 2009 and Kheiripour Langroudi et al., 2010a) one needs to use it in a more complicated geometry and compare the results of simulations and experiments. We identified the spheronizer geometry (also known as centripetal flow) to have several applications in the pharmaceutical and detergent industries and at the same time be simple enough, to be a good candidate for this purpose. We used a computational fluid dynamics (CFD) approach to model the flow in the spheronizer employing a Visco-plastic constitutive equation obtained earlier for the same granular material in the simpler geometry of the Couette cell. Average values and the distribution of stresses and solid fraction in this more complex flow were calculated and compared to measured values obtained in a home-made model instrument.

2 Literature Review

2.1 Quasi-Static (Frictional) Regime of Granular Flow

The first attempt to model granular flows was initiated by Coulomb (1773). For granular matter at rest, incipient motion can be achieved only when the applied stress overcomes static frictional contacts and dilates the material so that particles can slide past each other (Nedderman 1992). The simplest model for this incipient motion is given by:

$$\tau = \sigma \tan \phi + c \tag{2.1}$$

In this equation c represents the cohesion of the material, σ is the normal stress, τ is the shear stress, and ϕ is the angle of internal friction (a material property) that can be measured in a standard Jenike shear cell. Equation 2.1 represents the simple law of friction of two solids sliding on each other with the shear force proportional to the normal force, and where $\mu = \tan \phi$ is the friction coefficient. A similar condition also exists at the interface between particles and the walls of the container, only there the angle of internal friction is replaced by the angle of wall friction, ϕ_w. The angle $\phi_w < \phi$, since the wall is usually less rough than a powder-powder layer; this is mainly due to the larger void fraction near the wall (Tardos, et al., 2003).

It is assumed that once the material reaches the yield condition it behaves in a plastic mode and deforms indefinitely without further increase in stress. Plasticity-derived techniques have been used widely in soil mechanics (Jackson, 1983) and in predicting the flow from hoppers (Brennen & Pearce, 1978). As the material moves within the hopper, it is assumed that the material is always yielding so that: $\tau = \sigma \tan \phi + c$ everywhere

within the hopper. At large shear strains, the material is assumed to be at the critical concentration, v_c so that it appears incompressible. These authors showed that the flow rate from a hopper is independent of depth. This result confirms the analysis (Janssen, 1895) that showed that beyond a certain depth the weight of a bed within a bin is supported by friction on the sidewalls and the flow rate is depth-independent.

2.1.1 Frictional Nature of Granular Materials: Plastic Behavior of the Bulk

In Equation 2.1, tan ϕ, the ratio of shear to normal stress, is an apparent friction coefficient for the bulk. It is important to realize that granular materials, obey a plasticity rule only globally, i.e., it is the contact forces and not frictional forces, which govern the internal behavior of the material. As a consequence, force chains and spatially inhomogeneous stress distributions are characteristic of flowing granular materials. The inhomogeneous stress distributions result in force fluctuations inside the granular matter (Howell et al., 1999). It should be noted that the formation of force chains is more important for large particles (i.e. > 500 μm) than that of smaller particles (i.e. < 100 μm) (Tardos, et al., 2003). Most of the theoretical and experimental work concerning dense, slowly flowing granular matter, was performed on large and spherical particles (i.e. >2 mm in diameter and larger). The existence and behavior of force chains for small particles and particles with odd shapes are still a matter of debate.

2.1.2 Theories for the Quasi-Static Regime

Although a friction criterion (plasticity model) is the zero-order description of the solid-transition, the details are more complex as the initiation of flow is sensitive to the initial preparation of the sample and depends on both the initial solid volume fraction and the

history of previous deformations (Daerr and Douady, 1999). Modeling the initial deformation and the coupling between strain, stress, volume fraction and contact orientation, is the domain of soils mechanics (Roux and Radjai 1998). In spite of many microscopic studies (Herrmann et al., 1998), the relation to grain-level physical phenomena is not fully understood (Roux & Combes, 2001). Schaeffer (1978) used the Von Misses type yield criterion, written as:

$$\sum_{i=1}^{3}(\sigma_i - p)^2 = k^2 p^2 \quad \text{with} \quad p = \frac{1}{3} trT \tag{2.2}$$

where $k = \sqrt{2}\sin\phi$, is a characteristic constant of the material, and σ_i are the eigenvectors of T_{ij}. Combining the yield criterion and the co-axiality or Levy's flow rule (that relates the deviatoric stress and strain rate):

$$\tau_{ij} = \lambda \dot{\gamma}_{ij} \quad \text{where} \quad \lambda \geq 0 \tag{2.3}$$

(λ is a scalar constant) and combining Equation 2.2 and Equation 2.3, Schaeffer (1987) proposed a constitutive equation for incompressible granular material at yielding in the form:

$$T_{ij} = p\delta_{ij} + \tau_{ij} = P\delta_{ij} + \frac{\sqrt{2}\, p \sin\phi}{\left|\dot{\gamma}_{ij}\right|}\dot{\gamma}_{ij} \tag{2.4}$$

where:

$$\dot{\gamma}_{ij} = \frac{1}{2}\left(\frac{\partial u_i}{\partial x_j} + \frac{\partial u_j}{\partial x_i}\right) \text{ and } \left|\dot{\gamma}_{ij}\right| = \sqrt{\frac{1}{2}\dot{\gamma}_{ij}\dot{\gamma}_{ij}} \tag{2.5}$$

To obtain the general equation of motion one can combine the continuity and momentum equations with Equation 2.4 (constitutive equation) and get a similar form as

the generalized Navier-Stokes equations in fluid mechanics. The equation of motion for incompressible granular matter then takes the form (Tardos, 1997):

$$\rho_B \frac{Du}{Dt} = -\nabla p - \sqrt{2}\sin\phi\nabla \bullet \left(p\frac{\dot{\gamma}_{ij}}{\left|\dot{\gamma}_{ij}\right|} \right) + \rho_B g\,;\nabla \bullet u = 0 \tag{2.6}$$

In Equation 2.6, D/Dt is the material derivative, p is the average principal stresses and ρ_B is the bulk density. Tardos et al. (1998) solved the above equations for the simple geometry of plane Couette flow (two co-axial cylinders with a small gap) when the inner cylinder is rotating and the outer is stationary by assuming unidirectional flow ($\nu = 0$ *and* $u = u\,(y)$) in Cartesian coordinates. The continuity and momentum equations are satisfied regardless of the form of the function *u(y)* and hence the velocity distribution remains undetermined using the Schaeffer model. For this simple case, the components of the rate of deformation and stress tensor take the form:

$$\dot{\gamma}_{xx} = \dot{\gamma}_{yy} = \dot{\gamma}_{zz} = 0\ ;\ \dot{\gamma}_{xy} = \dot{\gamma}_{yx} = -\frac{1}{2}\frac{\partial u}{\partial y};\ \ \left|\dot{\gamma}\right| = \frac{1}{\sqrt{2}}\left|\frac{\partial u}{\partial y}\right| \tag{2.7}$$

$$T_{xx} = T_{yy} = T_{zz} = p\,;\quad T_{xy} = T_{yx} = -p\sin\phi \tag{2.8}$$

Solving the equation of motion in the z direction, these authors found the average stress to be hydrostatic or:

$$p = \rho_B g z \tag{2.9}$$

Correspondingly, from Equations 2.8 and 2.9 the shearing stress takes the form:

$$T_{xy} = \rho_B g z \sin\phi \tag{2.10}$$

This means that the shearing stress increases linearly with depth to reach a maximum at the bottom of the layer. Using the above consideration, one can estimate the torque on the rotating cylinder:

$$M_q = \pi \rho_B g h^2 R^2 \sin\phi \tag{2.11}$$

The above equation predicts quadratic dependence of the torque on the height of the sheared layer (h) and on the radius of the rotating cylinder (R).

The domain of validity of Schaeffer's law (Equation 2.4) is narrow and by itself is not enough to describe the regimes of granular flow under various conditions. The plasticity yield condition, which is valid only for incipient flows, makes the prediction of flow fields to be valid only in the slow regime where the deformations are small and it does not hold for continuously shearing systems at higher deformations where most industrial and geophysical phenomena occur. Another shortcoming of the ideal friction criterion is that it cannot describe the hysteresis observed in a stress-driven system. In a Couette cell, for example, one has to increase the applied shear stress up to a critical value to induce flow, but once it flows, the material stops only if the shear stress is decreased below a value less than the starting value (Forterre & Pouliquen, 2008). The origin of hysteresis in granular media is well illustrated by the toy model of a single bead flowing down a rough inclined substrate (Quartier et al. 2000).

As mentioned before the constitutive relation in Equation 2.4 requires that the material be in continuous flow, i.e. continuous yielding, so that the Schaeffer model (1987) predicts a flow domain with a non-zero velocity gradient. However, in practical situations like flow in a vertical rectangular or cylindrical bin, formation of shear bands and local

velocity discontinuities occur and make the velocity gradient to be zero at some points ($|\dot{\gamma}| = 0$) (Schaeffer, 1992). The combination of the stochastic flow rule with Mohr-Coulomb plasticity seems to be promising and can quantitatively model most flow geometries without empirically fitting the velocity profiles (Kamrin and Bazant (2007)). So far however, this approach has been applied only to systems with slow flow, e.g. quasi-static regime and only the velocity field (not the stress field) was calculated. We expect these authors to consider higher shear rates (when the collision also becomes important) in the future and calculate the velocity field as well as stress fields to generate a constitutive relationship that spans very slow to moderately high shear rates.

Another approach to describe quasi-static flows consists of explicitly writing non-local equations. Mills et al. (1999) have proposed constitutive equations in which stresses directly result from integration over force chains. Their model describes stationary dense granular flow along an inclined plane. The stress tensor is related via a constitutive law to quantities involving the properties and the structure of the whole granular material: the internal friction angle, the size of particles, and especially the correlation lengths attached to the transient strong contact network. The linear profile of the velocity field, and the scaling law between the flow rate, the height of particles and the inclination angle of the plane, are in good agreement with experimental results. However, their study is restricted to the one-dimensional case of the inclined plane geometry and has to be tested for other geometries as well as for 2D and 3D cases. Also a more precise analysis of the relation between the correlation lengths of transient chains in dynamic situations is of great importance.

Pouliquen et al. (2001) have proposed a simple model for slowly sheared granular flows, which is based on stress fluctuations. The basic idea of this model is based on a self-activated process, in which the shear deformations at a point induce fluctuations that may trigger shear at other positions. As a result, they obtained an integral rheological law, where the shear rate at a position is related to the shear rate in the vicinity. Quasi-static flows, like flow between vertical plates or in shear cells, are well described by the model. The model is also able to predict the onset of flow for the inclined plane configuration. Unfortunately, this model is also one-dimensional: the stress fluctuations are described by the z coordinate. A careful 3D analysis is necessary to better describe the fluctuations and shear induced motions. A second improvement to this model could be work on the finite duration of the jump. When yielding is activated at some place by a fluctuation, it takes a finite time for the particle to move to the next available space. Taking into account this time delay may allow describing more rapid flows.

In conclusion, several of these models have achieved moderate success, but they do not give a unified description of the transition between the quasi-static and the intermediate regimes.

2.2 Rapid Granular Flow (Collisional or Gaseous Regime)

Rapid deformations of dense granular materials occur mainly in geophysical phenomena such as avalanches. Such flows take place at bulk densities and strain rates at which the impulsive forces during collisions between pairs of neighboring particles are responsible for the transfer of momentum in the flowing material i.e. low bulk densities or very high deformations (Jenkins and Savage, 1983). It is assumed in this regime, that

grains interact by nearly instantaneous collisions in a way that is reminiscent of the classical picture of a molecular gas. This is the reason why the rapid granular flow is also known as a "granular gas" (Goldhirsch & Zanetti, 1993) and it can be modeled using the kinetic theory of gasses. In this rapid or gaseous regime of flow, each particle moves freely and independently of its nearest neighbors instead of moving in many-particle blocks. Bagnold (1954) was the first to suggest a model for rapid granular flow. He considered the collisions between particles of a rapidly sheared granular material consisting of identical spherical grains and suggested for the stress tensor a quadratic dependence on the shear rate:

$$\tau_{ij} = f_{ij}(\nu)\rho_p {d_p}^2 \dot{\gamma}^2 \tag{2.12}$$

The stresses reflect the internal momentum transport due to inter-particle collisions. Later experiments by Savage (1978) and Savage and Sayed (1980; 1982) on simple shear flow showed that the shear stress indeed depends quadratically on the mean rate of shear.

2.2.1 Granular Temperature & Kinetic Theory of Granular Material

The concept of granular temperature is perhaps the single most important key to understanding the behavior of rapid granular flows. Bagnold's picture of the individual granules moving in a shear flow invariably brings comparison with the motion of molecules in the kinetic theory of gases. Furthermore, inter-particle collisions will induce random velocities that are reminiscent of the thermal motion of molecules. Blinowski (1978) and Ogawa (1978) first recognized the importance of the velocity fluctuations and the means by which they could be included in a properly formulated continuum theory. Ogawa (1978) introduced the fluctuation temperature in terms of the mean kinetic energy

of the particles' velocity fluctuations. This so-called "granular temperature", which is the magnitude of all fluctuating velocities, then takes the form:

$$T = \left\langle u'^2 \right\rangle \tag{2.13}$$

Where *u'* is the instantaneous deviation from the mean velocity, and < > represents an appropriate average. T represents twice the energy per unit mass contained in the random motions of the particles. Comparing the thermodynamic and granular temperatures we see that both play similar roles in governing the behavior of their respective systems. In particular, both generate pressures and govern the internal transport rates of mass, momentum, and energy. Thus, while the term "temperature" sometimes leads to confusion, the physical analogy between the two temperatures is appropriate and its use has become standard throughout this field. Ogawa (1978) proposed a balance law for the granular temperature that related its rate of change to its production by the mean flow, its flux from one point to another in the flow, and its dissipation into true thermal energy. This author determined the total rate of change of fluctuation energy in such collisions by averaging over all possible collisions. This, with an estimate of the frequency of collisions, allows calculating the total rate of change of fluctuation energy and, finally, to infer how the mean stress and mean dissipation of fluctuation energy depend upon the collision parameters and upon the means of the density, fluctuation energy and strain rate. Later, Savage and Jeffrey (1981) argued that using the above procedure, the flux of fluctuation energy is not given, nor it is clear how the scheme might be extended in order to predict the form of this flux. This has been proven to be the main disadvantage of the method proposed by Ogawa (1978).

Savage and Jeffrey (1981) treated the rapidly deforming granular material by analogy to kinetic theory of dense gases, which enables them to use numerous results regarding collisions and averaging and avoid many of the difficulties confronted by Ogawa (1978). As in the kinetic theory of gases, the model proposed by Savage assumes that the granules interact by instantaneous collisions and that the granular temperature governs all transport rates. The proposed rapid granular flow theory only assumes collisional dissipation and, as collisions are taken to be instantaneous, the dissipation is represented as a coefficient of restitution, ε, i.e., the ratio of the approach to recoil velocities in the center of mass. Since granular temperature is produced by shear work one might expect a relationship between the shear rate $\dot{\gamma}$ and the magnitude of the granular temperature. One important difference between a kinetic theory for a classical dense gas and that for a rapidly deforming granular material is that in the granular material an inhomogeneity of the mean flow is necessary to force the collisions and to drive the velocity fluctuations. The temperature of a dense gas can also be influenced by the addition of heat throughout its interior or over its surface. In the new model, the importance of the mean deformation was reflected in the anisotropy of the distribution function that Savage (1984) proposed to govern the probability of collisions between pairs of particles. Collisions between particles in close proximity in the mean flow were regarded as more likely than those between particles swept apart. Savage (1984) considered a dense collection of identical spherical particles subjected to a rapid mean shear and, for perfectly elastic particles, calculated the components of the mean stress that result from the exchange of momentum in collisions. The second important difference between the kinetic theories for a dense gas and a rapidly sheared granular material is that collisions between particles of a

granular material are inelastic and hence involve a loss of energy. The energy associated with the granular temperature is dissipated by inter-particle collisions and therefore, left to itself, the granular temperature would quickly dissipate and the movement would stop. In fact, this is common experience; shaking a granular material-for example, a bottle of aspirin or a box of cereal-induces random temperature-like motions between particles, but once the shaking stops, the particles will almost instantaneously lose their granular temperature and cease all motion. To maintain the temperature, energy must be continually added to the random components of velocity to balance it; otherwise it is lost by dissipative collisions. Unlike a molecular system, the granular temperature comes about as a by-product of the flow itself and cannot be specified independently of the fluid mechanics, as one could fix the temperature of a molecular system by putting it in contact with a large isothermal reservoir. Determination of stress was improved by incorporating the energy lost in collisions for smooth inelastic particles by Jenkins and Savage (1983).

In order to have a better understanding of granular temperature, we should consider that the source of all energy is the work done on the system from the outside, either by body forces (such as gravity) or through the motion of the system boundaries. Shear work (the product of the shear stress and the velocity gradient) performed on the system converts some of the kinetic energy of the mean motion into granular temperature (which is the kinetic energy associated with the random particle velocities); this reflects the fact that both of the temperature mechanisms described above are related to the velocity gradient. Finally, the inelastic collisions between particles will dissipate the granular temperature into real thermodynamic heat. The magnitude of the granular temperature thus depends

on a trade-off between the temperature generation by shear work and its dissipation by collisional inelasticity.

While the above describes the global energy path through the granular system, the local value of the granular temperature may be affected by its magnitude in neighboring areas. This is a conduction-like process and occurs for physical reasons exactly analogous to the thermodynamic conduction in a gas; that is, as a particle follows its random walk through the material, it carries its random kinetic energy with it (a streaming temperature transport), and when two particles collide they exchange some of their random kinetic energy (a collisional temperature transport). Both mechanisms result in a diffusion of granular temperature through the material, and like its thermodynamic counterpart, granular temperature will be conducted along its gradients in the direction of diminishing temperature (Campbell & Brennen (1985)).

Another important concept about the granular temperature is that in the kinetic-theory picture of gases, the random velocities of the molecules are so large that the imposition of a mean velocity field provides only a first-order correction to the thermal velocities. In contrast, for granular materials, the random velocities are proportional to the mean velocity gradient and consequently will be much smaller than the mean velocities of the particles. Thus, when viewing a granular flow, the particle fluctuations are not as violent as one might expect.

2.2.2 Modeling of Rapid Granular of Flows

The physical similarity between rapid granular flows and the kinetic-theory of gases has led to a great deal of work on creating similar models for granular materials. The idea is to derive a set of continuum equations entirely from microscopic models of individual

particle interactions, if the particles are assumed to be rigid. The assumption of particle rigidity implies that all contacts occur instantaneously, only binary interactions need be considered, and surface friction or any other particle interactions are ignored. Furthermore, molecular chaos is generally assumed, implying that the random motion of even closely neighboring particles is independently distributed. The system of equations contains conservation of mass (continuity):

$$\frac{D\rho\nu}{Dt} + \rho\nu\nabla \cdot u = 0 \tag{2.14}$$

and also a conservation of momentum equation:

$$\rho\nu \frac{Du}{Dt} = \nabla p(\rho,\nu,T,\varepsilon) + \nabla.(\eta(\rho,\nu,T,\varepsilon)\nabla u) \tag{2.15}$$

Finally, there is an energy-conservation equation for the kinetic energy contained in the granular temperature:

$$\rho\nu \frac{DT}{Dt} = \nabla.(k(\rho,\nu,T,\varepsilon)\nabla T) + \tau : \nabla u - \Gamma(\rho,\nu,T,\varepsilon) \tag{2.16}$$

In Equation 2.16, k is the conductivity, $\tau : \nabla u$ is the temperature production by shear work, and Γ is the dissipation into thermodynamic heat by inelastic collisions.

The range of applicability of rapid flow theory is limited. For example the viscous nature of Equation 2.15 is not realistic in the solid phase stresses. Thus systems such as hoppers cannot be modeled by rapid flow theory. A key feature of hoppers is the frictional support of material by the vertical walls of the bin (Janssen, 1895). A viscous material produces no forces unless the material is in motion and can thus provide no such support. As Janssen's frictional support appears in static materials, it cannot be modeled

by the type of viscous material predicted by rapid-flow theory. In other words, either the material should not arch or this effect should come into the model. There have been attempts to add a frictional response to rapid flow models, most notably Johnson et al. (1990) but these are ad hoc models based on self-contradictory assumptions as they are formed by simply adding a rapid-flow model, based on instantaneous collisions, to a frictional model, based on long duration contacts.

Another problem is that all of the constitutive laws obtain their rates through the granular temperature T. This implicitly assumes that the magnitude of the thermal velocities ($T^{1/2}$) is much larger than the relative velocities induced by the shear ($d_p\dot{\gamma}$), which is only observed at extremely small solid concentrations. Predictions of Lun et. al. (1984) show that over most of the range of solid concentrations the mean shear and the temperature are equally important in driving the relative motion between particles, the collision rate, and thus the transport rates in a rapid granular flow. As the kinetic theories depend only on the temperature to govern transport, they are most likely to either underpredict the transport rate or overpredict the granular temperature. Furthermore, as the relative velocities induced by the shear rate are only in the direction perpendicular to the velocity gradient, this introduces anisotropies in the angular distribution of collisions about a particle (Campbell and Brennen, 1985). This collisional anisotropy was included in the earliest rapid flow models, like Savage and Jeffrey (1981) and Jenkins and Savage (1983), which only considered contact stresses but is absent from the model by Haff (1983).

Finally, the assumption of Boltzmann's molecular chaos in all kinetic theories, which says that the velocities or positions of colliding particles are un-correlated, is problematic.

This is because common granular flows occur at such large concentrations that any given particle will interact many times with its neighbors and it is likely that their velocities will be strongly correlated. Campbell (1985) and Campbell and Brenenen (1986) correlated the relative positions of particles and showed that true molecular chaos is unlikely in real granular systems although it is difficult to estimate the degree of error introduced by this assumption.

So far, the progress of rapid granular flow theory has largely been due to the interplay between theoretical models and computer simulations. The experimental data that do exist measure global properties-such as the stress/strain rate behavior of the system-with very few measurements of microscopic properties such as the granular temperatures and/or solid fraction fluctuations; the results are thus clouded by uncertainties about the actual material behavior inside the experimental device. Yet both theoretical analyses and computer simulations are based on material and boundary properties, and the behavior of the flow can be drastically altered by small changes in the chosen models. At the same time, there is little direct experimental evidence to assess the appropriateness of the model chosen. Much of the recent effort in the areas of rapid granular flow or kinetic theory has been directed towards issues that are of largely academic interest. This is either because, of unrealistic assumptions or because they are only of interest at small particle concentrations that are rarely found outside the laboratory or because the theories are limited only to ideal cases of spherical, uniform size, large, elastic particles (Campbell, 2006).

2.3 Intermediate (Frictional-Collisional) Regime of Granular Flow

In the “Intermediate” dense flow regime, where most industrial processes occur, the solid fraction is close to a maximum value and the flowing materials have the properties of the other two regimes, i.e. co-existence of enduring contacts (quasi-static) and

collisions (rapid). Ancey (2001) has shown that in a simple shear flow (i) networks of particles in close contact cover the flowing layer that greatly fluctuates in space and time (Radjai & Roux, 2002) (ii) these networks transmit strong forces, and (iii) they surround particle clusters, where the stress level is much lower.

Dense flows in the intermediate regime are beyond the quasi-static regime because the inertia of the grains and therefore the shear rate come into play. The assumption of binary, instantaneous collisions of the kinetic theory is also unrealistic (Jenkins & Savage, 1983; Goldhirsch, 1999). Due to the very strong correlations of motion and force, the theoretical description of these dense flows is very difficult (Pouliquen & Chevoir, 2002). Advances have come in the last decade from the combination of discrete numerical simulations and experiments on model materials in simple geometries. Campbell and co-workers (Zhang & Campbell, 1992; Campbell & Zhang 1992; Campbell, 1993) were among the first to study the phase change between fluid-like (intermediate) and solid-like (quasi-static) behavior in granular materials. These studies indicated that the transition could not be described in terms of rapid granular flow ideas (as was first proposed by Jenkins and Askari (1991)), but instead exhibited a quasi-static yield behavior. Later studies by Campbell on hoppers (Potapov & Campbell, 1996), in which the flow is clearly not rapid granular, indicated that the generally accepted assumption of quasi-static yield occurring at the internal angle of friction of the material could not explain the stress state within the hopper. In particular, standard quasi-static flow analyses assume that the ratio of maximum shear to normal stress should equal the internal angle of friction, which is treated as a material property. However the results by Potapov and Campbell (1996) showed that this ratio was far from constant and reached

its maximum value in the hopper throat. Finally, large-scale computer simulations of landslides, performed by Campbell et al. (1995), indicated that the ratio of shear to normal stress on the base of the slide increased with shear rate (i.e. the velocity gradient at the slide's base) even though both rapid flow and quasi-static flow theories suggest that this ratio should be independent of shear rate. This was an indication that the landslides were occurring in a new regime that is neither rapid nor quasi-static. Furthermore, these observations were consistent with the hopper simulation mentioned above, as the largest stress ratios were found in the hopper throat where the shear rates are the largest (as the velocities are highest and the channel is the narrowest). In the phase-change simulations, the stress ratio could also be interpreted as increasing with the shear rate. However, it was difficult to obtain rheological information from these studies as neither the density nor the shear rate could be sufficiently controlled.

This led to the more current investigations by Campbell (2002 and 2005), where it was proposed to include the inter-particle stiffness k in the model that made it possible to unify the various granular flow theories and fill in the gap between the quasi-static and rapid flow regimes and draw complete flow maps for shearing granular materials. This modeling effort was originally designed to quantitatively determine the effect of shear rate on the stresses in a dense granular flow and on the shear-to-normal stress ratio at either controlled stress or concentration. These authors were looking for flow regimes where the shear-to-normal stress ratio varied with shear rate as observed in the earlier studies mentioned above. Campbell's model used the soft-particle technique, which models the interaction between particles as a spring (which may be linear or nonlinear) in the direction along the particle centers that acts as long as the particles remain in contact.

Some mechanism is also added in parallel to the spring to dissipate the collisional energy and this is accomplished by putting a viscous dashpot in parallel with the spring. The contact model used in their studies is schematically illustrated in Figure 1.

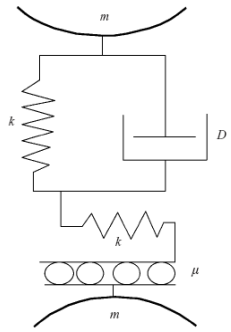

Figure 1: Schematic of the particle contact model

The spring has an associated stiffness *k*, which is linear in most parts of his study. This inter-particle stiffness governs how particles "see" each other mechanically and, determines the bulk elastic properties of the granular material. In the direction tangential to the contact point the particles are connected to a frictional slider with an associated friction coefficient, μ, connected in series with another spring also with stiffness k. Thus as the particle surfaces move relative to one another in the direction tangential to the contact point, the tangential spring will load until the tangential force reaches the friction coefficient times the normal force, at which point the surfaces slip relative to one another against a force equal to μ times the normal force. The simulation consists of integrating all equations of motion for all the particles in the system with forces derived from the contact model shown in Figure 1.

Campbell (2002) divided the entire granular flow field into two broad regimes: the *Elastic* and the *Inertial*. The *Elastic* regimes encompass all flows in which force is transmitted principally through the deformation of force chains for which the natural stress scaling is $\tau d_p / k$. As mentioned before, the hopper, landslide and phase-change simulations of Campbell indicated that the apparent friction coefficient, τ_{xy} / τ_{yy}, changes with the shear rate. This leads to a dimensional problem as the shear rate has units of (time)$^{-1}$, while the stress ratio τ_{xy} / τ_{yy} is dimensionless and can thus only be a function of dimensionless parameters. Campbell considered that the inverse shear rate represents the only time scale in rapid granular flow theory, while no time scale appears in quasi-static theories. Thus some other parameter must be introduced into the analysis, which contains units of time by which the shear rate can be scaled. The only possible candidates come from the particle contact model. As the particle surface friction and the coefficient of restitution are dimensionless, the most likely remaining possibility is the contact stiffness, *k*. A stiffness scaled with the shear rate has the form:

$$k^* = \frac{k}{\rho d_p{}^3 \dot{\gamma}^2} \tag{2.17}$$

This dimensionless parameter for the stiffness is the ratio of Bagnold's inertia, i.e. $\tau / \rho d_p{}^3 \dot{\gamma}^2$, to the elastic stress scaling, i.e. $\tau d_p / k$. Campbell (2005) then proposed a complete map for the regimes of flow (Figure 2). In this flow map Elastic-quasi-static refers to the quasi-static regime, elastic-Inertial refers to the Intermediate regime and Inertial-Collisional refers to the Rapid granular flow. This flow map indicates that rapid granular flows are seldom observed, for example 10 particle layers of 1 mm sand require

shear rates of about 100 s^{-1}. Deeper depths would require even larger shear rates and while such shear rates can be obtained in laboratory shear cells and computer simulations, they are not found in practice. His results also indicate that the limiting shear rates for changing the regimes of flow are relatively insensitive to the particle stiffness. Going to a softer material would decrease k and with it $k/(\rho d_p^3 \gamma^2)$, pushing the system towards an inertial flow, but at the same time would proportionally increase $\tau_0 d_p/k$, pushing the system away from inertial behavior, so that from Figure 2 a change in k is unlikely to cause a change in flow regime.

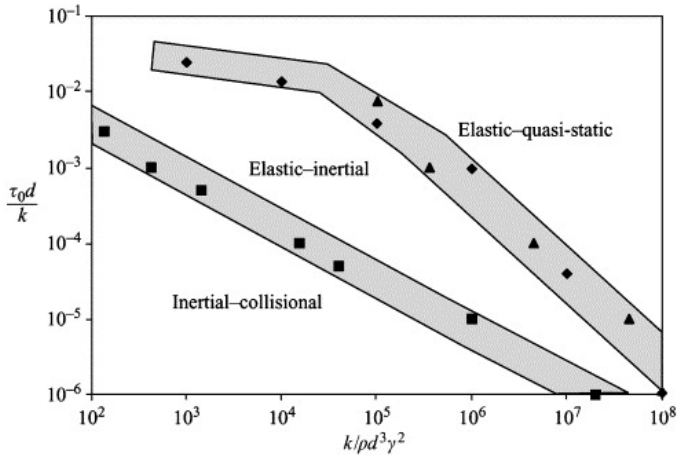

Figure 2: Different regimes of granular flow taken from Campbell (2005)

While a high speed laboratory shear cell can achieve the hundreds of inverse seconds of shear rate required to achieve Rapid Flow, shear rates in the hundreds of inverse-seconds, will not be found in any common granular flows, such as chutes and hoppers, all of which are gravity driven. However, under reduced gravity conditions, smaller shear rates are required to shift the regime to Rapid flow. Reducing gravity also reduces the driving force for the bulk motion and reduces the available shear rates proportionally. Although

Campbell was able to draw a general map for different regimes of flow, the results come from computations only and it is assumed that the stresses in the bulk appear to be homogeneous, while there are several experimental measurements that suggest stress inhomogeneity. In this model, applying even a small stress to the system results in flowing of the bulk, while it is well known that granular materials behave like visco-plastic fluids and they show a yield stress that is necessary for the system to overcome in order to flow (Losert et al., 2000).

Realistic granular materials consist of irregularly shaped grains, each with a finite stiffness (or Young's modulus). If no external force is applied to a dry granular material, it quickly loses all its kinetic energy in dissipative collisions and each grain comes to rest. In a dilute system, there are no residual contacts between grains and the total energy is approximately zero. However, for granular materials with larger bulk densities, there are contacts between grains in the relaxed state and a nonzero residual energy remains due to grain deformation and friction (Lois et al. 2006). If a shear stress is applied to the system, motion occurs if the stress is large enough to overcome the energy stored in the contacts. The minimum stress needed to initiate flow is the yield stress; it is zero below a critical packing fraction ν_c and is an increasing function of packing above ν_c (Aharanov & Sparks, 1999; Zhang & Makse, 2005). For granular shear flows with $\nu > \nu_c$, it has been demonstrated by Campbell (2002) that the stiffness of the grains plays an important role. Shear flows with $\nu > \nu_c$ are slowly moving in the quasi-static regime (Behringer et al., 1999; Mueth et al., 2000).

Savage (1998) brought the kinetic theory ideas into slow flow by splitting the individual particle velocities into fluctuating and mean transport components, and

employing the notion of granular temperature that plays a central role in rapid granular flows. He observed that on a somewhat larger scale, one can think of analogous fluctuations in strain rates. In other words at the individual particle level he considered the fluctuations in velocities while at somewhat coarser level the fluctuations in strain rate. Along with this theoretical evidence, there are experimental findings for velocity or strain rate fluctuations. Jaeger et. al. (1996) showed an important property of granular material which is partial fluidization in response to shear stresses.

2.3.1 Continuum theories for the Intermediate regime

One approach to model granular matter is the continuum theory for partially fluidized granular flows (Aranson & Tsimring, 2002). Capturing the hysteretic character of granular flows is the major motivation of a model developed through this theory. The granular media is described as the mixture of solid and liquid phases, whose relative fraction is controlled by a Landau equation (of phase transition). This theory is based on a combination of the equations for the flow velocity and shear stresses coupled with the order-parameter equation, which describes the transition between the flowing and static components of the granular system. When the shear stress exceeds a certain threshold, the granular material undergoes a transition from a solid state to a fluidized state (yield). The physical mechanism and properties of this transition are still not completely understood. In many important situations the granular material remains in a multiphase state when part of it is fluidized while another part is solid. This idea was borrowed from the Landau theory of phase transitions (Landau & Lifshitz, 1980). In the theory of partially fluidized granular matter, the shear stresses are composed of two parts: the dynamic part proportional to the shear strain rate and the strain-independent or static part. The relative

magnitude of the static shear stress is controlled by the order parameter (OP), which varies from 0 in the liquid phase to 1 in the solid phase. One of the advantages of this theory is that in partially fluidized flows, some of the grains are sliding past each other, while others maintain prolonged static contacts with neighbors. Accordingly, the stress tensor was written as a sum of the hydrodynamic part proportional to the flow strain rate, and the strain-independent part, i.e.:

$$\sigma_{ij} = \eta\left(\frac{\partial \upsilon_i}{\partial x_j} + \frac{\partial \upsilon_j}{\partial x_i}\right) + \sigma^s{}_{ij} \tag{2.18}$$

Here η is the effective viscosity, $\sigma^s{}_{ij} = \rho\sigma^0{}_{ij}$ for i≠j and $\sigma^s{}_{ii} = \rho\sigma^0{}_{ii}$ while the $\sigma^0{}_{ij}$ is the static stress tensor for the immobile grains. In the static state $\rho = 1$, and $\sigma^s{}_{ij} = \sigma^0{}_{ij}$, $\upsilon_i = 0$, whereas in a fully fluidized state $\rho = 0$, and the shear stresses are simply proportional to the strain rates as in ordinary fluids. Although the theory of partial fluidization has success in describing multiple flows within a single theoretical framework and can describe some unsteady flows, setting boundary conditions for the order parameter usually requires additional *ad hoc* assumptions. Also, the theory lacks any clear microscopic foundation and is not directly coupled to a constitutive stress model for static materials. Some attempts have been made to connect this approach to microscopic measurements (Volfson et al., 2003). Later improvements make it possible for the model to describe nontrivial behavior observed when triggering avalanches on an inclined plane and the model is able to reproduce known flow behavior in inclined chutes, avalanches, rotating drums, and simple shear cells without many fitting parameters but still fails to predict the correct rheology (Aranson & Tsimring, 2006).

Da Cruz et. al (2002) used a rheometer for the annular couette experiment. They measured the torque and rotational velocity for different size glass and polystyrene beads. Using these results, GRD MiDi (2004) defined the wall shear rate as $\dot{\gamma}_w = \frac{V_w}{d_p}$ while the velocity on the rotating wall is V_w. The dimensionless shear rate then takes the form: $\dot{\gamma}_w \sqrt{d_p / g}$. Figure 3 shows the effective friction μ_{eff} versus the dimensionless characteristic shear rate.

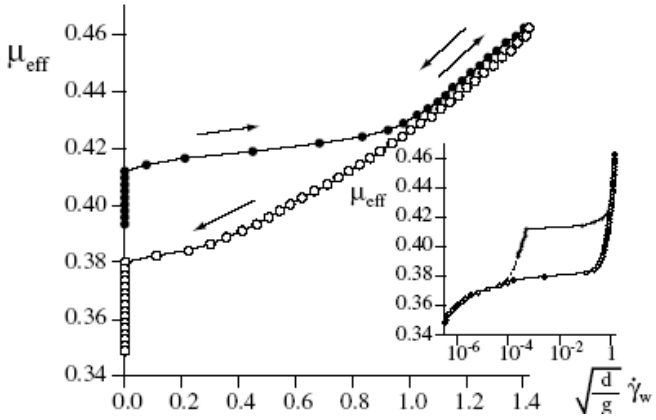

Figure 3: Effective friction as a function of the shear rate (GDR MiDi, 2004)

The effective friction in Figure 3 is obtained from torque measurements assuming a hydrostatic pressure distribution:

$$\mu_{eff} = \frac{\tau_w}{P_w} \quad \text{with } \tau_w = \frac{T}{2\pi R^2 L} \text{ and } P_w = \frac{1}{2}\rho g L \tag{2.19}$$

In the above equations T is the measured torque and L is height of the granular material, which is sheared between two coaxial rough cylinders. The roughness of the wall is made of glued grains. There is some missing data in Figure 3, between very small and moderately large shear rates and it is not clear why the increasing and decreasing stress curves are so different and it might be due to different force chain structures in the

two states. Also, defining the friction coefficient as the ratio of wall shear stress to hydrostatic pressure does not seem to be appropriate unless the normal stresses are equal. Later simulations by Da Cruz et al. (2005) showed that the normal stress components in the *x* and *y* directions are equal (i.e. $\sigma_{xx}=\sigma_{yy}$) for steady uniform shear flow (i.e. plane shear); this makes the definition of the friction coefficient acceptable. This observation contradicts the usual Mohr-Coulomb behavior in soil mechanics, where this ratio (σ_{xx}/σ_{yy}) is equal to an active or passive Rankin coefficient, different from unity (Nedderman, 1992). In the case of plane shear Da Cruz et al. (2005) defined the effective friction coefficient as the ratio of shear stress to the pressure inside the material $\mu^* = S/P$. It could also be defined as the ratio of the (total) tangential and normal forces on the wall $\mu_w^* = T/N$. Studies by Da Cruz et al. (2005) and Lois et al. (2005) showed that in the simple sheared configuration for rigid particles, dimensional analysis strongly constrains the stress/shear rate relations. For large systems (i.e., when the distance between the plates plays no role), the system is controlled by a single dimensionless parameter called the inertial number:

$$I = \frac{\dot{\gamma} d_p}{\sqrt{P/\rho_p}} \tag{2.20}$$

In Equation (2.20), P is σ_{xx} or σ_{yy} as mentioned before and ρ_p is the particle density. A physical interpretation of this parameter was given in terms of the ratio between two time scales (GDR MiDi 2004): (*a*) a microscopic time scale $\frac{d_p}{\sqrt{P/\rho_p}}$, which represents the time it takes for a particle to fall in a hole of size d_p under the pressure *P* and which gives the typical time scale of rearrangements, and (*b*) a macroscopic time scale $1/\dot{\gamma}$ linked to the

mean deformation. Small values of the parameter *I* correspond to a quasi-static regime in the sense that the macroscopic deformation is slow compared to the microscopic rearrangement, whereas large values of *I* correspond to rapid flows. Dimensional analysis shows that, to switch from the quasi-static to the inertial regime, one can either increase the shear rate or decrease the overburden or pressure. The inertial number is also equivalent to the square root of the Savage number or Coulomb number introduced by some authors as the ratio of collisional stress to total stress (Ancey et al., 1999; Savage, 1984). This parameter is the only dimensionless number for rigid particles (this is not the case for soft particles, in which an elastic time scale comes into play (Campbell 2002; Shen & Sankaran, 2004)). In steady uniform shear the solid fraction and the shear stress adjust in response to the prescribed inertial number. Da Cruz et al. (2005) showed the strong influence of *I* on two dimensionless quantities, the solid fraction and the effective friction coefficient. They proposed a constitutive model based on the discrete simulation of two-dimensional simple shear of a dense ensemble of disks in the absence of gravity. In their two-dimensional simulations, Da Cruz et al. (2005) found that the effective friction coefficient depends linearly on *I (*for $I \leqslant 0.15$) and starts to saturate for higher shear rates (the so-called friction law):

$$\mu(I) \approx \mu_{\min} + bI \tag{2.21}$$

This kind of friction law was already observed in previous simulations of the variation of μ with the shear rate, the pressure or the solid fraction (Savage and Sayed, 1984; Campbell et al., 1995). In the same range, Da Cruz et. al (2005) also found that the average solid fraction ν decreases approximately linearly with increasing *I,* starting from a maximum value ν_{max} (the so-called dilatancy law):

$$\nu(I) \approx \nu_{\max} - aI \tag{2.22}$$

Fig. 2.3.9 shows the functions $\mu(I)$ and $\nu(I)$ measured in the discrete numerical simulations of Da Cruz et al. (2005) carried out in two dimensions with discs (filled circles). The results confirm a proposal put forth by previous works (Savage and Hutter, 1989; Ancey et al., 1999) that establishes that the flow regime and rheological parameters scale with a dimensionless number that represents the relative strength of inertial forces with respect to the confining pressure.

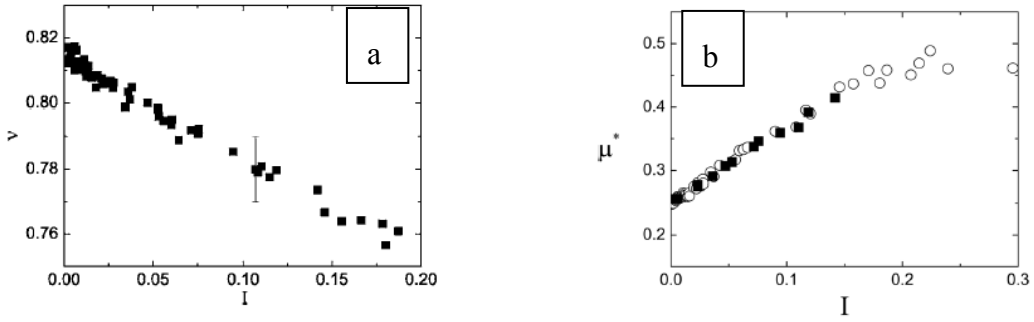

Figure 4: (a)Dilatancy Law, (b) Friction Law

As a consequence, for rigid grains, the shear stress is proportional to the confining pressure in simple shear between two horizontal plates, with the effective friction coefficient and the solid fraction being functions of I:

$$\tau = P\mu(I) \tag{2.23}$$

$$\nu = \nu(I) \tag{2.24}$$

From the dilatancy and friction laws, a visco-plastic constitutive law can be deduced, with a plastic Coulomb term and a viscous Bagnold term. These authors showed that this constitutive law is not very sensitive to the mechanical properties of the grains, once they are frictional, dissipative and rigid. Figure 5 shows a qualitative diagram of the flow

regimes and of the friction law. The quasi-static critical state regime corresponds to very small values of *I*, with nearly no variation of the effective friction coefficient.

Although the transition between the quasi-static regime and the dense flow (intermediate) regime is not very well defined, it is clear that the effective friction coefficient increases in the dense flow regime and should saturate in the fully collisional regime (the values of the effective friction coefficient in the figure are only indicative). By comparing results from simple shear test with experimental measurements of granular flows on rough inclined planes, (Pouliquen & Forterre, 2002; Pouliquen, 1999) showed that the friction coefficient is a function of the inertial number (*I*). Experiments in the same geometry by Jop et al. (2005) show that the friction coefficient ($\mu(I)$) starts from a critical value of μ_s at zero shear rate and converges to a limiting value of μ_2 at high values of the parameter *I*.

In the dense flow regime, in which variations of the volume fraction are small, an incompressible assumption is possible within the framework of Equations 2.23 and 2.24.

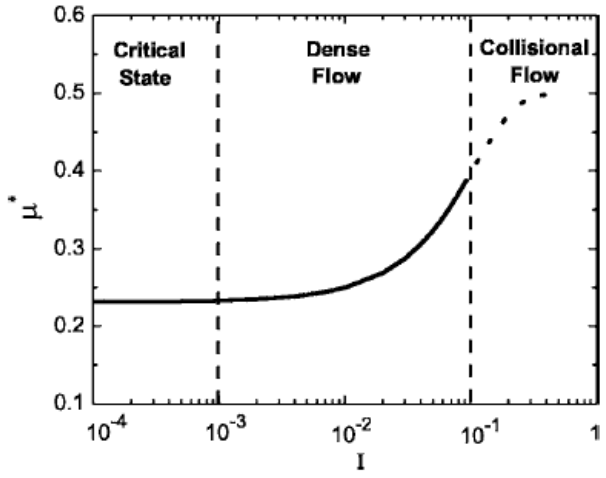

Figure 5: Diagram of the Granular Flow Regimes (Da Cruz et al., 2005)

The dilatancy and friction laws are decoupled, which allows one to neglect the variations of ν without losing the variations of the friction coefficient that characterize the viscous nature of the material (Jop et al., 2006). In this way the granular material is described as an incompressible fluid. Jop et al. (2006) proposed a 3D generalization of the friction law for granular materials. More recently Daniel et al. (2007) proposed a constitutive model by using the friction and dilatancy laws and generalized them to a 3D case. They tested their rheological model on flow between concentric cylinders (Couette flow) and the velocity distribution matches the experimental data by Mueth et al. (2000). However predictions for solid fractions only capture the trend for the experimental data and are unable to explain the fluctuations that occur in the experiment.

Tardos et al. (2003) studied the dependence of torque on the rotating cylinder on the shear rate in the annular Couette geometry. In their system the bed is closed and the materials are constrained from further dilatation. They found, not surprisingly, that the dependence of the shear stress on the shearing rate strongly depends on the way the bed is confined and is different from one experiment to another. Using a stagnant layer of particles loaded above the shearing gap (overburden) increased the confinement of the bed. However, those conditions could not be reproduced identically and different results were sometimes obtained with the same overburden. For this reason, these experiments could not be used to further prove the dependence of shear stress on shear rate.

2.4 Dilatancy and Shear Band Thickness in Granular Media

A unique property of granular materials was observed by Reynolds (1885) who named it "dilatancy". The concept of dilatancy is generally the expansion of the voidage that

occurs in a tightly packed granular arrangement when it is subjected to a deformation. In other word, in order for shearing to occur in a bed of closely packed particles, the bed must expand by increasing its void fraction (Figure 6). Many attempts have been made to include the effects of dilatancy in the theory (Nixon and Chandler, 1999).

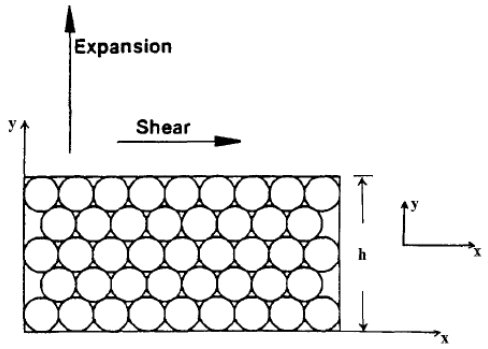

Figure 6: Illustration of dilatancy in close-packed spheres (Massoudi and Mehrabadi (2000))

Precise studies of dilatancy are hindered by the opaque nature of granular media and by the complexity of grain flows that in experimental situations never form a simple linear shear profile (GDR MiDi, 2004; Depkan et al., 2006). Hence, many basic questions are left unanswered. If a dense layer of granular material subjected to shear stress begins to fail at a slip plane, it can only undergo shear deformation if it also dilates (expands). In a real sample, the dilation does not occur uniformly throughout, but tends to be localized to a thin region around $10d_p$ wide (d_p is the particle diameter) known as a shear band (Howell et al., 1999). While many overall features of granular flows can be predicted using traditional models of plasticity, prediction of the thickness of shear layers remains unknown (Tejchman & Wu, 1993; Mohan et al., 1997). As mentioned before, when granular materials are sheared, a portion of the material does not exhibit sustained deformation (shear bands). Shear bands, localized regions where shear flows concentrate, form in many complex fluids under a wide range of circumstances and it can be formed by stress

inhomogeneity and flow instabilities. The flow of granular media is almost always inhomogeneous with the flow often localizing in shear bands near boundaries. For narrow granular shear bands, observations by sight suggest a clear distinction between the flowing and the non-flowing zone. However, careful studies of the apparent stationary region have revealed that there does not appear to be a strictly stationary zone in the vicinity of the flow. The thickness of the shear layer is influenced by the nature of the boundaries: when the flowing material is confined by smooth walls the bands are thinner while, it is found that the thickness of the shear layer is larger for the case of rough walls (Tejchman & Gudehus, 1993).

The failure of the frictional models to predict the thickness of the shearing layers has been attributed to the absence of a material length scale in their constitutive equations (Muhlhaus & Vardoulakis, 1987). To overcome this deficiency, the particle size must be incorporated in the constitutive equations. Two recently proposed models include the particle size as a length scale and these are the Cosserat model and the stochastic flow rule. Muhlhaus and Vardoulakis (1987), and Tejchman and Wu (1993) have developed Cosserat plasticity models for studying the development of shear bands in granular flow. In this model, the yield condition and the flow rule were modified to account for the influence of the coupled stress to provide a relation for the angular velocity. Mohan et. al. (1999) adapted this approach for modeling of slow shearing of granular materials through a vertical channel, plane shear without gravity and in cylindrical Couette flow. They defined R to be the ratio of stress arising from grain collisions to the total stress:

$$R = \frac{\rho_p d_p{}^2 \dot{\gamma}^2}{N} \tag{2.25}$$

where ρ_p and d_p are the density and mean diameter of the particles, $\dot{\gamma}$ is the shear rate and N is the total normal stress in the system. They considered the case of R<<1 (slow flow) in their Cosserat model (Mohan et. al. 1999). They included the coupled stress field, which is a result of tangential frictional forces between grains as well as an angular velocity field. This allows these authors to supplement the equation of balance of angular momentum to the balances of mass and linear momentum. They also extended the yield condition and flow rule used in classical plasticity to incorporate the coupled stress and the angular velocity. The resulting Cosserat model has a microscopic length scale, which determines the thickness of the shear layer (shear bands). These authors considered two cases for plane shear in the absence of gravity: (1) the two walls are of equal roughness, and (2) the upper wall is smoother. In both cases, the velocity fields decay rapidly with distance from the upper wall if the Couette gap is large compared to the grain size. If the roughness of the granular medium is exactly equal to that of the wall, it is predicted that it shears uniformly in the entire gap. In a cylindrical Couette flow between walls of equal roughness, the Cosserat model shows that the velocity decays rapidly with distance from the inner cylinder. This finding is in a good agreement with the velocity measurements reported by other scientists (Mueth et al. (2000); Loser, et. al. (2000)). In addition, Mohan et. al. (1999) found that if the wall roughness is less than that of the granular medium (i.e. $\phi < \phi_w$), then the shear layer thickness (Δ) increases with the Couette gap, but reaches an asymptotic value independent of the Couette gap in the limit $H/d_p \rightarrow \infty$ (H and d_p are the Couette gap and particle diameter, respectively). Further, Δ decreases when the angle of wall friction is reduced, and vanishes when the wall is perfectly smooth. In the case of fully rough walls when the wall friction is equal to the particle internal angle

of friction, Δ increases with the Couette gap as $(H/dp)^{1/3}$, and does not depend on ϕ. These cases have not yet been experimentally confirmed and are still questionable. This model also predicts a small increase in the solids fraction as one moves towards the outer cylinder. This increase, however, is substantially smaller than what was observed in the experiments of Mueth et al. (2000). This prediction may perhaps be corrected by incorporating elastic effects in the model. Another strange prediction from this model is that if the outer cylinder is sufficiently smoother than the inner cylinder, the shear layer is located near the outer cylinder and the material elsewhere undergoes little deformation. In contradiction with their prediction, our experiments at low shear rates (i.e. quasi-static regime) with a rough inner and smooth outer wall clearly show that shear layers are always located close to the inner cylinder (Kheiripour et. al., 2010c).

A more promising attempt to introduce the length scale in the model was done recently by Kamrin and Bazant (2007) who proposed a new model based on a stochastic flow rule inspired by Mohr-Coulomb plasticity. Their theory differs from all continuum theories in that it is derived systematically from a microscopic statistical model, which is called the "spot model" (Bazant, 2006). This model proposes a cooperative mechanism for dense random-packing dynamics, based on diffusing ''spots'' of interstitial free volume (Bazant, 2006). Simulations with the Spot Model could efficiently generate realistic flowing packings. Starting from a non-local stochastic differential equation, continuum equations were derived for tracer diffusion, given the dynamics of free volumes (spots). The model was applied to granular drainage in a silo and successfully reproduced realistic flowing random packings (Rycroft et al., 2006). In fact, Kamrin and Bazant (2007) provided a general mechanical theory (Mohr-Coulomb plasticity) of spot

dynamics. This model can predict shear localization that can occur in annular shear flows. Moreover, it should be noted that this simple model correctly predicts and places shear bands in geometries like the annular Couette cell. The main parameters that control the flow in the Couette geometry are the particle size, the radius of the rotating inner cylinder, and its rotation rate. The flow profiles have been found to be rate independent over a wide range of driving rates, in experiments in two dimensions (Howell et al. 1999), in three dimensions (Losert et al. 2000, Mueth et al. 2000), and in simulations (Latzel et al. 2003). In all cases, the flow decays rapidly away from the inner cylinder and particle shape and properties play an important role in setting the precise overall extent of the narrow shear bands (Bocquet et al. 2002), and the flow profiles near the wall can be influenced by the ordering of grains near the shearing wall (Mueth et al. 2000). Several recent experiments investigated individual particle motion in the Couette geometry (Schollmann, 1999; Mueth et al., 2000). These studies indicate that the mean particle velocity parallel to the shear direction $V(y)$ decreases faster than linearly away from the inner cylinder. The velocity profile in three dimensions was determined by Mueth *et al. (2000)*. Measurements were carried out in the interior of the material using x-ray and NMR techniques. Losert et. al. (2000) determined the particle dynamics and shear forces of granular matter in a Couette geometry. They found that the mean particle velocities during brief slips of the shearing cylinder decrease roughly exponentially with distance away from the moving cylinder. The average velocity of particles at the surface of the shear cell is shown in Figure 7 as a function of distance y from the rotating inner cylinder, for inner wall velocities U ranging from 0.24 to 24 RPM.

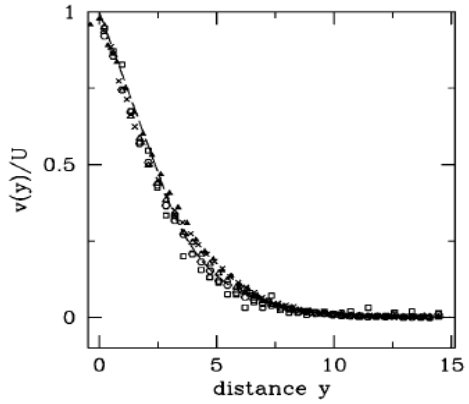

Figure 7: Mean Particle velocity as a function of distance (in particle diameter) from the inner cylinder (Losert et al., 2000)

In the case of flows generated in a split-bottom shear cell, where the grain flow is driven by the rotation of a bottom disc with respect to a cylindrical container, Sakaie et. al. (2008) addressed the dilatancy and shear band by imaging the 3D packing density of smooth and slow granular flows by means of Magnetic Resonance Imaging (MRI). In the split-bottom geometry the flow is driven from the bottom, not from the side walls and typically, a disc of known radius, mounted flush with the bottom (but smaller than the size of the container) is rotated at a certain rate. The differential motion of the disc and container creates a wide shear zone away from the side walls (Fenistein et. al., 2004). By imaging the local packing densities in this type of shear cell as a function of time for a range of filling heights, Sakaie et. al. (2008) explored the relationship between flow field and dilatancy. These authors showed that the relative change in density in the flowing zone is significant, around 10-15 % and that the dilated zone slowly spreads (up to 40 particle sizes) throughout the system as time progresses. This spread is consistent with the idea that the total, local strain experienced from the start of the experiment governs the amount of dilatancy (Da Cruz et al., 2005). For granular media, the shear bands

observed in chute, Couette, and split-bottom flows coincide with dilated zones (Mueth et al. 2000, Sakaie et al. 2008).

2.5 Conclusions

Large amounts of work have been performed on granular solids, especially in the physics community in the last ten or so years, and a multitude of new models and experiments have been conceived. The work is mostly concerned with rigid, round, in-elastic particles of mostly large size where all these new ideas are tested. The reality is that progress is being made and "theoretical granular physics" is a rapidly developing field. There is no doubt that in the not so distant future, this field will start to tackle industrially relevant problems, i.e., smaller particles that are not spherical, have a size distribution and exhibit plastic and/or sticking (cohesion) properties.

The present dissertation has its main goal to advance the field of "Powders and Granular Matter" into areas where industrially important materials are tested and pertinent information is extracted from measurements in simple flows to be further used in modeling industrially relevant geometries and devices. It is clear from the above review that industrial flows in hoppers, mixers and other machines which take place mostly in the intermediate regime of flow, are characterized by additional important parameters over and above those introduced by Jenike in 1954 (angles of friction and yield loci) and Savage and Jenkins in 1983 (coefficients of restitution and energy dissipation functions). Examples of such parameters are the stiffness coefficient, k introduced by Campbell, the order parameter coefficient introduced by Tejchman in 1993, the "friction and solid fraction laws" (and the coefficients within) introduced by Da

Cruz in 2005, just to mention a few. Taking a lead from these authors, the present work also introduces two new parameters which, however, can be directly measured for a given practical system as we propose an instrument to obtain them and a methodology to interpret them. We then use the new parameters obtained for a variety of industrially relevant powders in commercially available software taken over from computational fluid dynamics (CFD) and customize it for powder flows. In effect, we trade some mathematical rigor (present in the physics models) with a practical measurement and show that the approach is precise enough for practical purposes enabling thus to open the field to further industrially realistic measurements and modeling.

3 Stress Transmission through Granular Layers

3.1 Introduction

The transmission of stresses through stationary and sheared dense granular layers is a subject of fundamental interest in Powder Mechanics. Specifically, one seeks to find forces exerted on stationary walls and moving objects inside flowing powders as these are the result of transmitted stresses from boundaries and from the weight of the material. These stresses are transmitted differently when the powder is stationary from when it is shearing or even moving in plug flow.

Pressure (normal stress) measurements are relatively simple in fluids and entail mounting a pressure transducer at the point of interest. Granular layers present complications since Pascal's law does not apply and the formation of force chains in stationary or slowly sheared particle assemblies (in the quasi-static regime) results in stress inhomogeneities. These inhomogeneities and fluctuations can sometimes be as large as or even larger than the mean stress values (Liu et. al., 1995 and Howell et. al., 1999). Continuum models (Savage, 1998; Schaeffer, 1987; Srivastava and Sudaresan, 2003; Tardos, 1997; Tardos et. al., 1998; Tardos et. al., 2003; Tardos and Mort, 2005; Turek et. al., 2002; and Yu et. al., 1994) do not expose these kinds of behavior and only predict average stresses. While there have been several studies on stress inhomogeneities on the bottom surface of static granular piles (Liu et. al., 1995; Mueth et. al., 1998; and Corwin et. al., 2008), similar measurements in slowly sheared assemblies, where both inhomogeneities and fluctuations exist, are limited (Howell et. al., 1999 and Miller et. al., 1996). Yu and Tichy (1996) used a rotational shear cell to measure stresses in a shearing

layer, focusing on the rapid granular flow regime where particle interactions are dominated by collisions. The goal of the study by Yu and Tichy (1996) was to demonstrate the effect of "granular lubrication" and to calculate the total carrying force of the system and not to study the transmission of stresses in a granular layer.

The objective of the present study is to probe through a combination of experiments and discrete element method (DEM) simulations (for validating the experiments) the non-uniformities in stresses transmitted across a sheared granular layer. We employed the classical Jenike cell (commonly used to measure internal and wall friction coefficients) as well as a newly developed "fast" Jenike cell (described in section 3.3), where we added normal force (stress) transducers on the shearing bottom wall and applied known normal stresses to the upper surface of the granular layer. Using this experimental technique we compared the normal stress applied to the top surface of the particle assembly with stresses recorded by the normal stress sensors on the bottom. Particles of different sizes were tested in layers of different thicknesses and at different shearing rates and the transmitted stresses were recorded at several locations on the bottom surface and analyzed. Complementary DEM simulations (carried out by Dr. Jin Sun and Professor Sankaran Sundaresan at Princeton University through collaboration under DOE-UCR grant DE-FG26-07NT43070) were performed to further elucidate the connection between the spatial inhomogeneities and temporal fluctuations recorded by the sensors and the role of friction on side walls. Our measurements and analysis, described below, reveal that the normal stresses are transmitted through thin layers without significant attenuation *provided* the material is in *continuous shear*, but large fluctuations are introduced especially for rigid materials such as glass particles. The height (thickness) of the sheared

layer plays an important role in transmitting stress, much like that in Janssen's analysis of stresses in wall-bounded static assemblies (Nedderman, 1992).

3.2 Experimental

3.2.1 Selection and calibration of a sensor system to measure normal stresses

While the selection of a sensor system appears to be a rather mundane and simple undertaking, this is not the case for stress sensors used in granular systems. In fact, such instrumentation is not available commercially and there are two ways of solving the problem: either construct the system "in house" or re-engineer an existing system developed for a different application. We employed the second route after failing to develop our own sensors and being unable to use several other systems developed for different purposes by other vendors. Two systems, manufactured by Tekscan, Inc., one with and the other without remote sensing, were selected; a picture of the sensor is shown in Figure 8. Since these sensors were developed for a different application (namely, sensing forces in athlete's shoes and on car seats) and are made of very fine, interwoven plastic and conductive layers, it was necessary to apply a protective film and to re-calibrate the unit for each experiment. To perform the calibration, the sensor was mounted on a removable Lucite substrate to enable the transport of the calibrated device from calibration to the experimental unit.

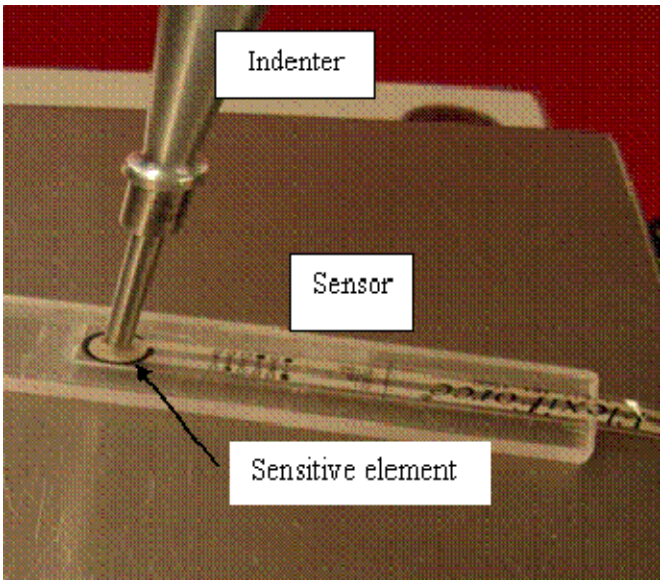

Figure 8: Picture representing the Tekscan stress sensor and the calibration unit

Calibration was performed in the instrument depicted in Figure 8 where pressure was applied on top of the sensor by an Instron-type indenter (Texture Analyzer) and the sensor was situated on the Lucite strip, as shown. The force applied by the indenter was measured by the Texture Analyzer and divided by the active area of the sensor (area delimited by the black circle, approximately 1.1 cm^2) to yield the appropriate applied normal stress. The indenter was chosen to match the size of the sensitive element and the calibration procedure was repeated several times before and during experiments. In this way, the normal stress applied on the sensor was transformed into a DC voltage that could be simply monitored by a data acquisition system controlled by a computer. Following calibration, the stress sensor and the Lucite strip are introduced into the powder flow by cutting an appropriate groove into the boundary (wall) so as to keep the sensor flush with the surface. Since the thickness of the sensor is less the 0.1 mm (see Figure 8) and is covered by a thin protective film, as mentioned above, there is practically no interference from the sensor to the moving powder layer. In addition, specific

experiments with sensors in different positions were carried out and no measurable interference was observed. The attenuating effect of the protective film is taken into account as the sensor is calibrated as shown in Figure 8.

3.2.2 Stress transmission through slowly shearing granular layers

Experiments were carried out in a conventional Jenike shear cell. A schematic representation of the granular layer with a normal stress applied to the top and a sensor mounted at the bottom is shown in Figure 9.

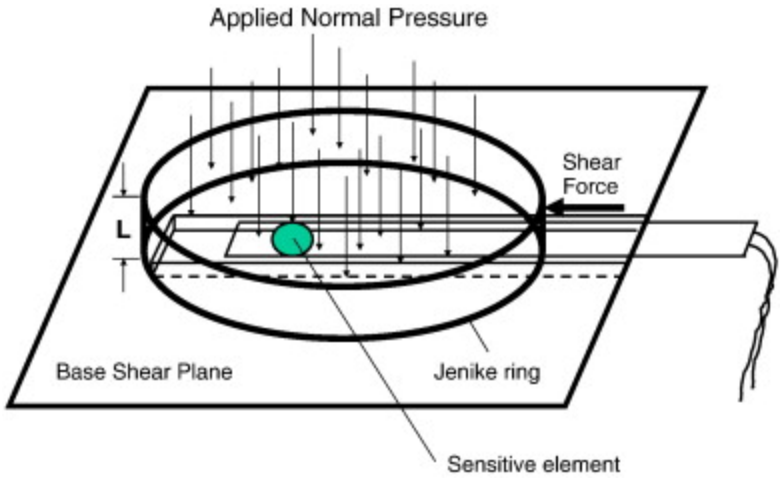

Figure 9: Schematic representation of Jenike cell arrangement

The load on the top was applied using the classical Jenike "frame" and the circular cover with a raised point in the center (Jenike, 1964) to assure that the stress is evenly distributed as shown in Figure 10a. Figure 10b shows the empty cell with the rough strip and the pressure sensor mounted on it. Two smooth (aluminum and Lucite) walls and several "rough" walls were used by gluing different grain-size sand paper on the wall of the device as seen in Figure 10b. One or more rings of the device were used in order to

increase the thickness of the granular layer. The sensor was located 7 mm off the central cord of the cell perpendicular to the direction of shearing at zero displacement as shown in Figure 10b. During a typical experiment, the cell moved at 2.3 mm/min over a distance of about 2 cm (Jenike, 1964).

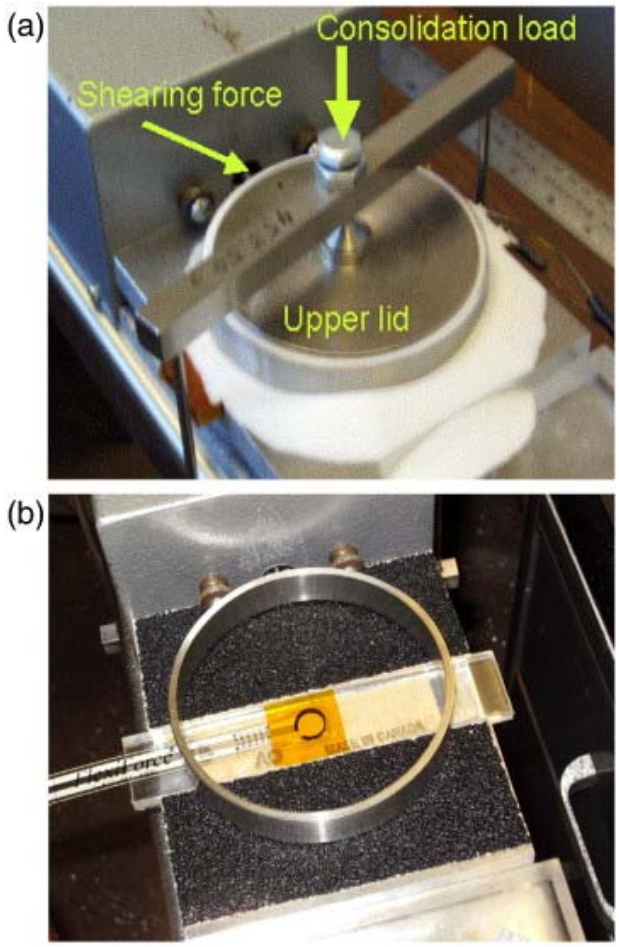

Figure 10: (a) Jenike shear cell; with sensor on (b) rough wall. Sensor is situated approximately 7 mm off-center at zero displacement

A variety of particles from large to fine, spherical and odd-shaped and cohesive and free flowing were tested; a sample is given in Table 1.

Table 1: Granular materials studied for investigating stress transmission

Particle Size [mm]	Material	Applied normal stress [kPa]	Layer Thickness [L, cm]	Remarks
5.0	glass	6.9 and 13.8	1.6, 2.6, 3.0, 6.0	spherical
3.0	glass	6.9, 13.8 and 20.7	1.6 and 2.6	spherical
4.0	polyethylene	6.9	6.0	not spherical
	polyethylene	6.9	6.0	and rough
2.0	glass	6.9 and 13.8	1.6, 2.6, 3.0, 4.7	spherical
	cast steel	6.9 and 13.8	1.6 and 3.0	
1.5	glass	13.8	1.5	
	glass	6.9	1.6 and 2.6	
1.0	glass	6.9	1.6, 3.0, 4.7, 6.4	
	crushed glass	6.9	1.6, 3.0, 4.7, 6.4	odd shaped
	polyethylene	6.9 and 13.8	3.0	not spherical
	cast steel	6.9 and 13.8	1.6 and 3.0	
	EPDM elastomer	6.9	3.0	shredded tire
0.5	glass	6.9	3.0	spherical
	glass	6.9, 13.8 and 20.7	1.6 and 2.6	not spherical
	sand	6.9 and 13.8	1.6, 2.6 and 3.2	angular
	detergent	6.9 and 13.8	1.6 and 2.6	cohesive
0.1	glass	6.9 and 13.8	1.6, 2.6 and 3.0	
	acrylic	6.9	1.6 and 2.6	not spherical

Particles chosen for study and given as examples below were imposed by the limitations of the DEM simulation (presented in the next section) that require very long times, of the order of weeks, for small particles. The overall behavior of the transmitted stress for other powders in Table 1 is qualitatively similar to the examples presented below.

Figure 11 gives a typical response curve, transmitted normal stress (in kPa) vs. time (in seconds), for a bed of 2 mm glass beads in a 2.6 cm thick layer. There are several stages in applying the load: in the empty cell, the measured stress was zero as it should be ("no load" in Figure 11). A normal stress of 6.9 kPa (1 psi) was then applied to the *static bed* and, as seen in the figure, the sensor only "recorded" approximately 1.4 kPa (0.2 psi). As the bed was sheared in the subsequent phase, the stress increased and started to fluctuate around the 6.9 kPa (1 psi) average value. As the normal stress on the top cover was increased to 13.8 kPa (2 psi), the average value measured by the sensor also increased and fluctuated around the same value as long as shearing was applied. The fluctuations are clearly large (≃ 50% of the average stress). At the point where the shearing stopped, the bed "froze" at about 13.8 kPa (2 psi) and the stress went to zero as the layer was unloaded.

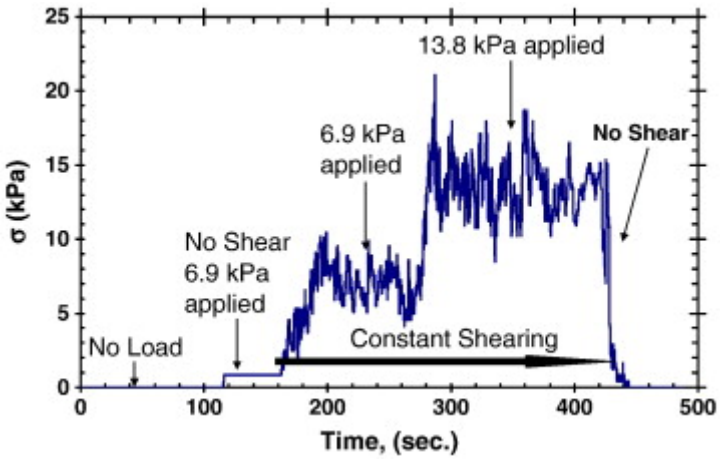

Figure 11: Normal stress variation in a Jenike shear cell: 6.9 kPa (1.0 psi) and 13.8 kPa (2.0 psi) applied to 2 mm glass beads. Layer height = 2.6 cm

Figure 12 presents additional results using larger particles: 5 mm glass beads and an applied normal stress of 6.9 kPa (1 psi). While the average stress during shearing was

only 5% higher than the applied normal stress, stress fluctuations were larger compared to the smaller particles (see Figure 11), about 70% of the average value. Results in Figure 11 and 12 are somewhat similar in that the measured stress is always smaller then the applied stress under static conditions and we observe "freezing" of the material once the shearing stops. While shearing is in process however, the applied and measured stresses become more or less equal. We note that the measured stress fluctuates, sometimes significantly, depending on particle size. This is mainly due to the fact that, since the cell has a constant volume, the number of larger particles is significantly smaller then the number of smaller particles (5 mm in diameter as compared to 2 mm in diameter). Consequently when the same load is applied, each larger particle carries a larger portion of the load. This larger portion is then transmitted to the transducer that either senses the presence of the particle (when the particles roles over it) or not (when the particle rolls off the sensor), giving rise to fluctuations that are smaller with smaller particles and larger with large particles.

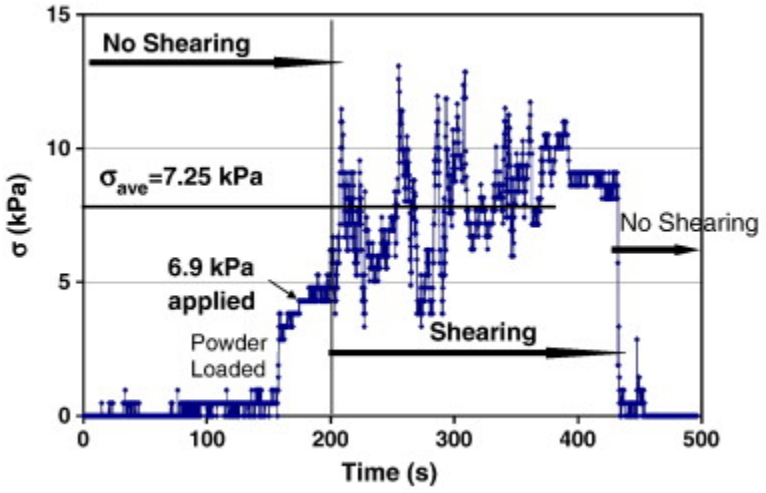

Figure 12: Normal stress variation in a Jenike shear cell: 6.9 kPa (1.0 psi) applied to 5 mm spherical glass beads. Layer height = 2.6 cm

Care was taken to use "small enough" particles so that the sensor can see a sufficiently large number of them at any given time: about 25 in the case of 2 mm in diameter spheres. Results with 5 mm particles are less reliable since the sensor can "see" only about 5–7 particles at any one time. This may have also resulted in larger fluctuations of the measured stress as mentioned above. To show the broadness of this observation we conducted experiments on materials with different physical properties as listed in Table 1. Figure 13 shows the results for the case of laundry detergent particles which are odd-shape and can be dry or coated.

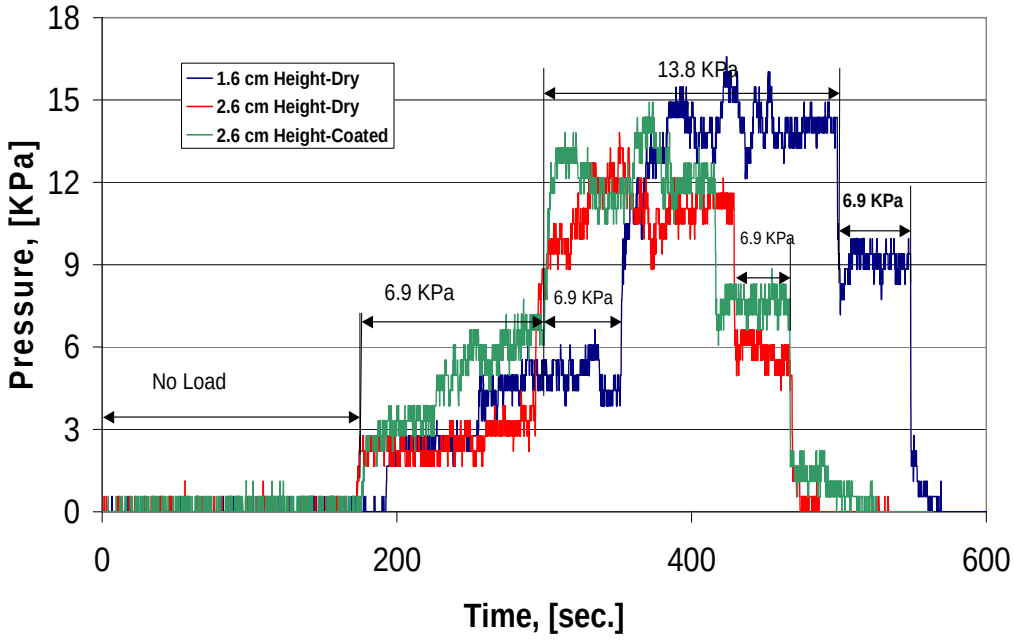

Figure 13: Stress transmission through detergents layers

In summary, we found that the normal stress was transmitted to the sensor mounted on the base mostly unaltered through thin layers of non-cohesive powders when the layers were in shear. The normal stress was not transmitted to the base uniformly in static layers

as the material "froze" depending on its history: an initially unstressed layer transmitted to the base only a portion of the normal stress while a previously stressed material maintained its internal stress levels until it was unloaded. While there are a number of theoretical studies to model granular beds (Campbell, 2006; Jackson, 1986; Luding, 2005; Mort et. al., 2003; and Moreno-Atanasio et. al., 2005) the subject of stress transmission was not addressed directly. Discrete element method (DEM) simulations of particles subjected to similar stress and deformation histories are helpful to understand these results more thoroughly. Unfortunately, such simulations proved to be extremely slow (of the order of weeks) owing to the very long shearing times at the slow shear rates employed in the experiments. It became apparent that experiments would have to be run at much faster rates to keep the running times as short as possible so that steady state could be reached much earlier. This prompted us to devise an experimental system to study stress transmission in more rapidly sheared dense assemblies and examine if the results obtained at faster shear rates differed from those described above. Such faster shear conditions are also more relevant to industrial applications.

3.2.3 Stress transmission through rapidly shearing granular layers

An instrument (henceforth referred to as the "fast" Jenike cell since the only difference compared to a conventional shear cell is its capability of faster shearing) was specially built to enable shearing of particles in the Jenike geometry at higher rates. The instrument was constructed as an addition to the moving arm of a tableting machine (donated to CCNY by Merck and Co. Inc.). A picture of the cell with the lower part of the driving mechanism and the detail of the cell itself with the stress sensor mounted on the bottom are shown in Figure 14. The dimensions of the cell and the stress sensor are identical to

those used in the traditional Jenike test. The loading of the cell with the normal force is also similar except that the weight is added at the top of the device instead of using the Jenike "frame" (Jenike, 1964).

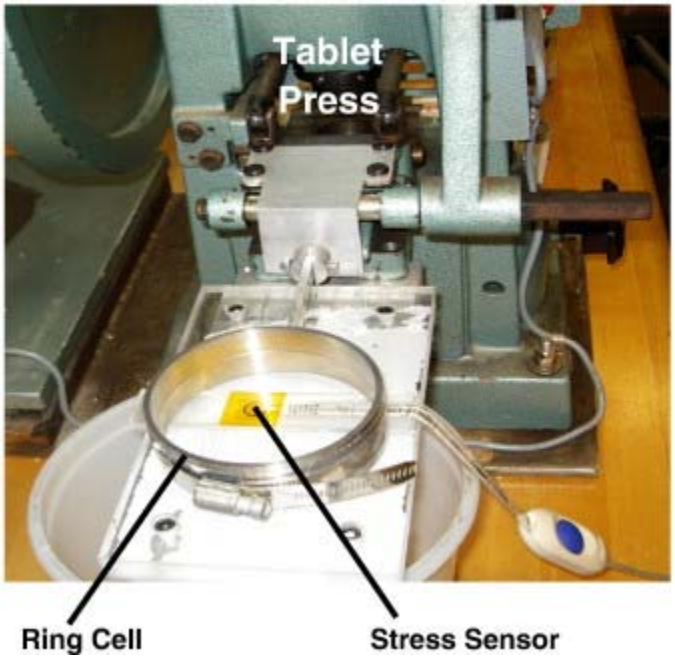

Figure 14: Picture of "fast Jenike cell" with driving mechanism

The cell executes a back-and-forth movement from the initial position shown in Figure 14. After a short pause, the back-and-forth movement is repeated. Usually, up to 4–5 cycles were performed during one experiment. The unit has adjustable speed from approximately 1.5 mm/s ($\sim$ 90 mm/min as compared to the traditional Jenike cell at 2.3 mm/min) to approximately 150 mm/s. Several experiments were performed at different speeds and with different particles, employing a single sensor in some and multiple sensors in the rest of the experiments. As seen in Figure 14, the lower plate used for these experiments was a Lucite sheet (angle of wall friction $\phi \sim 17°$ with glass

particles). The stress sensor was kept flush with the bottom at all times. Due to the relatively fast movement of the cell and the fact that there was a finite layer of material in the cell, the granules tended to move in a circulation type movement: up the approaching vertical wall and away from the departing wall. This created an uneven upper surface as the cell moved back-and-forth and resulted in the tilting of the applied weight. To diminish this movement and keep the weight horizontal, it was necessary to employ deeper cells made of up to four Jenike "rings" creating a cell that was approximately 60 mm deep in all experiments in this series.

A typical experimental result is shown in Figure 15. The cell was not sheared for the first 115 s of the experiment and therefore the stress in the figure is displayed only from t = 100 s. A normal stress of 6.9 kPa (1 psi) was applied, resulting in a jump in the sensed stress to about 3.8 kPa (0.4 psi). This behavior is similar to the one seen in the (conventional) slow Jenike cell (see Figures 11 and 12). Upon shearing at 15 mm/s, the sensed stress fluctuated significantly with an average of about 41% above the applied load.

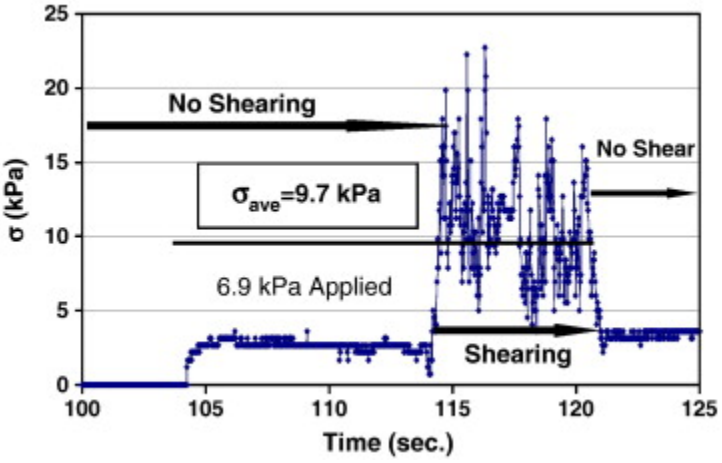

Figure 15: Normal stress variation in a fast Jenike shear cell. A normal stress of 6.9 kPa (1.0 psi) was applied to 2 mm spherical glass beads and the shearing was done at 15 mm/s.

The spatial non-uniformity of stress transmitted to the base was studied through experiments where two-sensor locations were used: (a) identical to the position in the conventional slow Jenike cell, i.e., 7 mm off-center (as shown in Figure 14) and (b) two sensors mounted as depicted in Figure 16; the positions of the sensors are 2.35 cm and 1.9 cm from the walls of the cell while the stroke of the movement is 5.25 cm.

Figure 17 and Figure 18 depict sample results obtained with the two-sensor assembly shown in Figure 16. The stress fluctuations were significant and were larger than what was observed earlier for the case of slow shear (see Figure 12). It appears reasonable to conclude that the fluctuations in dense assemblies increased with increasing shear rate (compare Figure 12, Figure 17 and Figure 18). Note that during the time when the cell is not under shear between cycles, the stresses recorded by the two sensors were essentially constant ("frozen"); this stress level at a given location on the base may be above or below the average value. It is also apparent from Figure 17 and Figure 18 that the stress transmitted to the base was spatially inhomogeneous as the stresses measured at different locations were quite different and also showed different fluctuations in time.

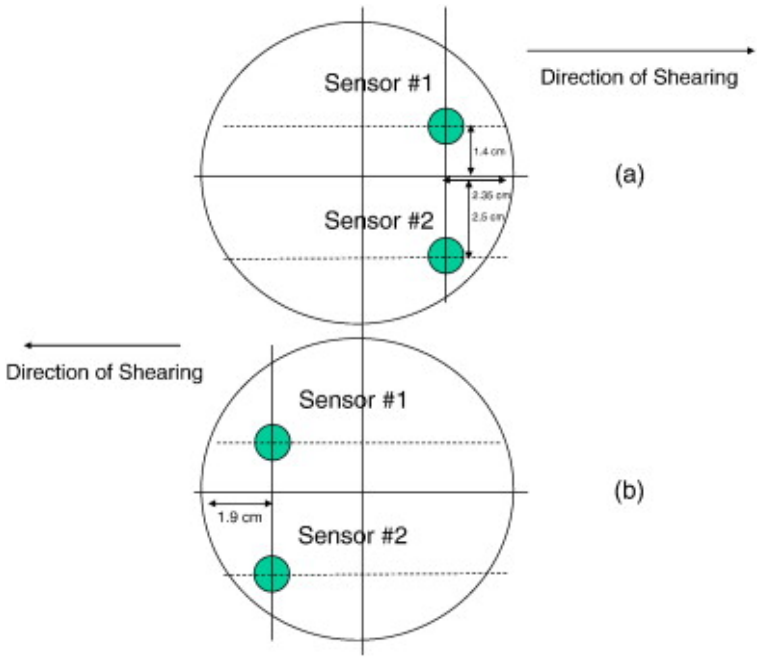

Figure 16: Measurements in the "fast Jenike cell". Position of the two stress sensors on the bottom plate of the cell: (a) ring movement to the right; (b) ring movement to the left

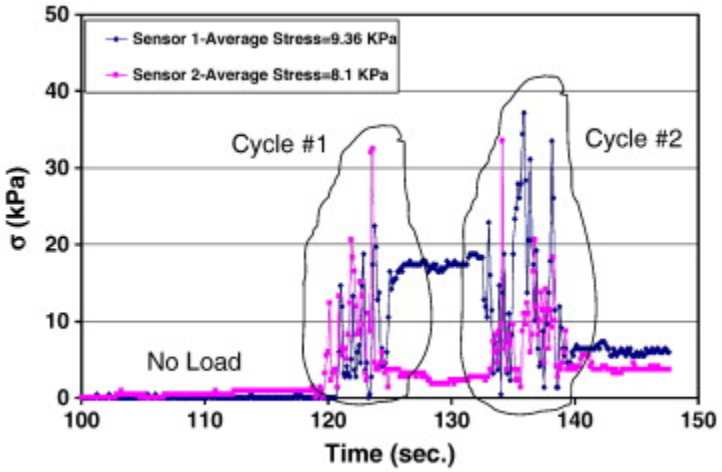

Figure 17: Measurements in the "fast Jenike cell" using two sensors. The sensor positions are shown in Figure 15. A load of 6.9 kPa (1 psi) was applied to a bed of 5 mm glass beads at $t = 118$ s. Layer depth = 2.6 cm, sheared at 16 mm/s. Between cycles the cell remained motionless with the applied load

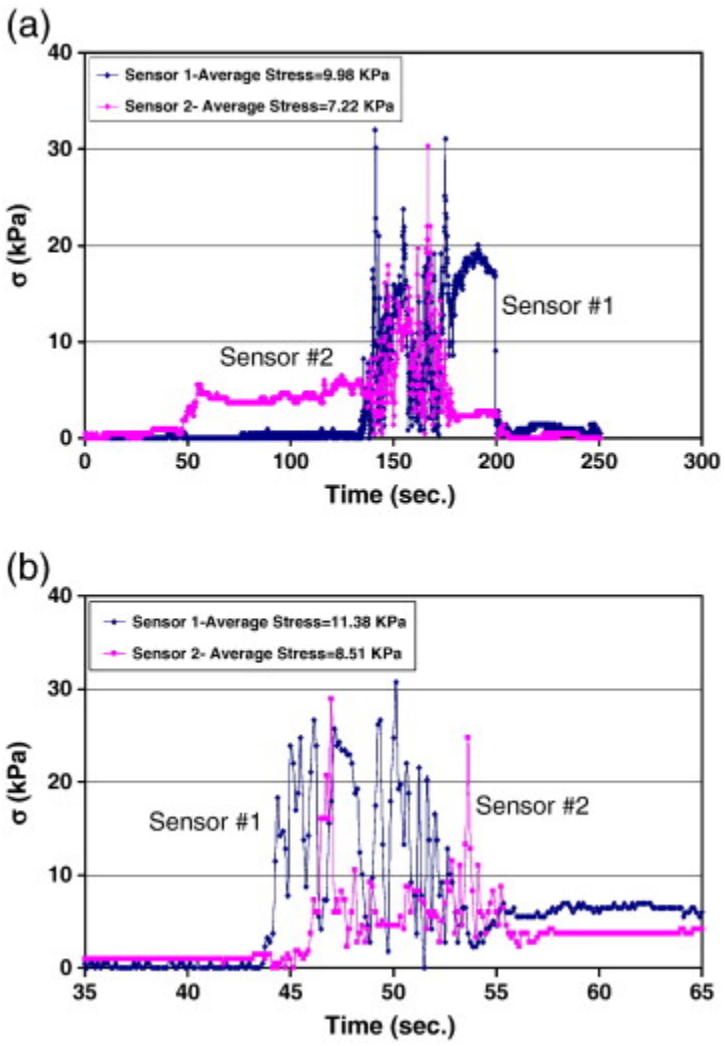

Figure 18: Measurements in the "fast Jenike cell" using two sensors. The conditions are as in Figure 17, except that only a single cycle is shown and the shear rates are (a) 1.8 mm/s and (b) 7.7 mm/s

3.3 Computational

The goal of the present computations is to elucidate the relationships between granular stress transmission, layer thickness and sensor size. DEM simulations were performed (by Dr. Jin Sun) using the LAMMPS code, a parallel particle simulator developed at Sandia National Laboratory (Plimpton, 1995). These simulations are based on a linear spring-dashpot model to calculate forces between particles, which interact only on

contact (Cundall and Strack, 1979). The value of the spring constant is chosen to be large enough to minimize particle interpenetration, yet not so large as to require an unreasonably small simulation time step. The tangential force at each contact is computed by keeping track of the elastic shear displacement throughout the lifetime of a contact. As the shear displacement increases, the tangential force reaches the limit imposed by a static yield criterion, characterized by a local particle friction coefficient μ. The tangential force is then truncated to satisfy Coulomb's law. The model allows for contact forces and friction between the particles and the walls in the same way as described for two particles, but with infinite mass and diameter for the walls. The simulation domain and the number of particles were chosen to correspond to those employed in the Jenike shear cell experiments; the shear was imposed in the simulations by moving the bottom wall at a prescribed velocity as in the experiments. The simulations were performed on two 3.0 GHz Intel Xeon dual core processors. The computational times range from about one day to a week, depending on the simulation time and number of particles.

3.3.1 Simulation of the Jenike shear cell experiment

Figure 19a shows a short-duration simulation corresponding to the Jenike experiment described in Figure 11, where a bed of 2 mm glass beads was sheared on a Lucite wall at a translational velocity of 2.3 mm/min (standard Jenike cell speed) with an applied normal stress of 13.79 kPa. The normal stress was calculated by summing all the contact forces between particles and the shearing wall over an identical circular area as the sensitive element of the experimental sensor (1.1 cm). The sensing element was situated as in the experiment (7 mm off-center). This simulation required very long computational time and so it could not be continued for the full duration of the experiment; as a result,

the fluctuations seen in the experiment could not be verified. Nevertheless, the normal stress measured on the sensor approximately agrees with the average value measured in the experiments.

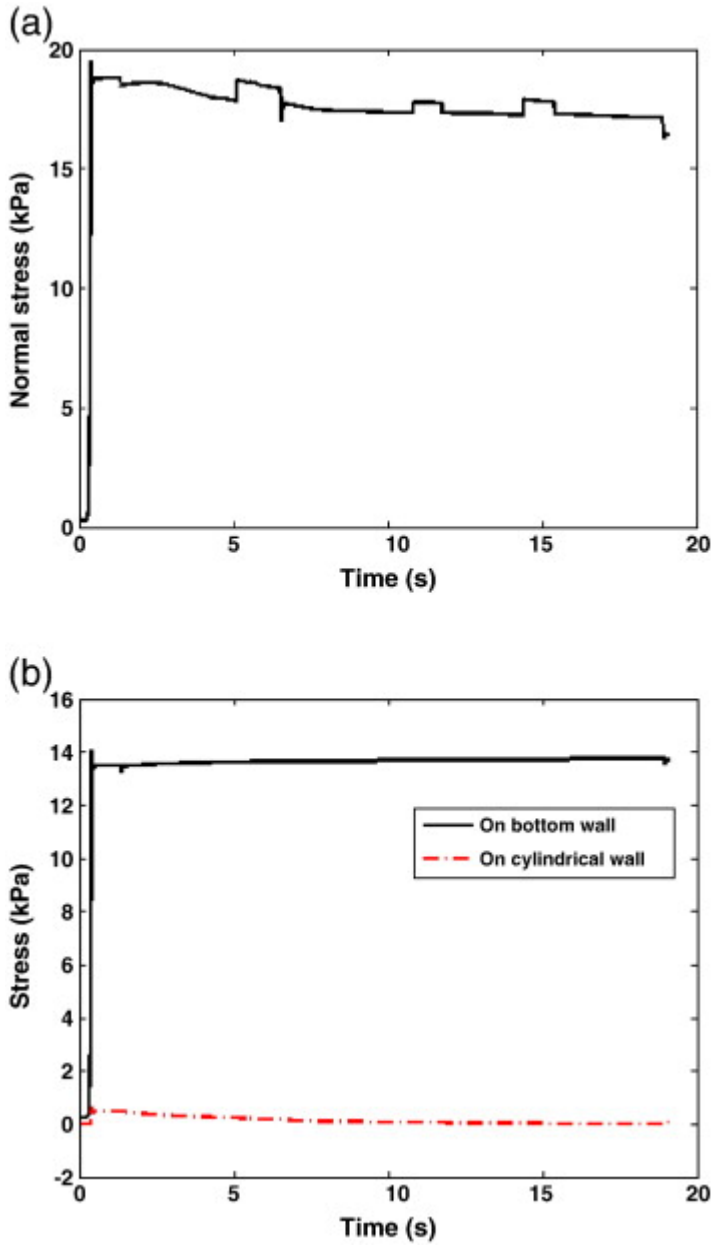

Figure 19: Simulation of Jenike experiment with 2 mm glass beads described in Figure 11. (a) Normal stress at the sensor location; (b) normal stress averaged over the entire bottom wall and the average shear stress supported by the cylindrical wall

Figure 19b shows the summation of all particle contacts on the bottom of the cell and one can see that the average normal stress at the base was indeed very close to that applied (with the side walls contributing a negligible amount). Results of the slow Jenike cell simulation did confirm that DEM could indeed be employed to explore stress distribution in this type of shearing experiment. However, in order to capture the dynamic fluctuations during the shearing process, one must either increase the simulation time (which was impractical) or perform simulations at faster shearing rates. As mentioned earlier, this consideration motivated the fast Jenike cell experiments and the corresponding simulations are discussed below.

3.3.2 Simulations of the "fast" Jenike cell

Normal stresses obtained using DEM simulations are shown in Figure 20, and these can be compared to the experimental results presented earlier in Figure 17. (D_s/d = 1.9, where d is the particle diameter and D_s is the diameter of the sensor area). The total number of particles in the experiment and in the simulation was the same ($\sim$ 5000); other geometrical and physical characteristics were also matched between the experiment and simulation. Figure 20 shows the normal stress response over two cycles of the (fast) Jenike cell (at 16 mm/s.). The circles on the time axis refer to the following events in order — load, begin cycle 1, hold following the end of cycle 1, start cycle 2, hold following the end of cycle 2; these are analogous to the stages in the experiments where the duration between the cycles (where the stresses stayed essentially frozen) was longer. One can readily see from Figure 17 and Figure 20 that in both simulations and experiments the normal stresses recorded by the two sensors oscillated significantly and that the range of the oscillations seen in the experiments was reproduced reasonably

accurately by the simulations. The different stresses measured by the two sensors are clearly visible in Figure 20 showing the spatially inhomogeneous nature of the stress distribution. The frequency of the oscillations differed somewhat between the experiments and simulations, which may be a consequence of factors such as sampling frequency and departure from spherical particle shape in the experiments.

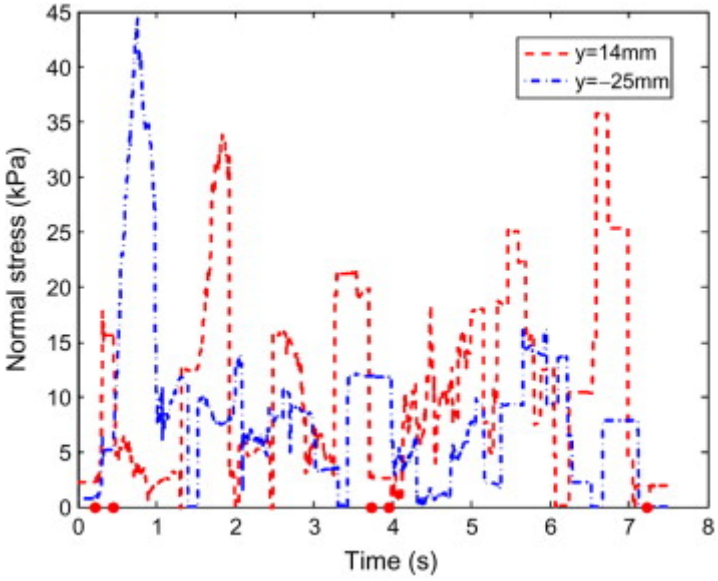

Figure 20: Simulation of Jenike experiment with 5 mm glass beads in "fast" Jenike cell (described in Figure 16). In the legend, the $y = 14$ mm and $y = -25$ mm indicate the two sensors with different distances to the central line as shown in Figure 15, $D_s/d = 1.9$.

3.4 Conclusions

The spatial non-uniformities and temporal fluctuations in the normal stress transmitted across a sheared granular layer have been studied through a combination of experiments in a Jenike shear cell equipped with normal force (stress) transducers embedded on the bottom shearing surface and discrete element method (DEM) simulations. Experiments

were carried out with particles of different sizes and layers of different thicknesses; the normal stress was measured at several different shearing rates and at several positions on the bottom surface. We found that the stress is transmitted mostly unaltered through layers of granular materials if they are subject to a continuous shearing. It is abundantly clear from our normal stress measurements using two sensors mounted on the shearing bottom surface of the commonly used Jenike shear cell that appreciable spatial inhomogeneity exists in the stress transmitted from the top to the bottom surface of the granular layer. Furthermore, each stress sensor records large temporal fluctuations in normal stress as the material is sheared. The spatial inhomogeneity (at any given time instant) and the temporal fluctuations (recorded by any one sensor) are of comparable magnitude. The stress fluctuations recorded by a sensor became larger as the sensor diameter to particle diameter ratio was decreased, layer depth was increased and the assembly was sheared faster.

DEM simulations employing a spring-dashpot model with appropriate constants to describe the stiffness and plasticity of the material are able to qualitatively reproduce the spatial inhomogeneity and temporal fluctuations seen in the experiments, thus validating the simulations. Further DEM simulations performed using a combination of static and dynamic sensors reveal the link between the spatial inhomogeneity and temporal fluctuations in normal stress in the sheared granular layer inside the Jenike cell. Although we did not measure shear stresses, it is expected that the same spatial inhomogeneity and temporal fluctuations must exist for shear stresses as well.

4 Development of a Rheological Model using a Couette Cell

4.1 Introduction

Powder flows have been studied extensively in the past starting with the pioneering work of Jenike (1964) and Jackson (1986). The accent on this earlier work was to establish the condition under which a stressed layer of powder will break and the material will start to flow. More recent studies were dedicated to modeling powder flows using mostly numerical methods: Muguruma et al. (2000), Srivastava and Sundaresan (2003), Luding (2005), Moreno-Atanasio et al. (2005), just to mention a few. Extensive work by Savage (1998) and Tardos and co-workers (1998), (2003) and (2005) looked into the slow and intermediate regimes of flow at slow and moderately high shear rates and the transition from one to another. The study of continuum models to describe powder flows was also undertaken by several authors (for example Schaeffer (1987) and Tardos (1997)).

The division of granular flows into slow or quasi-static and fast or rapid regimes is well documented (Campbell, 1990). The existence of a "transitional regime" where particle mobilization and/or shear are strong enough to dissipate significant energy through particle collisions, but do not completely eliminate the continuous particle enduring contacts is more recent (GDR MiDi, 2004) and (Tardos et. al, 2003). It was also shown theoretically that in order to change the regime of flow from quasi-static (dense, slow flow) to rapid granular (dilute and collisional), the solid fraction of the bed has to decrease (Lois et. al., 2007) but no direct experimental evidence is available.

The basic motivation for our work is to supply relevant experiments that allow the bed to dilate freely as shearing is increased and for inter-particle collisions to occur in a dense bed where particle–particle friction is also prevalent. We achieve these conditions in a Couette geometry where the inner cylinder is rotating and the outer cylinder is stationary. We over-impose a very slow axial flow of powders over the radial shearing of the powder thereby assuring a slight increase in the solid fraction of the bed. This procedure also ensures that the particle bed reaches a steady state in which the solid fraction is somewhat lower than that corresponding to maximum packing and hence collisions and relative movement between particles can take place.

There is theoretical evidence (DaCruz et. al., 2005 and Jop et. al., 2006) that in the intermediate regime, where the flow is fast enough but still dense, the friction coefficient (the ratio of shear to normal stress) increases from its constant value. While friction during very slow motion is only a function of the character of the surface and the normal load, at higher shearing rates, it becomes a function of the rate itself and increases as the rate of shearing increases. We provide experimental evidence that such an increase is real and significant and that the dependence on shear rate takes, in its simplest expression, the form of a power-law.

Furthermore, we use the experimentally measured friction coefficient as a function of shear rate to establish a yield condition and a constitutive equation that is valid in the slow, quasi-static and the intermediate regime. To extend the results from simple shear in the Couette device to more complicated geometries, we use a newly developed numerical scheme (FeatFlow-Ouazzi et. al., 2005) to solve the general equations of motion of an incompressible medium with the new constitutive equation. We show that the constitutive

equation and the numerical solver are general enough to generate useful information for more complicated geometries such as an eccentric Couette and a concentric Couette with a cylindrical obstacle in the shearing gap (Kheiripour Langroudi et. al., 2010a).

4.2 Experimental Approach

In this section, we present and discuss Couette experiments used to study the transition of powder flow from slow to moderately fast.

4.2.1 Batch and Continuous-flow Couette device

A schematic representation of the Couette device used during the present investigation is shown in Figure 21a with details of the sensors and the rotating cylinder given in Figure 21b. The vertical shear gap forms between the rotating and the stationary cylinders and both its width and height can be adjusted by appropriate choice of the radius and height of the rotating cylinder. The material is fed from above using a vibratory feeder (not shown in the figure) and is discharged by a screw-in-cylinder metering device (also not shown) that transfers the material to a precision balance for flow rate measurement. The walls of the Couette are made rough by gluing sand paper on the shearing surfaces as shown in the figure. The roughness of the walls is chosen to match or exceed the coefficient of internal friction of the material thereby trying to assure a non-slip boundary condition. By closing the discharge section, the Couette device can be operated in batch mode or, by feeding and removing material to achieve a steady state vertical flow, one can operate the device continuously. The material above the rotating cylinder (denoted overburden in the figure) is stationary and only provides dead weight to the shearing layer.

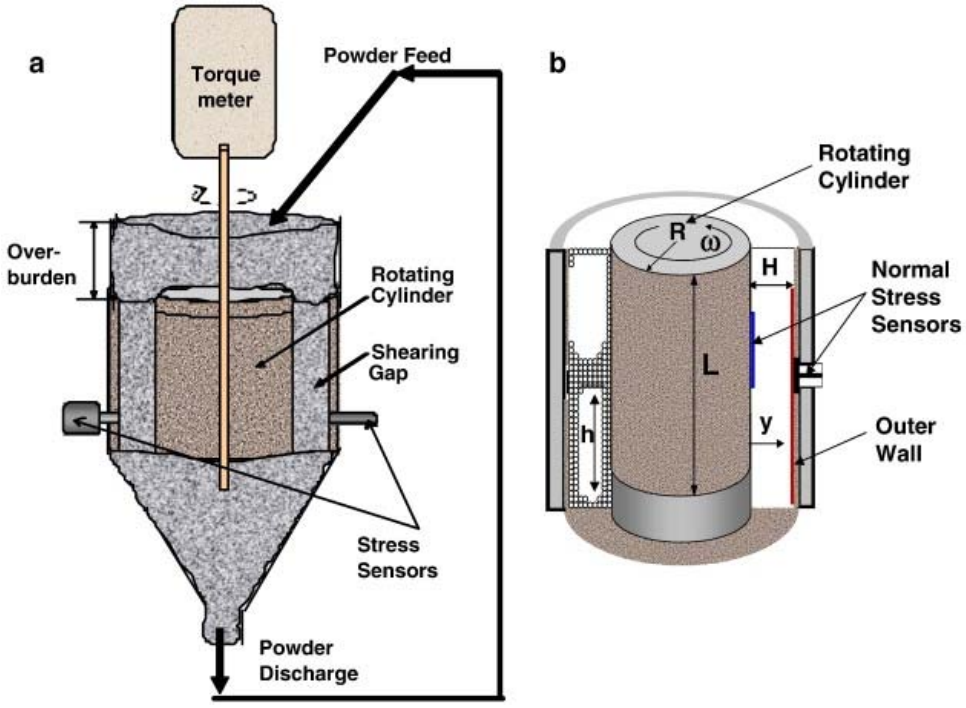

Figure 21: (a) Schematic representation of the axial-flow Couette device. (b) Detail of the shear gap

Experiments in the Couette device were performed without (batch) and with axial flow (continuous), and several depths of overburden to control the pressure in the shearing gap. Normal stresses were measured on both the outer, stationary wall as well as the inner, rotating (shearing) wall of the device as shown in Figure 21. Shear stresses were measured indirectly and recalculated from the torque on the rotating cylinder.

A typical batch, filling curve of the Couette is shown in Figure 22 for 1 mm in diameter round glass beads with a cylinder height of 20 in. and diameter of 1.5 in., in a housing of 6 in. in diameter (with a gap of 2.25 in.). We distinguish between the increasing portion of the torque as a function of height (LHS of the figure) and the torque due to packing of the material at constant height and as a function of time (RHS of the figure).

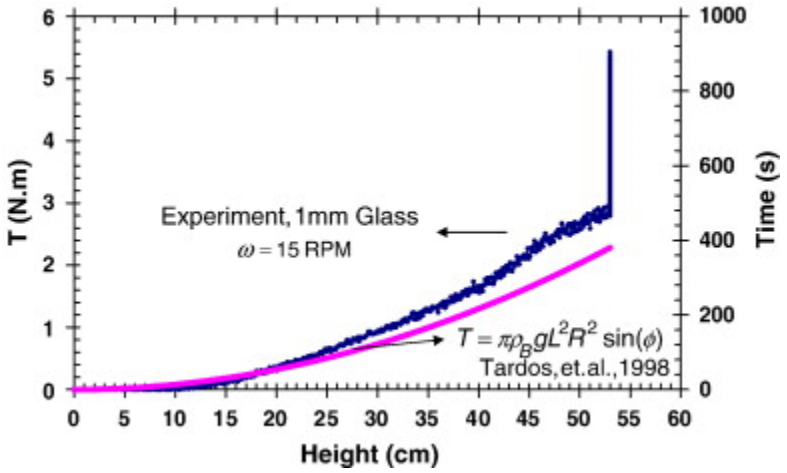

Figure 22: Filling curve: torque vs. height for 1 mm glass beads

First, we concentrate on the LHS region where the torque is height dependent as the Couette is filled with particles and fit the equation of the torque, T to the measured data as was done previously by Tardos et al. (1998):

$$T = (\tau R)2\pi Rh = \pi\rho_B g h^2 R^2 \sin(\phi) \qquad (4.1)$$

where $\tau = p\sin\phi$ is the shear stress and p is the average normal stress given by $p = \rho_B gh/2$. Other notations in Equation 4.1 are: ρ_B is the bulk density, g is the acceleration of gravity, h is the height of material in the vertical direction (function of filling time, see Figure 20b), R is the cylinder radius and ϕ is the angle of internal friction of the material. The implication of Equation 4.1 is that the shear stress τ is linearly dependent on the height h so that when the torque is calculated the height appears to the second power. In addition, the theoretical line fits the experimental results quite well suggesting that the shear stress is indeed a linear function of height as long as the material is continuously fed to the system. These general characteristics of the device were already established in our earlier work mentioned above.

We now concentrate on the second part of the curve where the torque increases due to packing of the material at constant height. Additional experiments were performed with a larger inner cylinder of 4 in. in diameter so that the shearing gap was approximately 1 in. and three different curves of the same kind are reproduced in Figure 23a for small (0.1 mm), medium (0.5 mm) and large (1.0 mm) diameter glass particles. One can easily see the different rates at which these particles pack at a constant shearing rate (15 RPM of the rotating cylinder): larger particles pack at a much higher rate due to their enhanced capability of bridging the relatively small shear gap. It appears from Figure 23a that the trends shown would continue but in reality, the range of the torque-meter is exceeded and the experiment has to be stopped. Figure 23b depicts similar behavior for the 0.1 mm in diameter glass beads but for a much wider shear gap (2.25 in.). Here, we calculated the average shear stress using Equation 2.27 and the linear speed is calculated from the angular velocity of the cylinder.

$$\tau_{ave} = T / 2\pi R^2 L \tag{4.2}$$

As seen in the figure, the torque increases significantly during the packing phase but does not exceed the range of the torque-measuring device. This is mainly due to the shorter cylinder used and by the relatively large shear gap that allows some additional movement of the granular layer in the radial direction. It appears from the figure that the torque has reached its steady state value at the lowest shear rate (blue curve) and we use this experiment to show how the shear stress depends on shear rate when the Couette is operated in batch mode (without vertical flow) at constant height. As seen in Figure 23b, increasing the shear rate (angular velocity of the inner cylinder) more than five-fold, does not result in any significant change in the shear stress: the material is in the frictional,

quasi-static regime and the average shear stress is practically independent of shearing rate.

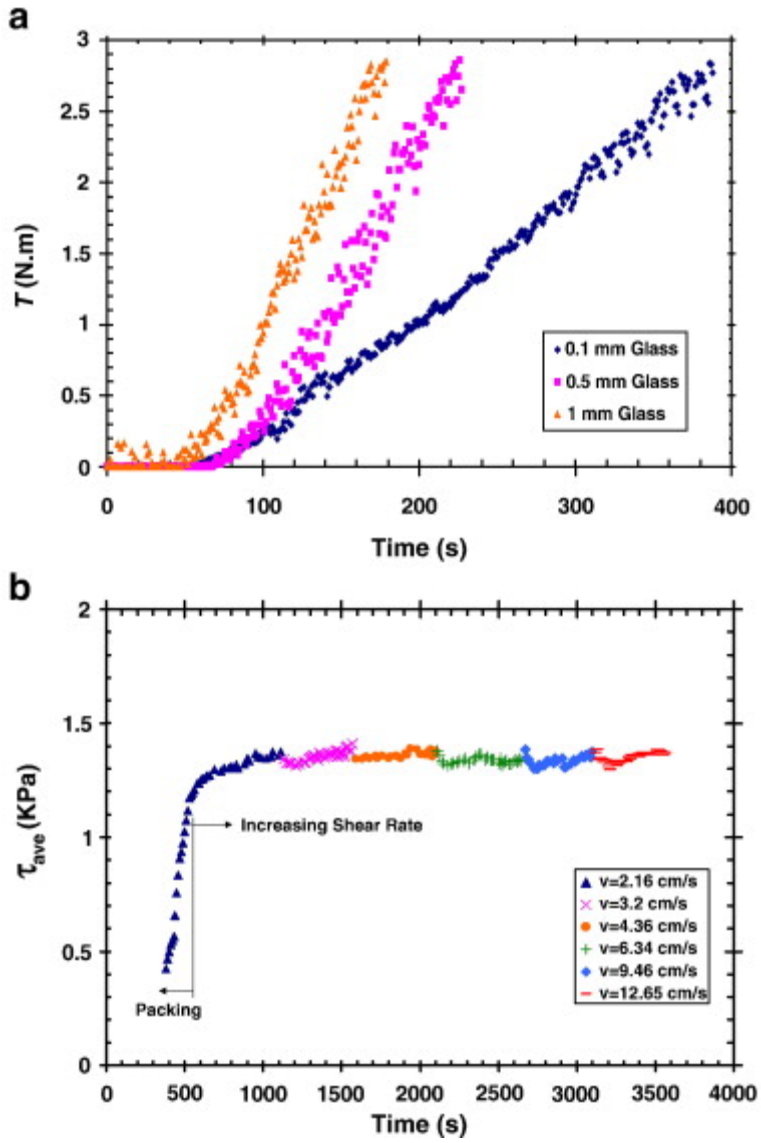

Figure 23: Batch Couette experiments: (a) torque vs. time for different particles; (b) shear stress vs. time and rotational speed

We reproduced in Figure 24 a similar experiment to that shown in Figure 23b but allowing the material to flow at a small rate vertically in the shear gap. The torque in this case decreases significantly due to a minute change in solid fraction (porosity) that allows

chains of particles to break as the inner cylinder rotates. Using Equation 4.2, the average shear stress can be calculated as a function of shear rate as shown in Figure 24. As seen, the shear stress exhibits two very distinct regimes: a quasi-static regime where the shear stress is mostly independent of the shear rate (at low shear rates) and an additional regime ("intermediate" as denoted in the figure) where the dependence takes the form of an increasing function. We assume that the behavior resembles a power-law with an index n. In fact, the power-law index appears to be variable, increasing at higher shear rates. One would assume that continuing to increase the shear rate would yield even higher values of the index n as the flow approaches the inertial regime (where the coefficient should be $n = 2$) but such experiments are outside the capability of our Couette device since centrifugal forces take over and the material is pushed radially outward and a slip condition sets in near the rotating cylinder.

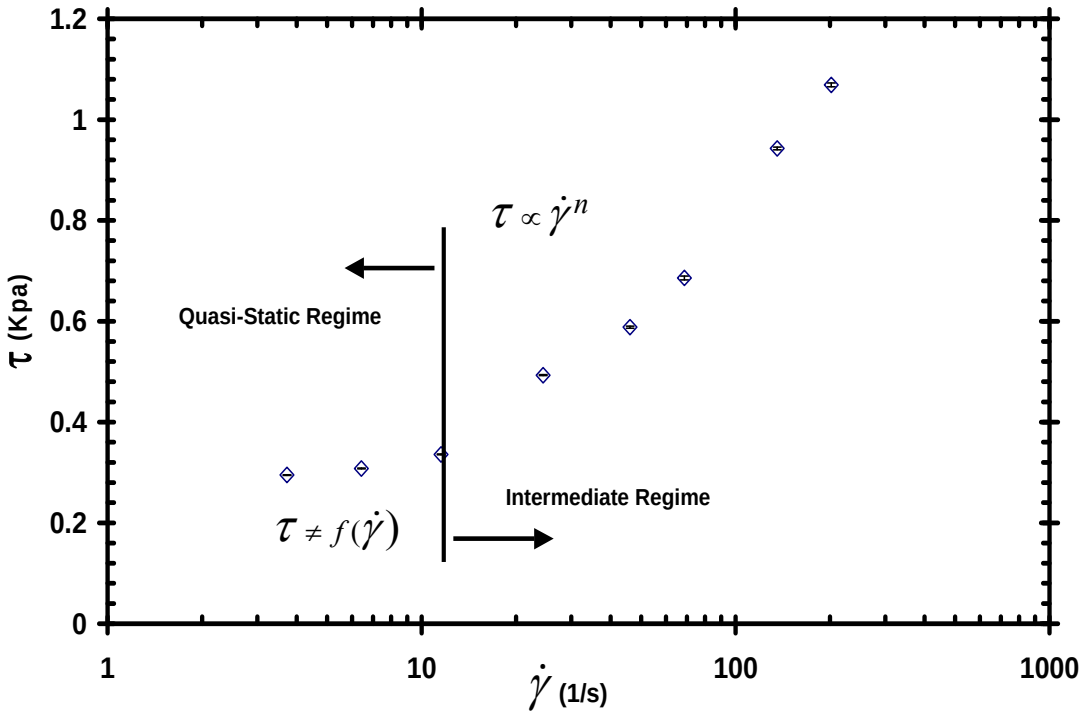

Figure 24: Axial-flow experiment in the Couette device: spherical glass beads, 0.1 mm in diameter

The purpose of these experiments was to show the significant difference in behavior of the shearing layer in the batch, no-flow and the continuous-flow device. While in the batch mode, the material continues to pack increasing its solid fraction as a function of time, in the flowing system a steady state sets in at an approximately constant solid fraction. This solid fraction is below a certain critical value, somewhat characteristic for each powder, where the material can "dilate" sufficiently and "flow" under shear. In this expanded, mobilized (sometimes also called "fluidized", even though there is no gas present to actually fluidize the powder) condition, the powder can transit from the quasi-static to the intermediate regime as the shearing rate is increased. We showed in separate experiments that the influence of the vertical flow rate is negligible if it can be kept small, just enough to prevent packing. The rest of this chapter is mainly concerned with this second case where there is a minute flow of material in the vertical direction and where a quasi-static, shear-rate-independent and an intermediate, dense-phase, shear-rate-dependent shear stress (torque) develops. The main goal of the experiments is to measure the shear and normal stresses on the shearing wall, their location and their ratio. We further propose a yield condition and a constitutive equation (closure) derived from experimental measurements and develop a new numerical scheme (performed for this geometry by S. Turek and A. Ouazzi in Kheiripour Langroudi et. al., 2010a) to solve the momentum equations with the newly proposed closure, to cover both regimes of flow.

4.2.2 Stress measurements in the continuous-flow Couette device

Experiments were performed to show the dependence of the shear and normal stresses on the shear rate. Materials with different sizes and shapes were tested to generalize the concept.

4.2.3 Average shear stress measurements and their location

Since there are no direct shear stress measuring sensors commercially available that can be employed in a dense granular bed, the shear stress on the rotating cylinder was measured indirectly using the torque on the shaft exerted by the granular medium on the entire length, L of the cylinder as in Equation 2.27. To explore the dependence of the shear stress on the depth of the granular layer, we employed cylinders of different lengths, L = 4, 8, 12 and 16 in. (and diameter of 4 in.) and calculated the average shear stress in each case. The experiments were performed with no overburden (material on top of the rotating cylinder, see Figure 21) using 0.5 mm in diameter glass beads. Results are given in Figure 25 where the average shear stress is given as a function of cylinder height, L for different shear rates by rotating the inner cylinder from 5 to 45 RPM. As seen, the shear stress is approximately linear as a function of height and depends strongly on shear rate as already shown above.

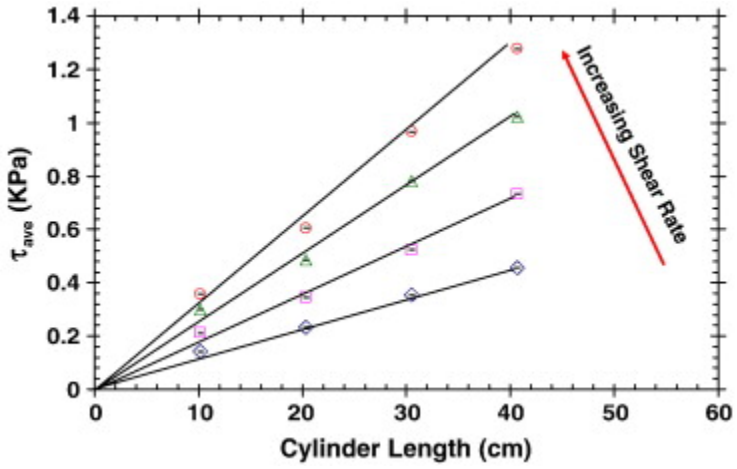

Figure 25: Average shear stress measurements in continuous Couette device using different overall lengths, *L*, cylinders at different shear rates

Another interesting observation is that, by forcing the trend of the experimental measurements to go to zero stress at zero height, data from the shortest cylinder (L = 4 in. in length) fall above the line at a somewhat higher shear stress. This behavior is due to friction between the lower cover of the cylinder and the granular material (in addition to friction in the shearing layer between the cylinders) which is not a linear function of height; this result was already demonstrated by DaCruz et al. (2005). When the length, L (height) of the shearing layer is small, the influence of this portion of the cylinder is significant and hence the torque is higher. At larger length (height), the influence of the bottom cover becomes less significant and the dependence is almost perfectly linear. The main conclusion from this measurement is that using cylinders longer (taller) than about 8 in. will mostly eliminate the influence of the end effect (lower cover) and that the value of the average shear stress will most likely occur at the middle point over the length, L.

4.2.4 Normal stress measurements

Figure 26 shows a schematic representation and a picture of the instrumentation to measure normal stresses inside the bulk material on the rotating cylinder at three depths (l_1, l_2 and l_3). The stress sensor is the same as depicted and described in chapter 3. As mentioned before it is made of a circular sensitive element 1.1 cm in diameter glued to the surface of the rotating cylinder and an electronic circuit situated inside the blue box in the picture. Since the cylinder is rotating inside the granular layer, the signal cannot be hard-wired but is instead transmitted by radio to a receiver connected directly to the data acquisition system. To our knowledge, this is the first time that such a measurement was undertaken on a shearing surface inside a granular medium. The cylinder used is 4 in. in diameter (this dimension is imposed by the size of the radio transmitter) and 20 in. long

(to accommodate the three radio transmitters). The outside diameter of the stationary cylinder that forms the Couette device (not shown in the figure) is 6 in. in diameter and thus defines a granular layer of 1 in. in thickness that surrounds the sensors.

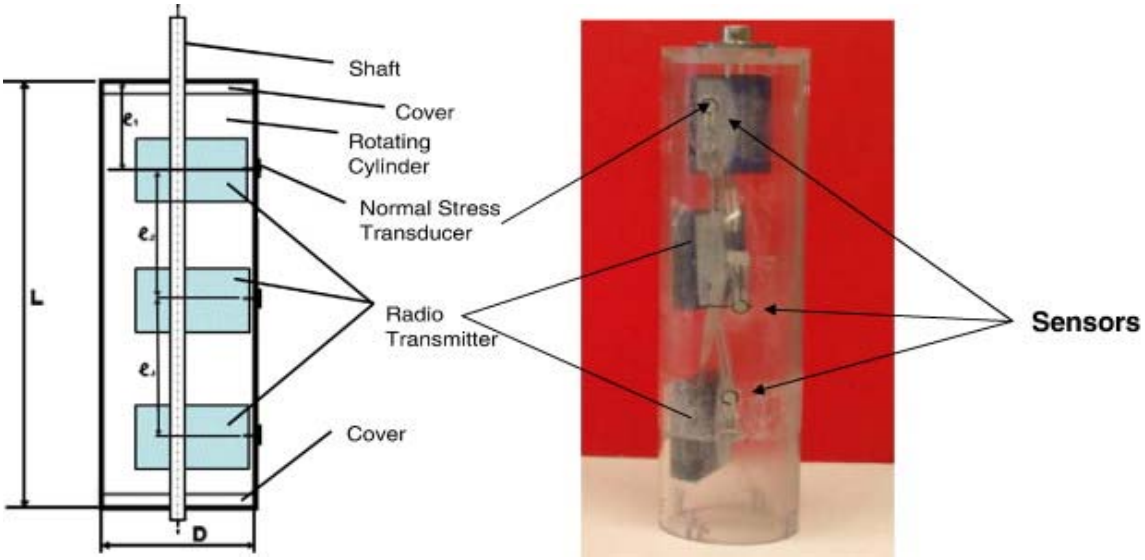

Figure 26: Schematic and picture of the Couette device with three remote normal stress sensors

These particular experiments were performed with an overburden of approximately 4 in. so that the depth of the three sensors was l_1–l_3 plus the overburden as shown in Figure 27. Different rotation rates from 5 to 60 RPM and glass particles of 0.5 mm (average) in diameter were used. The experiment was performed with a very small vertical flow rate of powder; this results in a very slow axial velocity in the Couette gap of less than 0.05 mm/s and does not influence significantly the flow and stresses in the radial direction. Figure 27 depicts the results of the stress measurements as a function of depth. The distribution appears to be linear with the error bars representing the fluctuation of stress and the dependence on the applied shear. As seen in Figure 27, the normal stress in the sheared layer is not shear-rate-dependent even at the highest shear

rate (at 60 RPM), within the error of the measurement and the presence of fluctuations. This allows the calculation of an average normal stress on the rotating cylinder that appears, according to these results, to reside in the middle of the cylinder ($L/2$). This is an important conclusion since it shows that both the average shear and normal stresses are practically located around the midpoint of the rotating cylinder at least under the experimental conditions of this experiment. In subsequent experiments only one normal sensor, situated at the midpoint on the cylinder, was used.

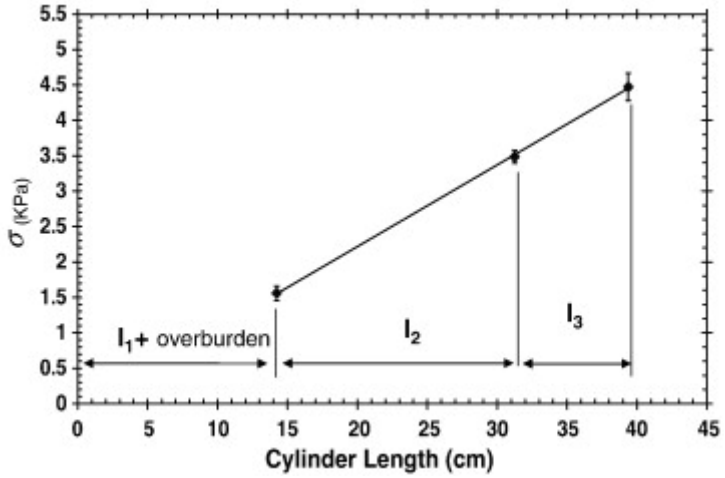

Figure 27: Normal stress as a function of height as measured on the shearing cylinder surface by remote sensing for 0.5 mm glass particles and rotation rates from 5 to 60 RPM

4.2.5 Ratio of shear to normal stresses in the Couette device

The most interesting result from the above measurements is that one can calculate the ratio of the average shear to normal stresses as a function of shear rate. A typical result is shown in Figure 28 where the average shear stress and local normal stress measured in the middle of the rotating cylinder ($L/2$) are shown as a function of shear rate. The

particles used are 0.1 mm in diameter spherical glass beads. The shear stress is the same as the one depicted in Figure 24 and the stress is practically constant at low shear rates and increases significantly as soon as the material reaches the intermediate regime of flow. The normal stress shows a very interesting behavior: it is constant and lower at low shear rates (where the shear stress is also constant) and then increases abruptly and remains practically constant thereafter even though the shear stress increases continuously.

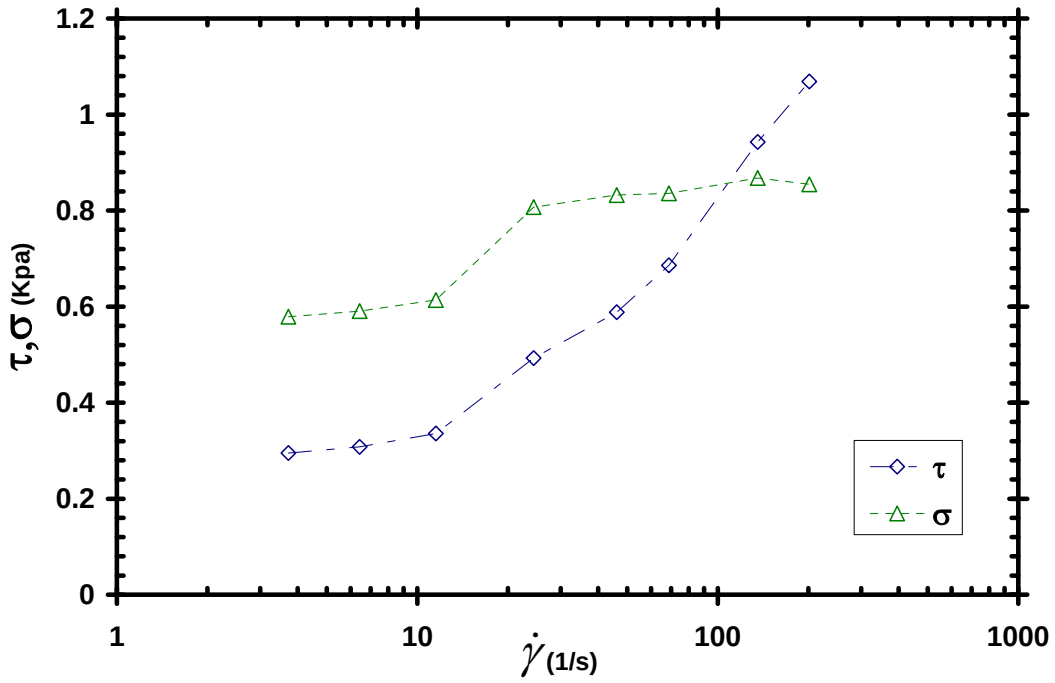

Figure 28: Shear and normal stress variations as a function of shearing rate in the Couette device; 0.1 mm in diameter glass particles

The ratio of the two stresses (apparent friction coefficient) is given in Figure 29 and, as seen, the ratio exhibits a similarly interesting behavior: at very low shear rates, the ratio is constant and only slightly lower than the tangent of the friction coefficient of glass particles (about 0.5) as one would expect from quasi-static flow theory. As the shear rate

increases beyond a certain critical value (in this case about 10 s^{-1}), the ratio of shear to normal stress increases significantly. This behavior is mainly due to the superposition of collisions between particles on the sliding friction of surfaces so that the overall shear stress and "friction coefficient" also increase. This kind of behavior was already suggested by simulations (Campbell, 2006 and Da Cruz et. al., 2005) but never actually measured experimentally before. It also shows that the material moves from the quasi-static regime to the intermediate regime of flow where collisions become more important and actually carry some load. A power-law type curve is fitted to the data: it shows a power-law coefficient of $n = 0.73$ and a constant coefficient $a = 0.45$ for zero shear rate.

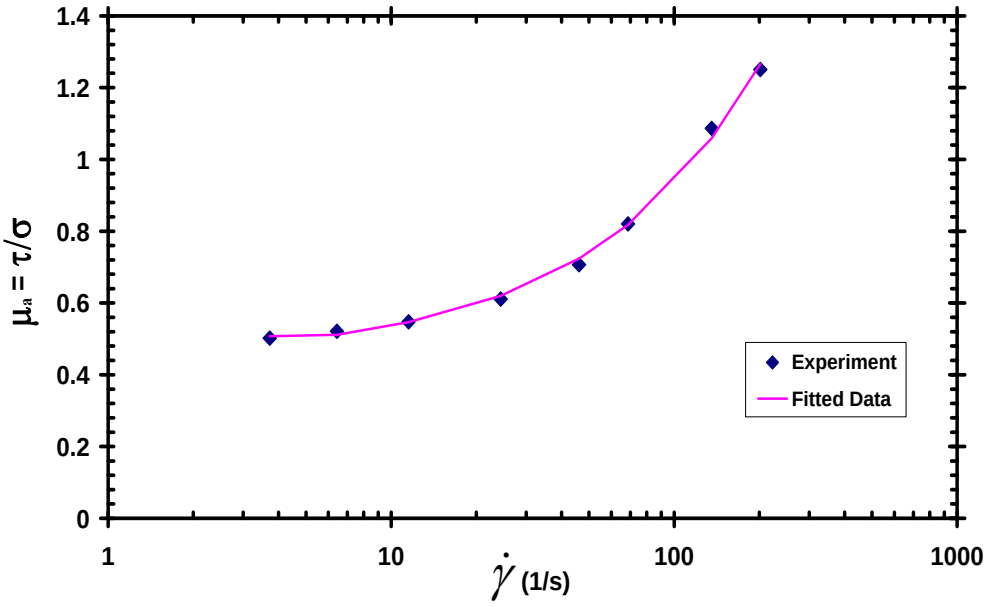

Figure 29: Measured ratio of shear to normal stresses (apparent friction coefficient) and fitted curve as a function of shearing rate for 0.1 mm in diameter round glass

We conclude that it is possible to measure normal stresses on the shearing wall of the Couette device inside the granular layer and calculate the ratio of the average shear to normal stress as a function of shear rate. It appears, as suggested by previous theoretical

simulations, that the dynamic angle of friction is reproduced by this ratio only at very low shear rates. As the shearing rate increases, the ratio of the stresses also increases due to collisions between particles that sustain loads in addition to dry friction that is prevalent at low shear rates. Our experiment could not probe the higher limit of the "friction coefficient" in the rapid granular flow regime (when only collisions are important) because of equipment limitations and the inherent presence of gravity that makes at least some enduring contacts between particles unavoidable.

4.2.6 Yield condition and constitutive equation

We try to generalize the above findings for the case when the powder transitions from the quasi-static to the intermediate regime of flow and propose a yield condition that holds at low and higher shear rates. We show below how the experimental yield condition obtained from experiments in the Couette device and given in Figure 29 can be inserted into the Schaeffer constitutive law (Equation 2.4). From Figure 29, one can fit the following equation to the data:

$$\frac{\tau}{\sigma} = a + b\left|\dot{\gamma}\right|^{n} \tag{4.3}$$

where τ and σ are the shear and normal stresses and "a", "b" and "n" are coefficients characterized by the experimental curve. We use the notation for the modulus (absolute value) of the shear rate to designate that only its magnitude is of relevance and not its direction. A slight generalization can be obtained by replacing the constant coefficient "a" by $\tan\phi$ to obtain:

$$\frac{\tau}{\sigma} = \tan(\phi) + b\left|\dot{\gamma}\right|^{n} \tag{4.4}$$

This equation has the advantage that it reduces to the Coulomb yield condition at zero shearing rate. The error between Equations (4.3) and (4.4) comes from the complex way the two stresses are measured using independent instrumentation and calibration procedures for the torque and normal stress, respectively. An equivalent representation of the Coulomb yield condition $\tau = \sigma \tan\phi + c$ can be obtained from the characteristic Mohr circle, by replacing σ by p and τ/tanϕ by q/sinϕ, in the form (Nedderman, 1992):

$$q = p\sin\phi + c\cos\phi \tag{4.5}$$

where q is half of the difference between the principal stresses and "c" is referred to as "cohesion". The deviatoric part of the Schaeffer's law for flow of a dry powder in the quasi-static regime (Schaeffer, 1987) is:

$$\tau_{ij} = \frac{\sqrt{2}\, p \sin\phi}{\left|\dot{\gamma}_{ij}\right|}\dot{\gamma}_{ij} = \frac{\sqrt{2}\, q}{\sqrt{z}}\dot{\gamma}_{ij} \tag{4.6}$$

where $\dot{\gamma}_{ij} = \frac{1}{2}(\nabla u + (\nabla u)^T)$ is the rate of deformation tensor, $\left|\dot{\gamma}_{ij}\right|$ is its magnitude and z is twice the second invariant defined as $z = 2\gamma_{II} = \dot{\gamma} : \dot{\gamma} = \left|\dot{\gamma}_{ij}\right|^2 = tr[(\dot{\gamma}_{ij})^2]$. One recognizes the Coulomb yield condition (Equation 4.5) (with c=0) in the numerator of Equation 4.6. We replace "q" from Equation 4.5 in Equation 4.6 with $c = b\left|\dot{\gamma}_{ij}\right|^n$, to obtain:

$$\tau_{ij} = \sqrt{2}p\{\sin\phi + b\cos\phi\left|\dot{\gamma}_{ij}\right|^n\}\frac{\dot{\gamma}_{ij}}{\left|\dot{\gamma}_{ij}\right|} \tag{4.7}$$

or in terms of the variable "z":

$$\tau_{ij} = \sqrt{2}p(\sin\phi\ z^{-\frac{1}{2}} + b\cos\phi\ z^{\frac{n-1}{2}})\dot{\gamma}_{ij} \tag{4.7'}$$

This is the constitutive equation for the modified Schaeffer's law that includes the behavior at higher shear rates, characteristic of the "intermediate" regime of powder flow. The first term on the right hand side of Equation 4.7 corresponds to the plastic deformation (frictional or solid-like behavior) while the other term corresponds to the viscous behavior (liquid-like) of the granular material. In simple shear flow, in Cartesian coordinates (small gap) where u = u_y and v = 0, Equation 4.7 takes the simple form:

$$\tau_{yx} = p\sin\phi(1 + b\cot\phi\left|\dot{\gamma}_{yx}\right|^{n}) \tag{4.8}$$

One has to note that the deviatoric part of the stress, Equation 4.7 does not go monotonically to zero as the shear diminishes because the magnitude of the shear appears in the denominator. There is a physical and mathematical discontinuity at this point that, in practice, results in the formation of narrow shear bands and that has to be overcome by the numerical method (Ouazzi et al. (2005)). From a practical point of view, a modified Couette device with slow axial flow superimposed on the shearing motion, in which the materials can freely dilate and collide, can be used to determine the values of *b* and *n* for any material that is somewhat free flowing. These values can then be used in Equation (4.7).

4.3 Continuum theoretical approach

In this section a fluid mechanistic continuum approach using the constitutive equation developed above, will be presented. The purpose is to predict theoretically, experimental results obtained in this work using the simple geometry of the concentric Couette device. Based on these calculations we then predict results for more complex geometries, namely an eccentric Couette and one that has a cylindrical obstacle in the shearing zone.

4.3.1 Equation of motion

Powder flows are treated using general constitutive laws for non-Newtonian fluids (Ouazzi et al., (2005)). The powder is assumed to be an incompressible continuum that obeys conservation of mass:

$$\frac{D\rho}{Dt} = \frac{\partial \rho}{\partial t} + \nabla \cdot (\rho u) = 0 \tag{4.9}$$

where $D * / Dt$ is the material derivative and u is the velocity vector. Since we assume that the bulk density ρ is a constant, the continuity equation reduces to the divergence of the velocity $\nabla \cdot u = 0$. The powder also obeys a conservation of momentum equation:

$$\rho \frac{Du}{Dt} = -\nabla \cdot T + \rho g \tag{4.10}$$

where the stress tensor is given by $T_{ij} = \tau_{ij} - pI$ and where I is the unit tensor. To complete the problem, a closure is required in the form of a constitutive equation that correlates the deviatoric part of the stress tensor τ_{ij} with the velocity.

The above problem can be similarly formulated in the framework of the Cauchy momentum equation valid for incompressible, non-Newtonian fluids and powders:

$$\rho \frac{Du}{Dt} = -\nabla p + \nabla \cdot \left(\mu(\gamma_{II}, p) \dot{\gamma}_{ij} \right) + \rho g, \quad \nabla . u = 0 \tag{4.11}$$

where we take $\tau_{ij} = \mu(\gamma_{II}, p) \dot{\gamma}$. To complete the problem, the nonlinear pseudo-viscosity $\mu(\gamma_{II}, p)$ is defined as a function of the second invariant of the rate of deformation, or the variable “z”, and the normal stress “p”:

1. Newtonian fluid, $\mu(z,p) = 2\mu_0$, where μ_0 is the fluid viscosity, (4.12-1)

2. Bingham solid $\mu(z,p) = 2\mu_0 + \sqrt{2}\,\tau_0 z^{-\frac{1}{2}}$, where τ_0 is the yield strength, (4.12-2)

3. Powder in the quasi-static regime, $\mu(z,p) = \sqrt{2}\,p \sin\phi\; z^{-\frac{1}{2}}$, (4.12-3)

4. Power-law fluid $\mu(z,p) = 2\mu_0 z^{\frac{n-1}{2}}$, ("n" is the power law index), (4.12-4)

5. Modified Schaeffer law, $\mu(z,p) = \sqrt{2}\,p[\sin\phi\; z^{-\frac{1}{2}} + b\cos\phi\; z^{\frac{n-1}{2}}]$. (4.12-5)

A comparison of Equation 4.11 with the classical Navier-Stokes equations (obtained by using Equation 4.12-1) reveals that the ordinary viscous terms (proportional to the viscosity ,μ_0) have been replaced by shear-rate independent terms (Equations 4.12-2 to 4.12-5) that contain the magnitude of the shearing rate $(1/\sqrt{z})$ in the denominator. This means that these equations are mathematically more complex than the Navier-Stokes equations and apply only to the region where the material is deforming.

The main mathematical problems of the generalized incompressible continuum model (Equation 4.11) can be summarized as follows:

• Mathematical analysis: There is a lack of research concerning the existence of solutions for the flow of such "fluids" except for special cases (Hron et al., 2003), furthermore the dynamic equations (Equation 4.11) show some instability (Bulícek and Kaplický (2008),

Bulícek et al. (2005), Prasad and Rajagopal (2006), Malék et al. (2002), Renardy (2003), Schaeffer (1987) and Schaeffer (1990)).

• Singular viscosity: The part of the stress tensor containing $1/\sqrt{z}$ is well defined only for nonzero values of the rate of strain tensor and for 'non-negative' pressures, which requires some stabilization techniques of singular phenomena due to the nonlinear viscosity (Ouazzi et al. (2005)).

• Discretization method: It is well known that the computation of solutions to such incompressible systems requires that some care is taken in the choice of the approximating spaces in order to make the discrete problem well posed. Moreover, since a large number of successful spaces satisfying the above condition are nonconforming that present a locking phenomenon for problems involving the rate of deformation tensor, some consistent stabilizing term is required (Turek and Ouazzi (2007)).

• Nonlinear multigrid solver: for this highly nonlinear problem, coupling the pressure and the velocity, there is almost no alternative to linearization using Newton's techniques and therefore efficient multigrid methods for these new types of saddle-point problems need to be developed (Turek (1998), Turek et al. (2002)).

Figure 30 shows the ratio of average shear to normal stresses on the rotating cylinder vs. the shear rate from a numerical solution (performed by Turek and Ouazzi in Kheiripour Langroudi et. al., 2010a and reproduced in Appendix) using the new constitutive equation (Equation 2.37-5) and compares calculations with experimental data for 1 mm in diameter spherical and crushed glass (with rheological models and physical properties given in Table 2).

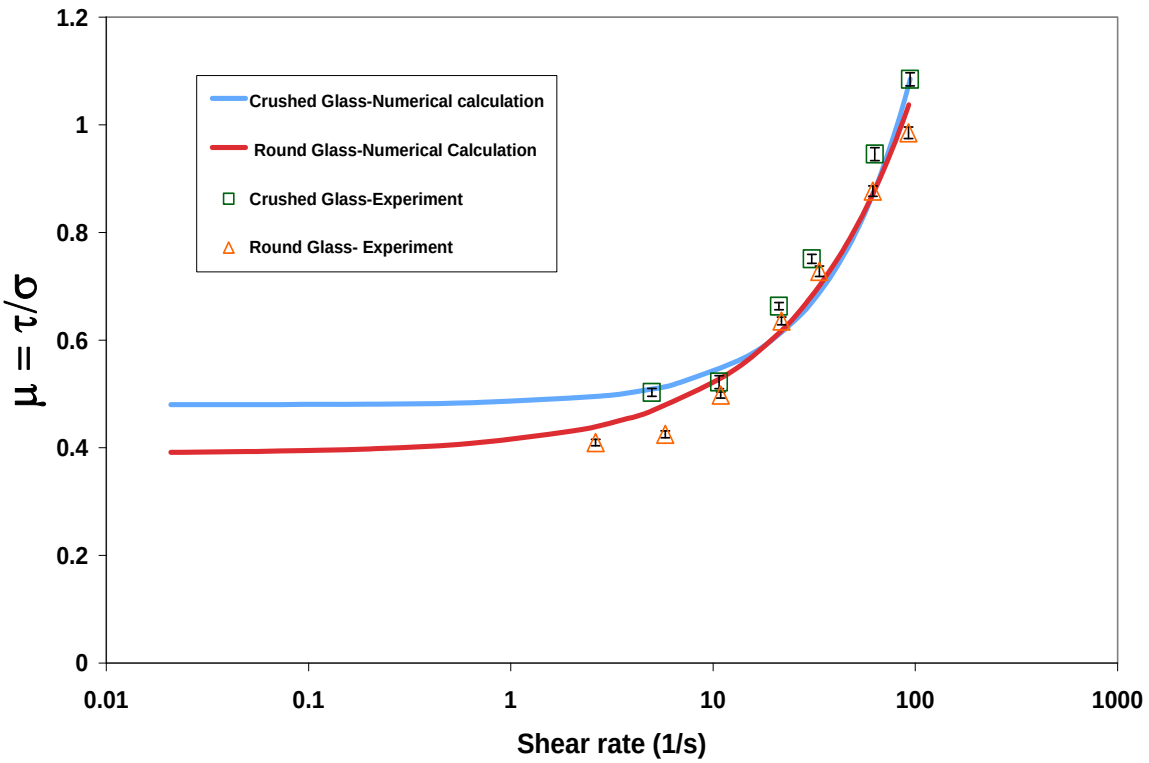

Figure 30: Numerical solution of the ratio of average shear to normal stresses vs. shear rate (using the new constitutive equation, Equation 4.7); Concentric cylinders with 1 mm round and crushed glass particles

Two regions can be seen: solid-like behavior at low shear rate where the ratio is constant and independent of the shear rate reflecting quasi-static flow, and fluid-like behavior as the shear rate increases beyond a critical value where the ratio is dependent on shear rate. The result in Figure 30 shows that the simplifications introduced by the continuum approach and the numerical method used, do not introduce excessive errors. The advantage of the numerical solution is that velocity, stress distributions and overall torque can, in principle, be calculated for different geometries.

We repeated the above measurements and theoretical calculations for several particles and we show in Figure 31 an example where we give the friction coefficient of smooth

($\phi = 26^o$) and rough ($\phi = 36^o$) Polyethylene particles (4 mm in size and cylindrical shape) at different shear rates, the rheological parameters for each case and a picture of the particles. The coefficients "a" is higher for the rough material due to higher surface friction, as one would expect. In fact, the experiment shows that our Couette device is sensitive enough to distinguish between different surface roughnesses.

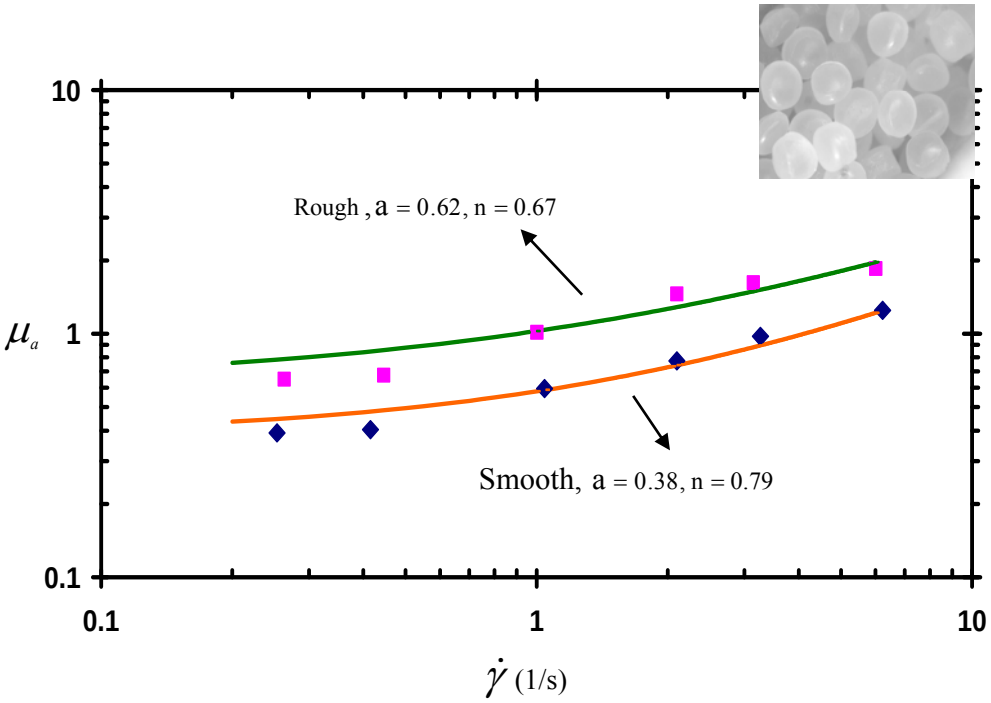

Figure 31: Apparent friction coefficient for 4 mm in diameter rough and smooth Polyethylene particles

4.4 Effect of Physical Properties on the Rheological Behavior

In order to generalize the rheological model obtained from our Couette cell we tested a large number of particles with different physical properties such as size, size distribution, shape, surface roughness, rigidity and elasticity. These are summarized in Table 2.

Table 2: Physical properties and rheological model obtained in the Couette cell for different particles; ϕ^o and $\phi_w{}^o$ are internal and wall angles of friction, a and n are from the fitted model to Equation 4.3

Material	MPS (mm)	Shape	Remarks	(Φ^o)	($\Phi_w{}^o$)	Rheological Model, a	Rheological Model, n
Glass	0.1	Round	Rigid	27.0	25.3	0.45	0.73
Glass	0.5	Round	Rigid	27.1	25.7	0.45	0.70
Glass	0.5	Odd	Rigid/Crushed	26.0	24.1	0.43	0.94
Glass	1	Round	Rigid	27.4	24.2	0.39	0.72
Glass	1	Odd	Rigid/Crushed	34.6	30.4	0.48	1.03
Glass	2	Round	Rigid	28.2	25.5	0.44	0.78
Glass	3	Round	Rigid	28.4	24.6	0.42	0.75
Polyethylene	4	Odd	Cylindrical/ Smooth	35.7	33.7	0.62	0.67
Polyethylene	4	Odd	Cylindrical/ Rough	25.6	22.4	0.38	0.79
Polyethylene	0.3	Odd	Soft/Compressible	25.3	23.9	0.43	0.45
Polyethylene	0.5	Odd	Soft/Compressible	27.9	25.5	0.45	0.68
EPDM	1.5	Odd	Soft/Elastic	31.1	24.2	0.39	1.11
Detergent/HP	0.45	Odd	Soft/Deformable	30.5	29.8	0.57	1.21
FCC Catalyst	0.07	Odd	Rigid/Broad Size Distribution	37.1	36.3	0.70	0.69

As seen in Table 2, the coefficient *n* varies for different materials from about 0.3 to approximately 1.3 as a function of particle shape, surface roughness and particle softness and elasticity, etc., and cannot be taken as a constant. Simple addition of the stresses from the quasi-static and the intermediate regime i.e., taking $n = 1$ (as was proposed earlier by Jackson (1986)) only applies for specific cases. We also see that the coefficient "a" reaches approximately $\tan \phi_w \sim \tan \phi$ when the shear rate tends to zero (quasi-static regime of flow) and this is when the plasticity rule (Coulomb criteria) applies. Results with spherical glass particles of different sizes reveal that by just increasing size the

power law index remains almost unchanged. Comparison between round and crushed glass (0.5 and 1 mm) shows that the shape has an important role on the rheology of the powder bed. The power law index "n" is much higher (~1) for crushed glass than that for round glass beads (~0.7). This shows that collisional effects are dominant for an odd shaped particle, as "n" is a characteristic for viscous behavior. Irregular-shape and broader size distribution increase the contact areas between particles so that the viscous term of the constitutive equation becomes dominant. The effect of surface roughness, as described above, was considered using smooth and rough Polyethylene. We found that rough and smooth materials of the same size and shape behave differently. The coefficients "a" is higher due to higher surface friction. Smooth particles exhibit a larger coefficient "n" (0.79 as compared to 0.67 for rough particles) which means that collisions can occur more frequently and this effect dissipates more energy by friction.

Regarding some more complex effects such as for example particle material hardness (rigid vs. soft particle), this set of experiments does not yield unequivocal answers, as we did not find two powders with the hardness being the only difference between them. However, when a particle is elastic and/or soft it can deform to some degree under shearing and the excess deformation requires more shear stress (torque) so that a large index "n" was obtained for EPDM as compared to more rigid particles such as glass and polyethylene. A somewhat similar effect can be seen for the case of detergent granules that exhibit the largest "n" among all materials as this is the most deformable particle among all (in addition of having a wide particle size distribution), and if shearing rates are increased excessively, the deformation becomes permanent. The effects of compressibility and elasticity can be investigated looking at the two polyethylene

particles (0.3 and 0.5 mm) and the elastomer powders, respectively. A more careful study of this later effect (looking also at solid volume fraction during flow) is presented in Chapter 6.

4.5 Conclusions

In this chapter flow of dry, frictional powders in the quasi-static and intermediate regimes using the simple geometry of the Couette device was studied. We measure normal and shear stresses on the shearing surface and propose a constitutive equation valid in both regimes. We found that it is possible to measure normal stresses on the shearing wall of the Couette device inside the granular layer and calculate the ratio of the average shear to normal stress as a function of shear rate. It appears that the dynamic angle of friction of the powder is reproduced by this ratio only at very low shear rates. As the shearing rate increases, the ratio of the stresses also increases due to collisions between particles that sustain some load. We show that a modified Couette device with slow axial flow superimposed on the shearing motion can be used to determine the constants (b and n) of a yield condition for any material that is somewhat free flowing and thus can be used as a "powder rheometer". The yield condition is valid in both the quasi-static as well as the "intermediate" regimes of flow and contains a term characterizing "solid"-like behavior and an additional term that captures some "fluid"-like properties at higher shear rates.

We found that while the sizes of particles does not have major impact on the rheological parameters, size distribution, shape, surface roughness, ability to dilate or pack, deformability and elasticity strongly affect the rheology of the bulk. Odd-shaped

particles with the same average size as spherical particles yield a higher power-law index. Rough and smooth materials of the same size and shape behave differently: the rough material shows a higher constant coefficients “a” due a larger friction coefficient while the smooth particles have a higher exponent “n” because of less force chains (due to smaller friction) and more freedom of movement. Particles with more ability to dilate i.e., exhibit larger inter-particle spaces, show less dependency of shear stress to shear rate while deformation and elasticity increase the rheological index “n” as more shear stress is required for the same shearing rate for elastic and/or deformable powders.

Development of a Navier-Stokes-type set of equations for granular matter from the yield condition obtained in the modified (with continuous axial flow) Couette cell and use of this equation in the momentum balance to solve for the flow and stress fields, fits into a “Fluid Mechanics” type view of powder flow. As an example of the possibilities of this approach we use the constitutive equations obtained by the above method in a new, specially developed numerical scheme realized in the FEM package FeatFlow (this work was performed by S. Turek and A. Ouazzi in Kheiripour Langroudiet. al., 2010a and is given in Appendix) to solve the continuum equations of motion and to obtain stress and velocity distributions in the powder. While the measurements to obtain the constitutive equation are performed in a *concentric* Couette device, the numerical scheme is used to predict the torque and stresses in two additional geometries: an eccentric Couette device where the inner, rotating cylinder is placed off-center with different eccentricities and a more complicated geometry where a cylindrical body is introduced in the middle between the rotating and stationary cylinders and obstructs part of the shearing gap. The importance of these examples is that once the constitutive model for a certain powder is

determined from the Couette experiment, various geometries can be studied, i.e., stresses and velocities can be calculated, using established numerical methods. A concrete example of such a calculation is given in the last chapter of the thesis for the geometry of centripetal ("spheronizer") flow.

5 Powder Flow Patterns and Shear Band in a Continuous Couette Cell

5.1 Introduction

This chapter contains several studies of dense granular flows in the axy-symmetric Couette geometry with a slight axial (vertical) flow. This part of the work was performed through collaboration with The Procter and Gamble Corporation, (Dr. Paul Mort) and some results are presented in Kheiripour Langroudi et. al., 2010c. The flows comprise a variety of particulate materials with different shapes and size distributions. We try to use "real", industrially important materials to expand basic physical and engineering research in granular dynamics. Work described in previous sections suggests additional studies with particles possessing distributed characteristics, such as size and shape, to uncover interactions between flow and stress fields that might otherwise go un-noticed with model materials such as spherical glass beads. In this chapter, we present experimental studies using two techniques: 1) analysis of tracer particles to elucidate flow patterns; and 2) measurement of solid fraction distributions as a function of radial position in the shear flow. The combination of techniques allows for detailed observation of flow patterns and is essential in understanding the micro-behavior of powder flows. Two tracer methods are used, one is based only on particle size, and the other is based on color. The colorimetric method enables multi-variate analysis of size, color and shape on a per-particle basis (Mort et al, 2004).

Local solid fraction measurements were used in the past for packed powders by employing a capacitance probe [Louge et al., 1996, Louge and Opie, 1990 and Louge and Keast, 2001]**.** In the present study, we use the dependence of solid fraction on position

and shear rate to determine the thickness (width) of the shearing layer in the Couette device. The main objectives of solid fraction measurements were to study the effect of radial and axial flows on mixing in the Couette, e.g., the relation between dispersion and convection and to find the effect of shearing rate on dispersion. We also used tracer studies in the axial Couette flow to elucidate the effect of flow and shear gradients on size segregation of polydisperse samples. We found evidence of radial gradients suggesting a coupling between solid fraction and shear rate across the gap.

Many of the existing theories for flowing granular materials relate the applied stress to the average porosity (solid volume fraction) and the velocity. These flows usually do not develop simple linear shear profiles (GDR MiDi, 2004; Depken et al., 2006) and therefore measurements of average solid volume fraction (bulk density) cannot probe dilatancy. Several recent experiments investigated individual particle motion in the Couette geometry (Schollmann, 1999; Mueth et al., 2000). These studies indicate that the mean particle velocity parallel to the shear direction $V(y)$ decreases faster than linearly away from the inner wall (i.e., the moving boundary in the Couette). The velocity profile in three dimensions was determined by Mueth *et al. (2000)*. Measurements were carried out both in the interior of the material using x-ray and NMR techniques, and on the bottom surface of the Couette cell by optical imaging. These measurements showed that the velocity profile on the bottom surface and in the interior is similar. Losert et. al. (2000) determined the particle dynamics and shear forces of granular matter in a Couette geometry. They found that the mean particle velocities during brief slips of the shearing cylinder decrease roughly exponentially with distance away from the moving cylinder.

They showed that the velocity profile is localized in a shear band five to ten particles thick located close to the moving wall for the case of spherical particles.

Positron emission particle tracking (PEPT) is another technique for studying the shear band. Seville and Tardos (2004) applied this technique in a batch Couette cell (without axial flow) and found that for crushed glass particles (odd shape) the shear band extends as far as 14 particle sizes.

As discussed before, in more complex 3D geometries such as the modified Couette cell, in which the bottom is split into a rotating and a static part, shear zones with up to 40-particle diameters are observed (Fenistein et al. 2004). Sakaie et. al. (2008) used Magnetic Resonance Imaging (MRI) for the study of the 3D packing density of granular flows generated in a split-bottomed shear cell, where the grain flow is driven by the rotation of a bottom disc with respect to a cylindrical container. By imaging the local packing densities in the shear cell as a function of time and for a range of filling heights, they explored the relationship between flow field and dilatancy. The picture that emerges is that the amount of dilatancy grows with the total amount of local strain experienced and saturates when the local strain becomes large. They showed the relative change in bulk density in the flowing zone is strong and saturates around 10-15 %. Experimental measurements of particle dynamics on the lower surface of a three-dimensional Couette cell containing mono-disperse spheres were reported by Mueth, (2000). By directly measuring the velocity, velocity fluctuations, and density within the system, these authors found a power-law relationship between shear rate and fluctuation amplitude, $\delta v \propto \dot{\gamma}^{\alpha}$, with $\alpha \approx 0.52$. This form is consistent with the predictions of hydrodynamic and kinetic theories for granular flow proposed by Bocquet et al. (2002). Mohan et. al. (2002) used a

Cosserat model for finding the shear layer thickness (shear band). This model has a microscopic length scale, which determines the thickness of the shear layer. In a cylindrical Couette flow between walls of equal roughness, the Cosserat model shows that the velocity decays rapidly with distance from the inner cylinder. This finding is in good agreement with the velocity measurements reported by others (Mueth et al. (2000); Losert, et. al. (2000)). In addition, these authors also found theoretically that the shear layer thickness decreases when the angle of wall friction is reduced, and vanishes when the wall is perfectly smooth. Also the shear layer thickness is at its maximum value when the wall friction is equal to the particle internal angle of friction (ϕ). These cases have not yet been experimentally confirmed and are still questionable. This model also predicts a small increase in the solid fraction as one moves towards the outer cylinder. This increase, however, is substantially smaller than that which was observed in the experiments of Mueth et al. (2000).

5.2 Tracer Study

5.2.1 Material used during the study

One set of experiments was performed with a commercial granulate (detergent), denoted in this study as "white base" with a relatively wide particle size distribution as shown in Figure 32. The median particle size is approximately D_{50}=0.45 mm while the width of the distribution is D_{90}/D_{10}~4. This is the same powder presented in Table 2, Chapter 4 and denoted "Detergent/HP". To create the tracer, the same white base was dyed red by spray-on in a fluidized bed mixer to provide colored particles with size and

morphology that are practically identical to the white base. Bivariate analysis of the tracer (size and color) was done using color image analysis.

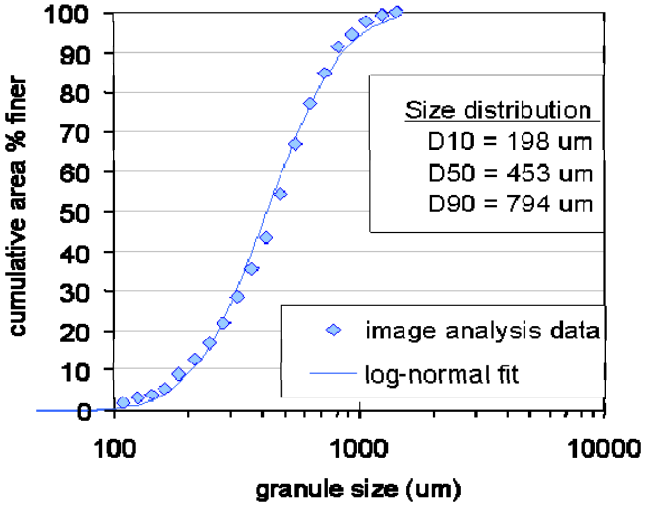

Figure 32: Size distribution of "white base"

Figure 33 shows the time dependent size distribution of the white base as it emerges from the bottom outlet of the axially flowing Couette device.

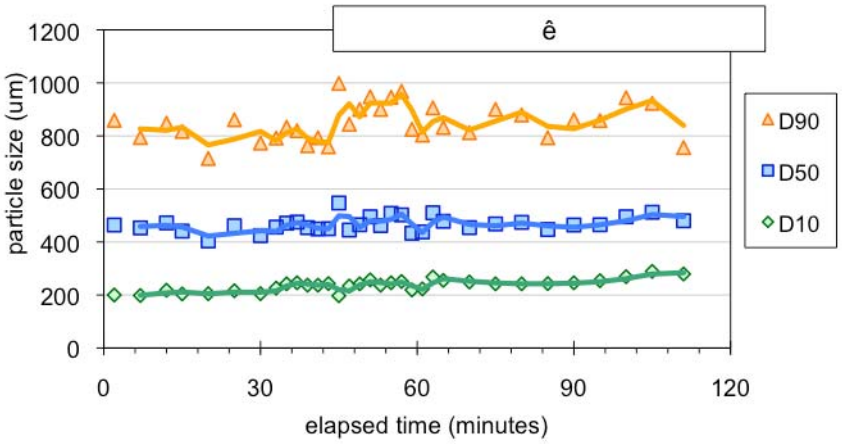

Figure 33: Time dependent size distribution of white base

While there are some fluctuations especially in the size of the larger particles (D_{90}), the distribution appears steady and time independent around the values shown in Figure 32.

This behavior indicates that axial flow achieves a steady state without significant temporal variation.

A second set of experiments was performed in the Couette shearing cell using three kinds of monodisperse round glass beads of 0.1 mm, 0.5 mm and 1 mm in diameter; physical characteristics and rheological models are given in Table 2. In this case, the 0.1 mm glass beads were used as base particles while the larger particles were used as tracers. Identification of the tracer was done by sieving.

5.2.2 Tracer experiments

A schematic representation of the axial-flow Couette with tracer particles inserted into the shearing zone is shown in Figure 34. The insertion is made in such a way as to produce a narrow "pulse" of red tracer particles on an otherwise white background.

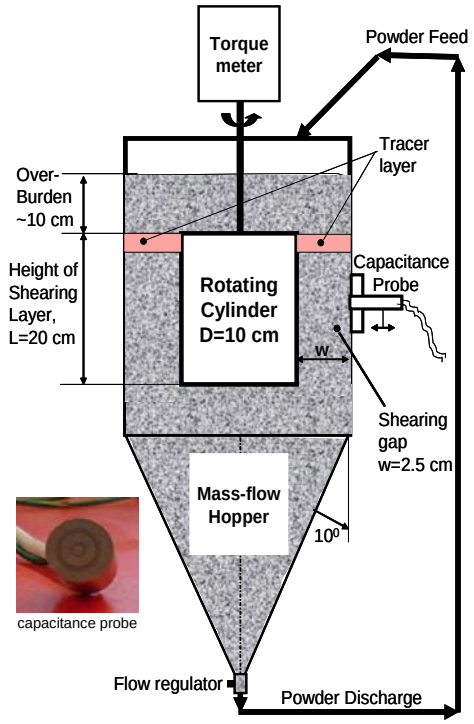

Figure 34: Schematic of the tracer experiment

Additional white base granules are provided to fill the space above the rotating cylinder (overburden in the figure). The experiment is performed by rotating the inner rough cylinder and feeding and discharging material continuously to maintain a constant overburden. The outflow of the mixture from the bottom of the Couette is collected at approximately one minute time intervals. Samples (of approximately 80 grams) were collected and analyzed using color image analysis shown in Figure 35 (SolidSizer*, JM Canty Inc. Buffalo, NY). The powder sample is fed through a vibratory feeder at controlled rate to form a mono-layer "curtain" of particles that fall from the chute in front of the color sensitive camera. The important parts of the system are the mono-layered curtain, the front (reflective) lighting system and the fast frame color camera and analysis software for particle detection. The automated procedure identifies particles as 2D images using threshold brightness and then calculates size, shape and color for each particle image (Figure 36).

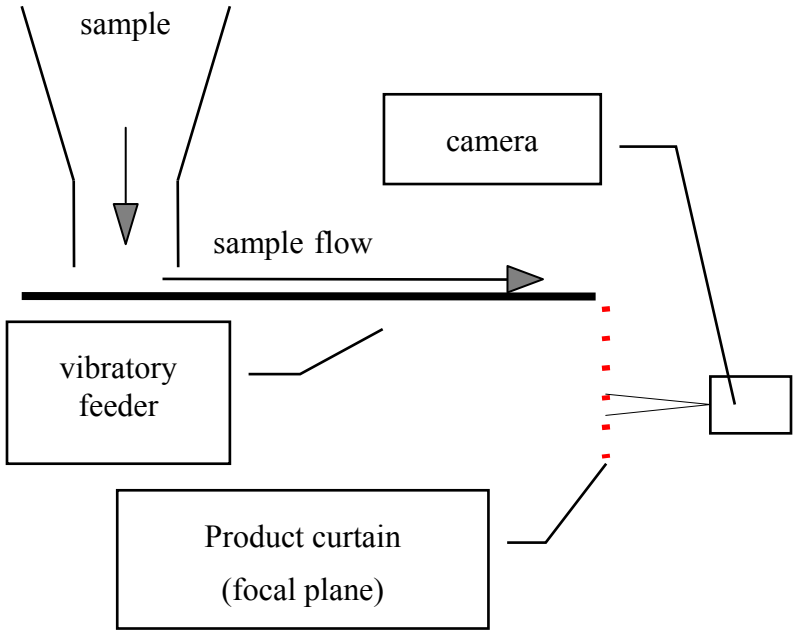

Figure 35: Schematic of the Colorimeter. SolidSizer, *JM Canty Inc*

Sufficient frames are obtained to sample 10,000 particles from which size and color distributions are calculated.

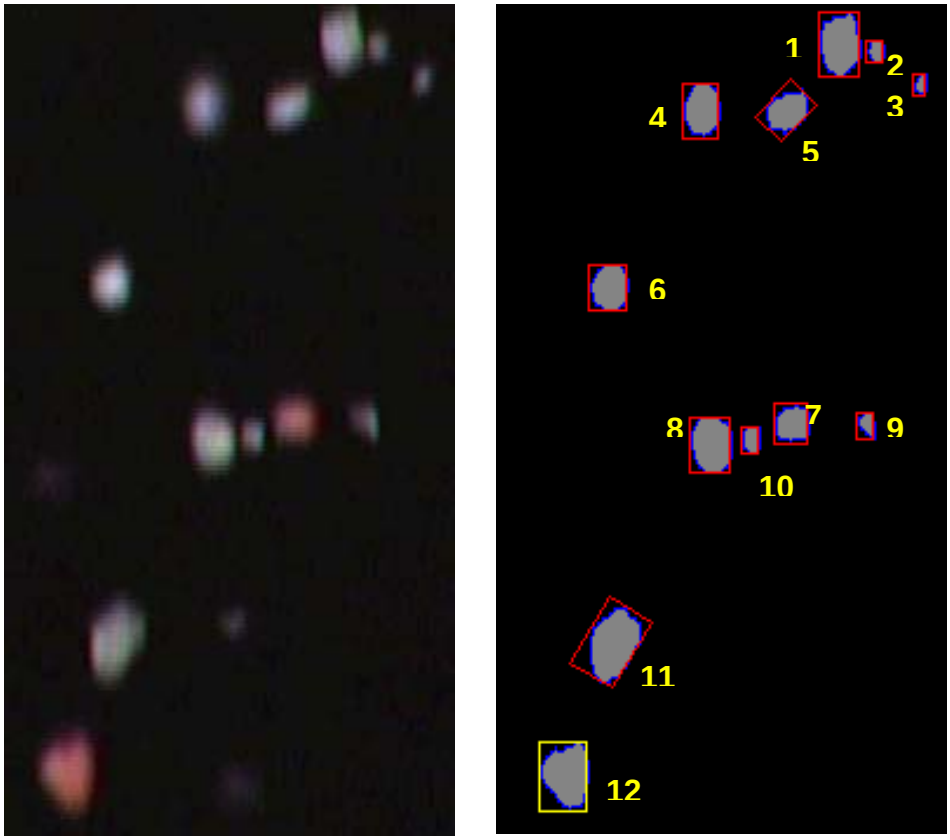

Freeze-frame image of particles

Binary image after brightness thresholding

Figure 36: Bivariate image analysis for size and color

Particle color is measured from the color-camera by identifying three major colors R-red, G-green and B-blue from the reflected light on a black background. Since the tracer particles are red (in this case), the amount of red (R) relative to the total brightness (R+G+B) was used as a relative red characteristic [R%=R/(R+G+B)]. White base particles have a relative balance of colors, i.e., a peak of R% ~ 31%. Red tracer particles

have a discrete peak at R% ~ 37%. Based on these measureable color differences, a threshold of R% > 36% was used to identify tracer particles. For example, in Figure 36, particles 7 and 12 are identified as tracers based on their color being above the red threshold, while the remaining are white base particles.

5.2.3 Results and discussion of tracer experiment

Figure 37 gives a typical result from a tracer experiment using the white base and red tracers, as concentration versus time. Each data point in the Figure 5 represents one sample taken from the hopper outlet. For each sample, the image analysis was done to measure the concentration of red particles versus white particles, based on particle color threshold described previously. The concentration of the tracer is made dimensionless with the average concentration C_0, as $C_\theta = C(t)/C_0$ while time is made dimensionless with the average axial velocity, u and the average bed height, L as $\theta = tu/L$. The axial velocity is calculated as an average from the vertical flow rate and the dimension of the shearing gap. The Peclet number is defined as Pe=uL/D, where D is the dispersion coefficient.

Figure 37 shows the experimental values (in blue, diamonds) and four theoretical response curves using the classical Residence Time Distribution model (Levenspiel, (1972)) for several different values of the parameter D/uL=1/Pe from 0.002 (small dispersion) to 0.2 (large dispersion). As seen, the experimental data are apparently bi-modal having a main peak with limited dispersion (D/uL ~ 0.015) and the delayed peak having more dispersion. Overall, the data fall somewhere in the middle of the range showing that the flow is somewhat dispersive with a diffusion coefficient of approximately D~1.1 cm^2/min (resulting from 1/Pe~0.02).

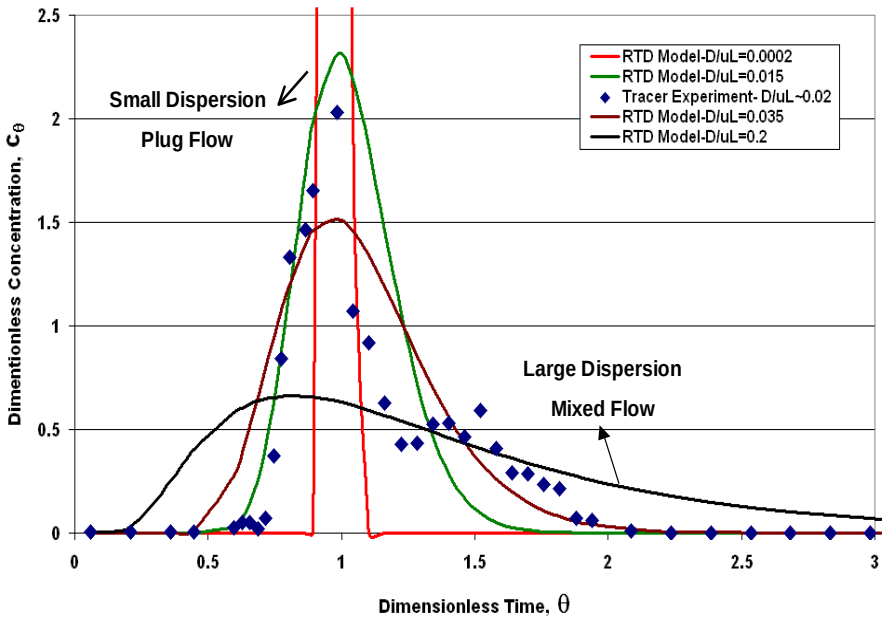

Figure 37: Dimensionless concentration vs. dimensionless time for red tracer particles

The time required for the main peak of tracer to move through the device is approximately 32.6 minutes (Figure 38a); notice that initial tracer particles appear as early as 20 to 25 minutes. It is interesting that the relative size of the red tracer particles is coarser just before the main peak time (t_{peak}) and then becomes finer over the duration of the peak, before stabilizing with extended time (Figure 38b). This trend of tracer particle size with flow time is even more apparent when the tracer size is normalized to the base particle size (Figure 38c). Further, the weighted composite of the normalized size distribution (Equation 5.1) plotted against offset time ($t - t_{peak}$) over a peak interval of about +/-12 minutes (Figure 38d) shows a trend of particle size with time, suggesting coarser tracer particles have a faster axial flow speed compared to finer tracer particles in the Couette. The size trend function is overlaid on the data of Figure 38c; for

visualization, the trend is extrapolated beyond the range of its applicability. Note the trend function pertains only to the transition from base to tracer particles in the domain of the main peak of tracer flow (~20 to 45 minutes).

$$Dx_{tracer}/Dx_{base} = 20\%*D10_{tracer}/D10_{base} + 60\%*D50_{tracer}/D50_{base} + 20\%*D90_{tracer}/D90_{base} \quad (5.1)$$

This analysis suggests a potential linkage between particle size, velocity gradient across the gap in the Couette (radius) and the observed axial flow rate; i.e., coarser particles apparently migrate toward the higher shear field near the inner moving surface while finer particles migrate toward the outer radius of the Couette.

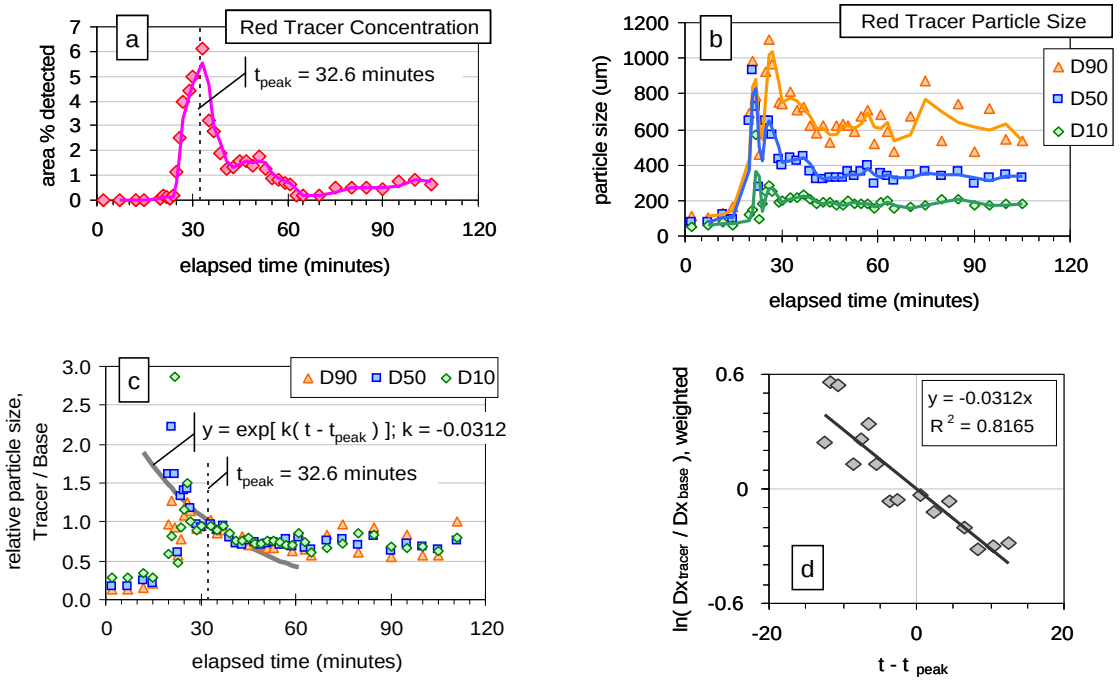

Figure 38: Raw data for tracer flow: a) tracer concentration over time; b) tracer particle size distribution over time. Analysis of tracer flow data: c) normalized particle size distribution (Tracer/Base) with overlaid size function; d) regression analysis of normalized size data, offset to the peak tracer flow time (tpeak)

As a proviso to the above discussion, one has to observe that the trajectory of particles in the axially flowing Couette is actually not simple and is comprised of flow in the

shearing gap in addition to radial flow in the mass flow conical hopper. However, while the hopper flow may marginally contribute to the measured dispersion, it is unlikely that the hopper flow is causing acceleration of the coarser particles. The observed size effect is most likely related to the shear gradient in the Couette cell.

To examine the flow pattern in more detail, we performed a controlled experiment using model materials with only two sizes of glass bead particles, 0.1 mm beads as base particles and 0.5 mm beads as tracer. The experiment was performed by filling the bed with base particles and establishing a steady state flow by maintaining a constant overburden and changing the feed (at time t=0) to 0.5 mm particles thereby creating a "step". The evolution of the step was then followed at the discharge of the Couette device, taking samples at regular time intervals as described above. The tracer was separated by sieving and by measuring the weight fraction of larger particles in the discharged stream.

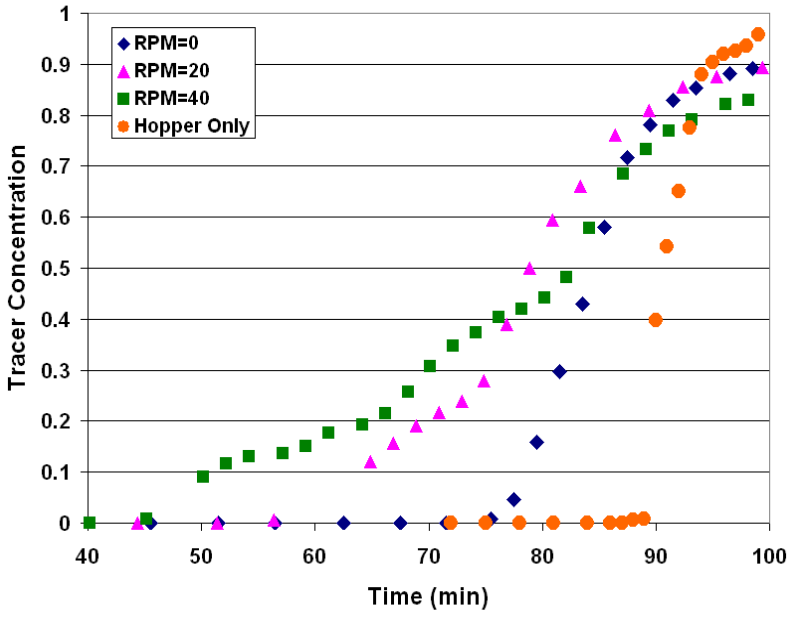

Figure 39: Tracer experiment with 0.1 and 0.5 mm glass

The experiments were performed with different axial flow rates and several different shear rates. A typical set of results is given in Figure 39 as the weight fraction of 0.5 mm glass beads versus time. The response in Figure 39 is given starting at a time t=40 minutes for three shear rates at 0, 20 and 60 RPM (there were no large particles detected before t=40). The fourth experiment in Figure 39 (hopper only) is the response to the same transition of 0.1 mm particles to 0.5 mm glass beads only using the hopper and no insert in the Couette device. The data is shifted 70 minutes to the right as the time of flow through the hopper only is much shorter compared to the whole device. This experiment was performed to show that in the mass flow hopper with polished metal walls, the flow of the material is almost perfectly plug flow with an almost flat velocity distribution and significant slip on the wall. This behavior can be inferred from the steepness of the response in Figure 39.

As seen in the Figure 39, the average time for the "step" to move through the device is about 75 minutes when the bed is at rest (no shear). Increasing the shear rate reduces this time significantly at constant axial flow rate (~2.8 g/sec) to 56 minutes at 20 RPM and 45 minutes at 60 RPM. We also calculated dispersion coefficients characteristic to the response curves depicted in Figure 39.

Table 3: Dispersion coefficient of 0.5 mm in diameter round glass beads at different angular velocities (RPM) of the inner cylinder

Rotation Rate(RPM)	Time for first tracer to exit (min)	**D** (cm^2/min)
0	**75.5**	**0.19**
20	**56.4**	**0.36**
60	**45.2**	**0.58**

The data is given in Table 3 and values appear to be quite close to those obtained with the detergent, despite the fact that the geometry is slightly different, i.e., the shear gap is 1.27 cm larger and the average size of base particles (glass) is smaller (0.1 mm compared to an average of 0.45 mm).

We see from the above results that dispersion (mixing) increases by increasing shear rate as particles closer to the rotating cylinder move faster axially than those situated towards the stationary wall. This suggests that a shear band forms near the rotating cylinder where both shearing and axial flow are more intense and a plug flow type of pattern develops outside of the shearing band as shown schematically in Figure 40.

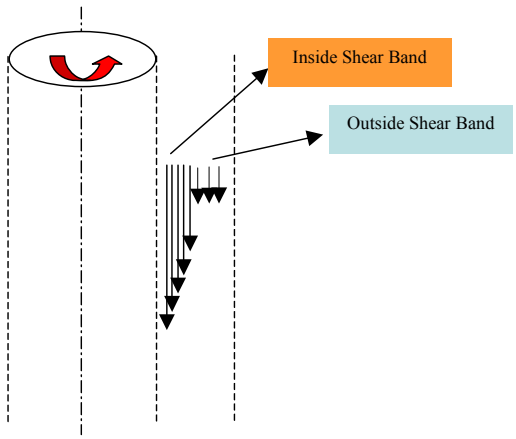

Figure 40: Schematic representation of the shearing layer

This figure also explains the previous finding where larger particles flow faster in the shear gap then smaller particles. This is because in the sharing band the material is looser and less compact, i.e., has a lower solid fraction, and larger particles have enough space to move faster. The disadvantage of the present experiment is that it gives no precise indication as to the relative thickness of the shearing band to the overall width of the

shear gap. Theoretical calculations (for example Tardos et al, 2003) suggest for the shear band an overall thickness of around 10-13 particle sizes in diameter. This solution applies to plane shear, to the case when velocity fluctuations become large and the granular temperature comes into play. Other values from experiments suggest 5-10 particle diameters for tightly packed smooth particles and up to 40 particle sizes in the split-bottom cell, as discussed above (see also Table 5). Work to measure the actual thickness of the shearing band in relation to the width of the shear gap in the axially flowing Couette device is described in part 3 of this chapter.

5.2.4 Segregation studies

Even though larger tracer particles were found to move faster in the shearing band, axial segregation in a continuous steady state flow is not significant. To demonstrate this behavior more thoroughly, an additional experiment was performed with 0.1 mm in diameter glass beads as base particles. The "step" was created as described previously but instead of mono-disperse particles; a 50/50% mixture of 0.5 and 1 mm glass beads was used as tracer. Results from this experiment are shown in Figure 41.

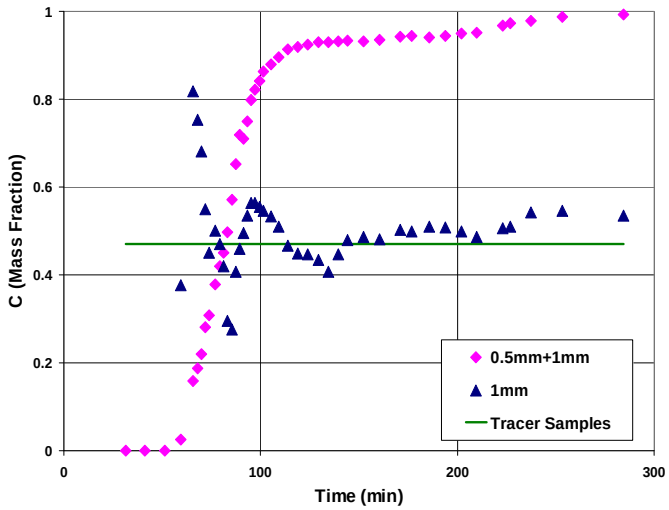

Figure 41: Segregation studies with 0.1, 0.5 and 1 mm in diameter glass particles

The blue triangles show the mass fraction of 1 mm diameter particles relative to the total tracer composition. The red diamonds show the mass fraction of the tracer mixture (0.5 and 1 mm diameter glass beads) relative to the total experimental composition (0.1, 0.5 and 1.0 mm beads). The undisturbed tracer sample composition (ratio of 1 mm beads to the 0.5 and 1 mm tracer blend) is also shown in the figure (green line). The mass fraction of the largest particles, 1mm in diameter, shows an initial maldistribution as the concentration fluctuates when the flow is disturbed by the step function in somewhat similar way as the red tracer in the experiment with the white base detergent (Figure 38). Subsequently however, the concentration becomes stable at approximately the value of the composition of the undisturbed sample (~50/50%). This clearly shows that there is no significant axial segregation in the continuous Couette cell at steady state. Rather, segregation seems to be driven by a radial gradient in the flow field and is therefore seen only as the flow transits from the base to the tracer particles. A schematic picture of the coupling between radial gradients and axial flow is depicted in Figure 40.

5.3 Solid Volume Fraction and Shear band Thickness

5.3.1 Measurement of Solid Fraction in a Continuous Couette Cell

Solid volume fraction can be measured using the capacitance probe available commercially from Capacitec, Inc. (Louge and Opie, 1990; Louge et. al., 1996). The commercial instrument is made to measure small distances with great precision but it was modified for the present experiment to detect solid fraction. This is achieved by filling the "detection volume" of the probe with powder and performing a thorough calibration of the powder's dielectric constant at different porosities. The knowledge of the porosity

in the shearing bed and its variation is crucial to understanding the behavior of the material. There is a significant difference in the behavior of the shearing layer in the batch, no-flow and the continuous-flow Couette cells (Kheiripour Langroudi et. al., 2010a). It was shown in this work that while in the batch mode the torque increases continuously, by draining a small amount of material in the axial direction (continuous Couette), the value of the torque decreases and it reaches a steady state. To investigate the reason for such a change we measured the solid fraction in both batch and continuous modes. Mounted on the stationary wall, the probe measures the change in solid fraction in a semispherical volume of about 3 mm in diameter. To reach inside the shearing gap, the probe is physically pushed inside, parallel to itself in equal steps of 1 mm using a caliper.

We showed previously (Kheiripour Langroudi et. al., 2010a) that there is no path from quasi-static to rapid (collisional) flows by increasing the shear rate, if the particles are constrained from further dilation. In fact in our traditional Couette cell (batch mode, without axial flow) stress builds up and the torque increases in such a way that the range of the torque- meter is exceeded and the experiment has to be stopped. However, by continuously removing a small amount of material in the axial direction, the torque (shear stress) decreases and the regime of flow shifts from quasi-static to "intermediate" where the shear stress-shear rate relationship exhibits a power-law dependence (Kheiripour Langroudi et. al., 2010a).

A picture of the capacitance probe used in this study, the electronic circuit together with the calibrating cylinder is given in Figure 42. The probe is mounted flush to the outer wall of the calibrating cylinder, as shown. The porosity measurement requires a very thorough calibration since the capacitance of the powder varies with the amount of gas

(air) trapped in the system. The system depicted in Figure 42 achieves this by filling the cylinder with the appropriate powder and tapping it continuously so that densities from free filling to highly packed can be achieved. The conditioned signal is then connected to a data acquisition computer specially designated for this measurement. In a real experiment, the probe is mounted similarly onto the outer wall of the Couette device in a position opposite to the normal stress measuring device so as to measure the normal stress and the porosity at the same height in the bed.

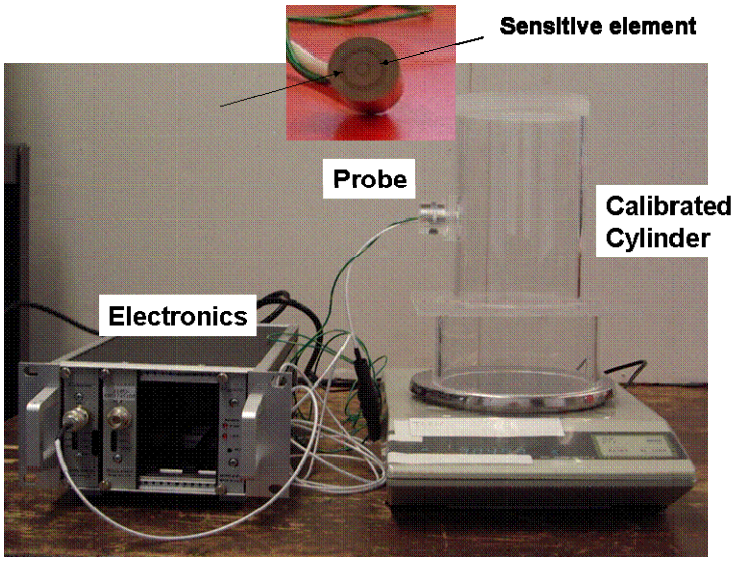

Figure 42: Capacitance probe and calibration circuit with detail of the probe head

We show several examples of solid volume fraction measurements in both batch and continuous modes at two different positions. Figures 43 and 44 show simultaneous results of torque and solid fraction in the two modes of operation, batch and continuous, on the outer stationary wall (Figure 43) and in the shearing zone (Figure 44) for 0.5 mm crushed glass as a function of time. The experiment entails the filling of the bed with particles to an overburden height of approximately 20 cm and measuring the torque and solid fraction

in the batch mode. Subsequently, a constant axial flow is established and the torque and solid fraction are again monitored as a function of time.

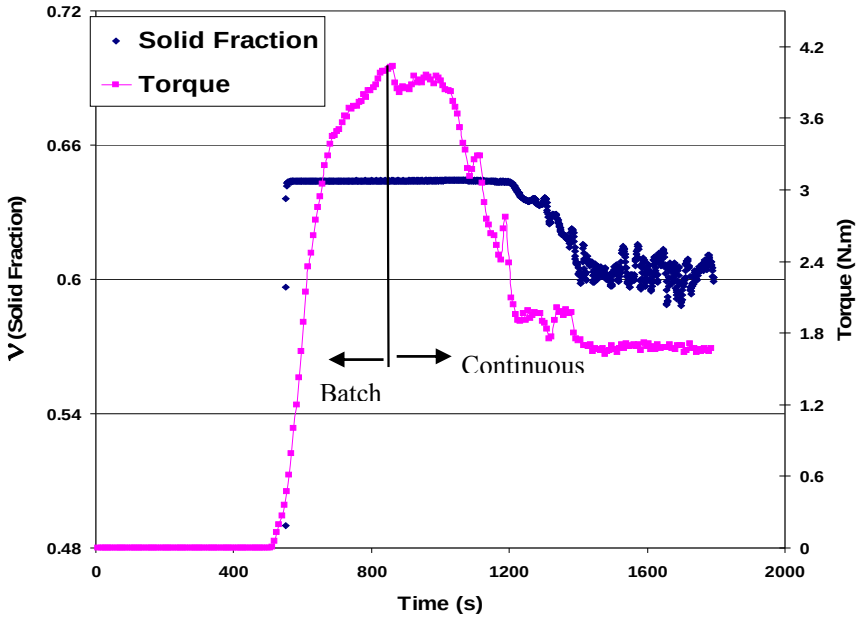

Figure 43: Torque vs. solid fraction measured on the stationary wall in batch and continuous Couette for 0.5 mm crushed glass

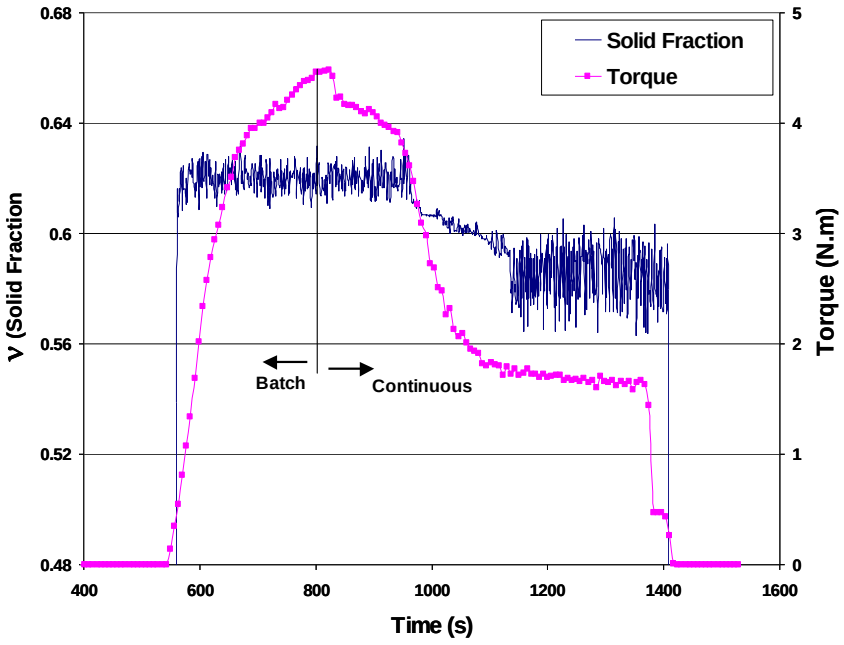

Figure 44: Torque vs. solid fraction measured on the stationary wall in batch and continuous Couette for 0.5 mm crushed glass

As seen in Figures 43 and 44, the torque increases when the bed is in batch mode; the solid fraction also increases and reaches its maximum value as the granular bed is constrained from further dilation. Upon continuous removal of particles ("continuous" in the figure), the torque reaches a maximum and then starts to decrease to reach a steady value. The solid fraction exhibits similar behavior except that it takes somewhat longer for the axial flow to affect the decrease in solid fraction. In both cases, one can see that after starting the axial flow (denoted by "continuous" in the figure), both torque and solid fraction decrease but the response of the torque is faster. In addition, the fluctuations of solid fraction increase when one goes from batch to continuous mode. The decrease in solid fraction indicates that the change of regime happens because particles gain freedom of movement in the space around them so that they can actually move freely past one another and may also collide. Comparing Figures 43 and 44, it can be seen that it takes more time for the particles trapped outside of the shear band to start dilation compared to the particles inside the shear band due to the fact that the axial flow has more impact on the active shearing zone than on the dead zone (as shown in Figure 40). Also, by comparing results from Figures 43 to 44, the average value for solid fraction is less when it is measured close to the rotating wall (inside the shear band) compared to the outer wall (outside of the shear band) even when there is no axial flow, due to the shearing in radial direction, as this flow is more intense near the shearing wall. The same argument can be used to explain the fact that fluctuations in solid fraction are higher everywhere for the case of continuous compared to the batch mode. During a similar experiment with finer and more deformable powder, 0.3 mm ground (odd shape) Polyethylene (Figure 45), we again see that the axial flow prevents the bed from further packing and increase in torque.

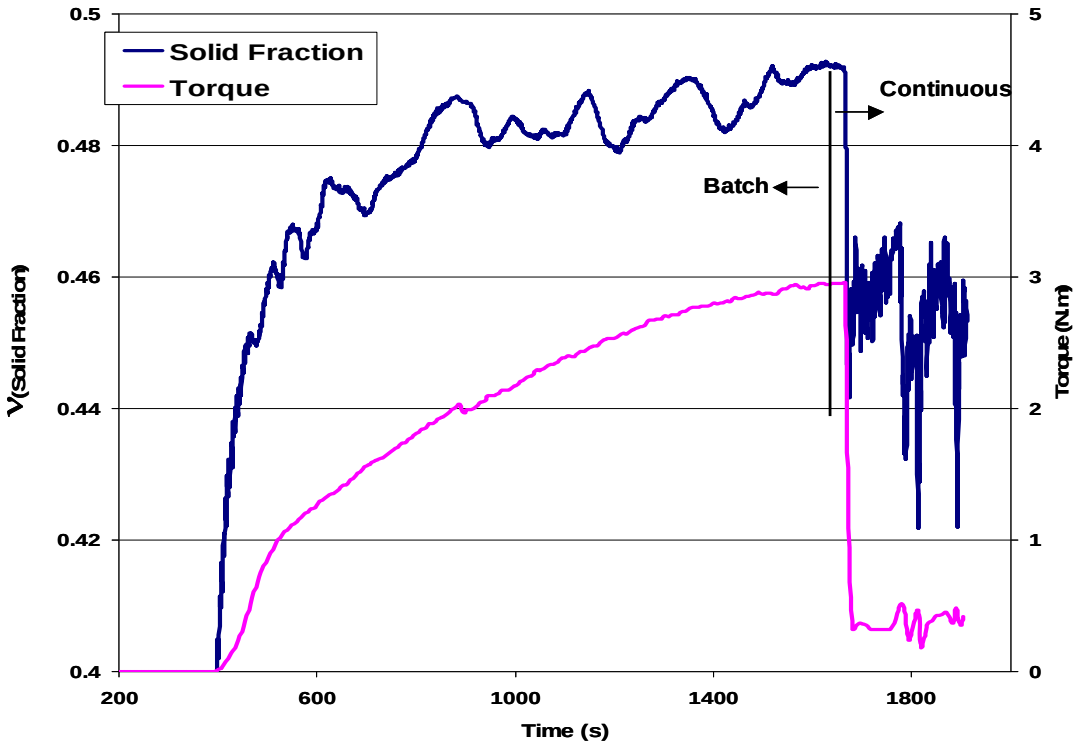

Figure 45: Solid fraction and torque in the Couette with 0.3 mm Polyethylene chips

Furthermore, both the torque and solid fraction respond faster to the onset of axial flow (denoted "continuous" in the figure) than in the case of the more rigid (glass) powder and they decrease together almost simultaneously. Change in solid fraction by imposing the axial flow is higher for the fine, odd-shaped (more compressible) particles as compared to the rigid (incompressible) powder. Table 4 shows the average value and standard deviation of solid fraction for different particles in batch and continuous modes at a constant angular velocity of 15 RPM. In all cases, the solid fraction decreases and its fluctuations increase by changing the mode of the experiment from batch to continuous. Note in Figure 45, that the actual change in solid fraction by imposing the axial flow for ground Polyethylene (soft, compressible) is higher because the packing is not complete and the solid fraction is still increasing when the change from batch to continuous mode

occurs. For all other cases the solid fraction reached its maximum value and it does not have the tendency to further increase; this can be confirmed by comparing the standard deviation of solid fraction of Polyethylene particles and glass particles.

Table 4: Solid fraction in batch and continuous Couette for different materials

Material	ν (Batch)	Standard Deviation	ν (Continuous)	Standard Deviation	Change in ν (%)
1 mm Round Glass	0.6405	0.00253	0.6161	0.00638	2.44
0.5 mm Round Glass	0.6356	0.00021	0.6046	0.00565	3.1
0.5 mm Crushed Glass	0.6441	0.00011	0.6133	0.00552	3.07
0.3 mm Crushed PE	0.4832	0.00568	0.4484	0.00931	>3.48

5.3.2 Identifying the Shearing Layer Thickness in a Continuous Couette Cell

Further measurement of solid fraction on the stationary outer wall of the continuous Couette cell at different angular velocities shows that increasing shearing rates results in packing of the material. Measurements of solid fraction close to the inner rotating cylinder, on the other hand, show that by increasing the shearing rate, the bed of granular matter dilates more and this is in agreement with the tracer experiment presented previously. Having two distinct behaviors (packing vs. dilation) in different regions indicates that shearing of materials inside the shear band pushes some materials toward the outer wall**.** Figure 46 shows results of a measurement for 1 mm round glass particles at nine positions as the capacitance sample head is moved from the outer stationary wall towards the inner rotating cylinder in steps of about 1 mm. Since the shearing gap is about 25 mm wide (about 1 inch), there are at most 25 steps. Each data set corresponds to

a certain distance from the rotating wall that has been specified by particle size. For example, data at $25d_p$ results from a measurement flush with the stationary, outer wall while a measurement at $6d_p$ is six particle diameters away from the rotating wall. It is clear that the solid fraction increases by increasing shear rate further from the moving wall at $25d_p$, $23d_p$, $21d_p$ and $19d_p$ (blue lines in the figure).

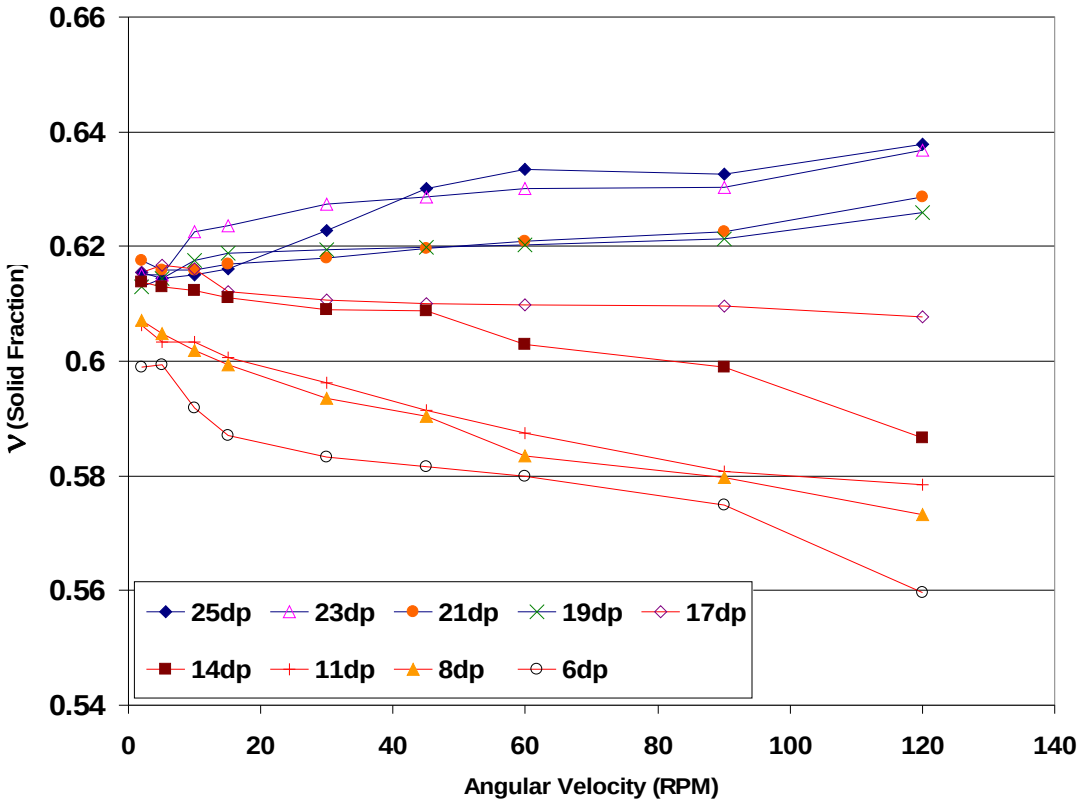

Figure 46: Solid fraction at different shearing rates and distances from the rotating wall in a continuous Couette experiment for 1 mm round glass

Closer to the inner rotating wall (17-particle sizes in diameter and less), the solid fraction tends to decrease by increasing shearing rate (red lines in Figure 46) indicating that the active shearing zone has been reached. We conclude that in this case the thickness of the shearing layer is around 18-particle sizes. This shows that continuous removal of

particles increases the thickness of the shear band since in a tightly packed bed of this width it was found the layer to be of the order of only 10 particle sizes (GDR MiDi 2004).

5.3.3 Effect of Shape on Thickness of the Active Shearing Zone

In order to consider the effect of shape on the width of the active shearing zone we used 0.5 mm crushed (odd shape) glass particles (Figure 47). Unlike in Figure 46, in this figure, we plotted the solid fraction data versus the distance from the moving wall (left side of the figure) with the shearing rate as a parameter. We found that almost all curves intersect at a distance of approximately 24-particle sizes away from the moving wall in such a way that beyond that point, the particle is located in the packed zone and below it the particle is in the shearing zone.

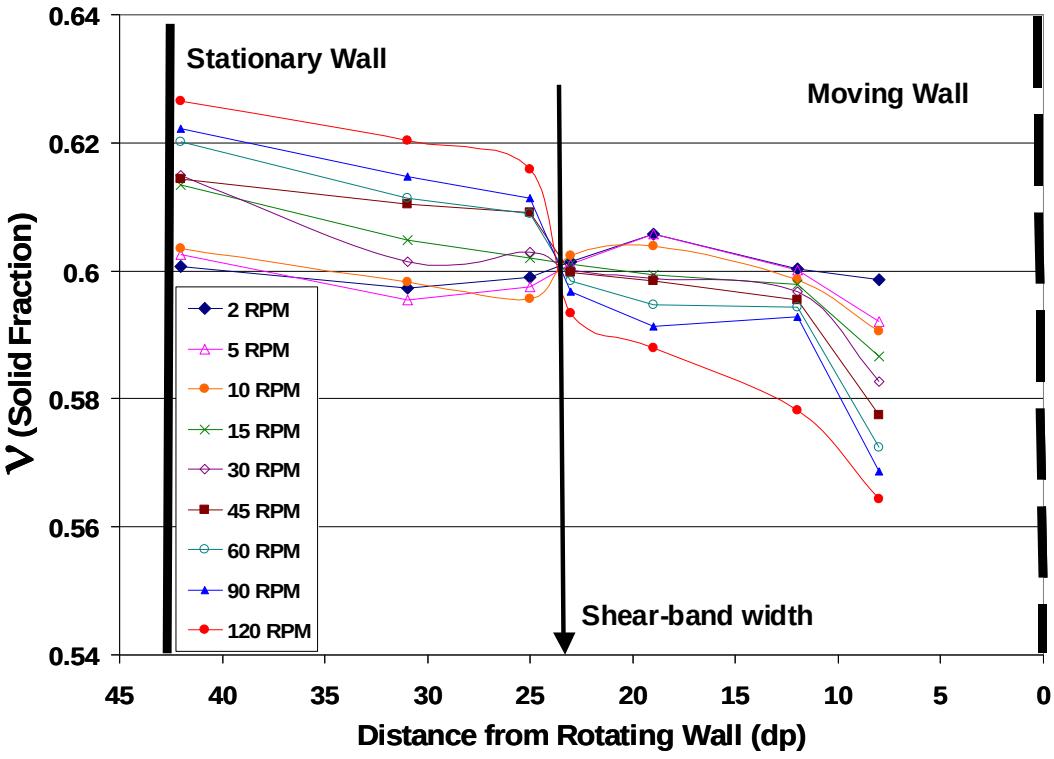

Figure 47: Solid fraction at different distances and shearing rates from the rotating wall in a continuous Couette experiment for 0.5 mm crushed glass

Compared to 1 mm round glass, we can see that the shear band extends by at least 7-particle sizes for the odd-shaped particle. Having irregular shape helps the particles to arrange in different configurations so that the shear band increases. Previous PEPT (positron emission particle tracking) measurement for the same particle (0.5 mm odd-shaped) yielded 14-particle sizes for the case of a batch Couette experiment without axial flow. This confirms that the axial flow increases the width of the shear band by up to 10-particle sizes or almost by a factor of two. Table 5 contains data from our measurements presented above (using the capacitance probe) and additional measurements with 0.5 mm spherical particles, data for 0.5 mm odd shaped particles and data from other researchers.

Table 5: Shear Band Thickness (expressed in number of particle diameters) in different types of Couette cells obtained from different experimental techniques

Material	Particle Size (mm)	Shape	Type of Couette	Wall Roughness	Technique	Shear Band (d_p)
Mustard Seed	**1.8**	Round	Batch	Rough	MRI Mueth et. al., 2000	**6-10**
Glass	**0.3**	Round	Split-Bottom	Rough	CCD Camera Fenistein & van Hecke, 2003	**Up to 40**
Glass	**1**	Round	continuous	Rough	Capacitance Probe	**17-19**
Glass	**0.5**	Round	continuous	Rough	Capacitance Probe	**16-18**
Glass	**0.5**	Round	continuous	Smooth	Capacitance Probe	**9-11**
Glass	**0.5**	Odd	Batch	Rough	PEPT Seville & Ingram, 2004	**14**
Glass	**0.5**	Odd	continuous	Rough	Capacitance Probe	**23-25**

It can be seen in the table the large variation of shear band thickness with experimental conditions. The largest width appears to occur in the split-bottom cell (up to $40d_p$)

followed by the odd-shaped particles in the axially flowing bed (23-25d_p) and by the round spheres in the same bed. A smaller thickness is exhibited by all batch flows where the flow is constricted and confined without the possibility of dilation.

In all previous experiments, the roughness of the rotating wall was chosen to be very close to the internal friction coefficient of the particles. In order to study the effect of wall roughness we used 0.5 mm round glass (ϕ~27°) and substituted the rough wall with a Lucite wall on which the wall friction is less than the particle internal angle of friction (ϕ_w~11°)**.** The result is show in Table 5 and one can observe that the thickness of the active shearing zone (shear band) decreases by 7-8 particle sizes when a rough wall is replaced by a smooth wall. This is expected since, due to slip on a smooth wall, the velocity of particles close to the rotating wall is always lower than on the rough wall so that the particle velocity in the angular direction decays faster and closer to the moving wall.

5.4 Conclusions

We found that the flow pattern inside a Couette cell with axial flow is dispersive and mixing increases by increasing the shearing rate. In addition, while the Couette cell with axial flow of polydisperse material comes to a steady state, there is evidence that radial gradients in the flow field may couple with particle size and shape distributions. In essence, larger particles migrate to higher shear zones while smaller particles move in the direction of lower shear. This conclusion is consistent with literature discussions of avalanching on a free surface where larger particles move to high-shear regions and smaller towards the lower – the main difference is the presence of the free surface that

does not exist in the Couette device. By analogy, the dilation that is enabled by the Couette cell's axial flow is similar to the cascading free surface in the avalanche or heap flow. We see that in dense granular flows with distributed sizes and well-defined shear regions, particles move along shear gradients according to their relative size.

Comparing the results at zero shearing rate with values at higher shearing rates it was found that the particles inside the shear band move faster axially than those trapped outside of the active shearing zone. The picture that emerges is that in the region where the bed is highly sheared, the axial velocity is somewhat higher in the average and the solid fraction is lower. Shearing extends into the bed to some depth depending on particle shape and size while beyond that zone the bed is packed and moves slowly in the axial direction.

Employing a capacitance probe, we showed that addition of the axial flow to a regular Couette cell, results in decrease of the solid fraction that provides space for the collisions between particles to occur. Our experimental results revealed that while on the outer stationary wall particles pack at increasing shearing rate, they dilate when the solid fraction is measured close to the rotating wall. Furthermore, we used the capacitance probe to measure solid fraction as a function of position and shear rate in the shear gap and thereby measured the thickness of the shearing layer. We found that, the shearing layer starts when the solid fraction decreases due to an increase in shear rate (velocity in radial direction decays as one moves from the rotating to the stationary wall). Previous studies in a traditional Couette cell predicted the shear band to be 10-14 particle sizes close to the rotating wall and our experiments show an increase to between 18-24 particle sizes when the axial flow is present. The solid fraction decreases and its fluctuations

increase when the material is allowed to dilate by superposing an axial flow on the Couette cell's tangential and radial flow fields. From the experiments conducted in the Couette device, it appears that the axial flow rate has a minor influence on solid fraction, i.e., once the material is flowing the solid fraction does not change significantly upon an increase in the axial velocity. We found experimentally that the thickness of the shearing layer increases by replacing round by odd shaped particles. In addition, decreasing the roughness of the rotating wall decreases the thickness of the shear band significantly.

6 Importance of Dilatancy on Rheology and Flowability of Compressible Powders

6.1 Introduction

In this chapter we present our attempts to find the connection between rheology, dilatancy and mass flowability of compressible powders (Kheiripour Langroudi and Tardos, 2010). Rheological properties were obtained in the Couette shearing cell (Kheiripour Langroudi et al., 2010a) presented in Chapter 4 where it was shown that even this geometry, well-studied in the field of Non-Newtonian Fluid Mechanics, had to be modified for powders by adding a slow axial flow super-imposed on the radial shear field, in order to allow the powder to actually dilate (Kheiripour Langroudi et. al., 2009). In this geometry we were able to measure shear (from torque) and normal stresses (with a remote sensor developed in Kheiripour Langroudi et al. (2010b) and presented in Chapter 3) inside the active shearing zone of the granular layer and we found that the regime of flow can be shifted to intermediate from quasi-static if the particles can dilate (collisions can occur). A numerical scheme (FEM) was able to use the continuum equations of motions and validate the experimentally obtained data (Kheiripour Langroudi et. al., 2010a, results are presented in the Appendix A). In an attempt to study the flow pattern of granules in the Couette device, it was revealed that the Couette geometry with a secondary axial flow develops an increased width of the shear band compared to the batch Couette so that the continuum approach becomes more applicable (Kheiripour Langroudi et. al., 2010c).

The basic motivation for this work is to investigate the impact of solid fraction on the rheology of compressible powders and to find a relationship between dilatancy and mass

flowability through an orifice in a continuous type of flow. There is a lack of relevant experiments that allow the granular bed to dilate freely and for inter-particle collisions to occur during flow. In addition, as soon as gravity is introduced into the plane shear geometry or if the shearing is performed in a rotational shear cell, the stress distribution is no longer homogeneous across the shearing zone and the flow-fields are not uniquely defined.

6.2 Rheological Properties and Solid Fraction for Compressible Powders

To study the rheological behavior of compressible powders and to consider the effect of dilatancy, we use the same Couette-type cell (described earlier in Chapter 4) in which the particles are sheared in the gap between an inner rotating vertical, rough cylinder and an outer stationary cylindrical (also rough) wall. The walls of the Couette are made rough by gluing sand paper on the shearing surfaces. The roughness of the walls is chosen to match the coefficient of internal friction of the material thereby assuring a non-slip boundary condition. All Couette experiments were performed with the four inches in diameter and eight inches high, rotating cylinder and six inches in diameter outer housing with relatively low overburden of approximately four inches. The size of the shear gap in all cases was one inch. Couette experiments in this chapter were obtained in the presence of a secondary axial flow (continuous mode) to make sure that both, collisions i.e., a quasi-static, shear-rate-independent and an intermediate, i.e., shear-rate-dependent shear stress (torque), can develop.

A capacitance probe (described in Chapter 5, Figure 42) was attached to the Couette cell to measure solid volume fraction outside and inside of the shear band. The active

portion of the probe is about 10 mm in diameter and approximately 30 mm in length. To measure the solid fraction on the outer wall, the probe is mounted flush to the surface so that it does not disturb the flow. For measurements inside the shearing zone, the probe is inserted to a certain distance from the wall but due to its small dimensions it is expected to only disturb the flow in its vicinity. Furthermore, the "measuring" volume is situated at the inner end of the probe where disturbances due to its presence are minimal (Kheiripour Langroudi et. al., 2010c).

Two different polyethylene powders (previously shown in Table 2, Chapter 4) were selected and physical properties of these materials are summarized in Tables 7. One can see from Table 6 that the two materials are quite different in size and size distribution in that PE-2 is about twice as large compared to PE-1 in average particle size and also somewhat less dense.

Table 6: Physical properties of the polyethylene powders (PE-1 and PE-2)

Material	E (Modulus) MPa	Bulk Density (g/cm^3)	MPS (um)	d_{50} (um)	d_{90}/d_{10}	Span
PE-1	**5.11**	**0.938**	**277**	**298**	**421/136**	**1.54**
PE-2	**4.76**	**0.924**	**500**	**513**	**730/301**	**1.43**

Also, in order to consider the effect of shape and surface texture, scanning electron microscopy (SEM) for the powders have been performed and Figure 48 shows the images. It can be clearly seen that PE-2 is roundish agglomerate with very rough surfaces while PE-1 is a cleaved particle with different shapes and a wide particle size distribution.

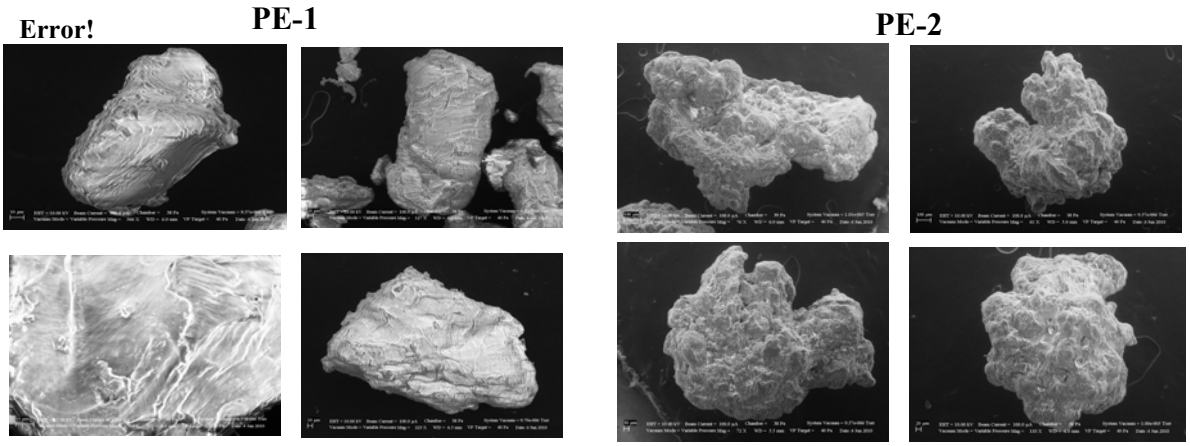

Figure 48: SEM images of the PE-1 and PE-2 done by Dr. Kevin Sung

One important physical characteristic of these Polyethylene powders is their compressible nature. In other words they have the ability to pack or dilate during the flow. To better understand the difference between these particles and glass particle (assumed to be an incompressible powder) the change in bulk density by increasing the pressure on the bulk of granules is illustrated in Figure 49.

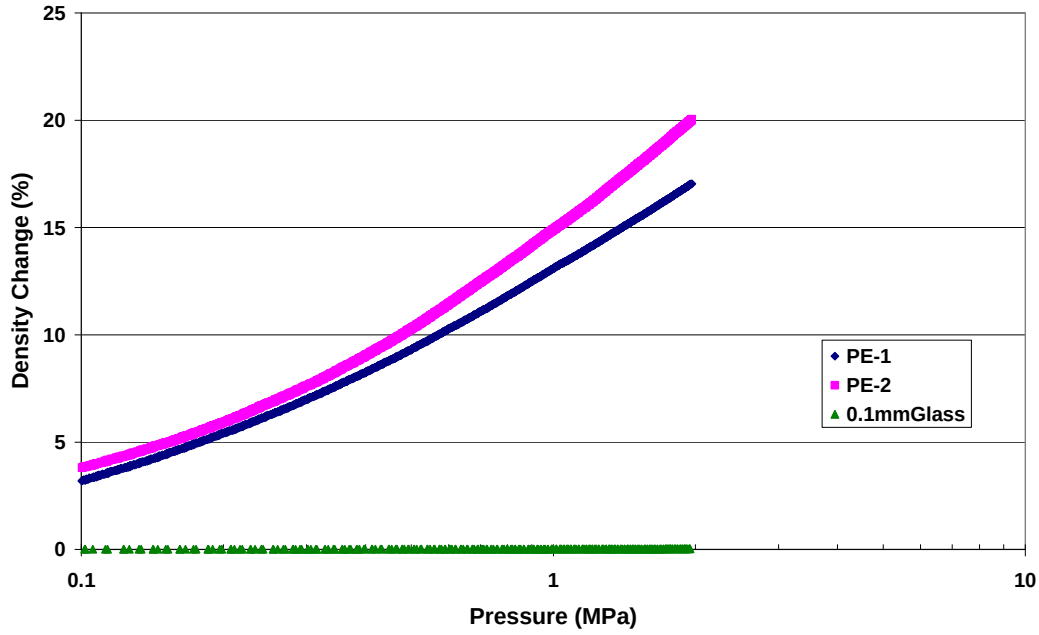

Figure 49: Density change in bulk of particles vs. applied pressure for PE-1, PE-1, and spherical glass

The results depicted in Figure 49 were obtained using an Instron-type indenter (Texture Analyzer). It can be seen that while the change in density for Polyethylene particles is about 20%, this quantity is almost negligible for glass material and it clearly shows that what we mean by the term "compressible" for Polyethylene granules. In fact the compressibility of PE-2 is higher than that of PE-1 as it packs more under the same pressure.

To measure the shear and normal stresses on the shearing wall, and the ratio between them (friction coefficient), we follow the methodology described in Kheiripour Langroudi et. al (2010a&b, Chapter 4). We showed before in Chapter 4 that the normal and shear stresses are linear with cylinder height and therefore the average normal stress is located at the midpoint of the rotating cylinder as is the shear stress calculated from the torque on the cylinder (Kheiripour Langroudi et. al., 2010b). Under these conditions, the "friction coefficient", can be calculated by dividing the values of the average shear stress to the average normal stress. Figure 50 and 51 show the measured normal and shear stresses on the rotating rough cylinder. The stress is given as a function of the product between the shear rate and the particle diameter $(\dot{\gamma} d_p)$ so that all data for the two materials could be shown together on the same graph. The same scale is used in Figure 52a where the "apparent friction coefficients" for the two polyethylene is given as the ratio of the two stresses. At slow shear, the ratio is constant and very close to the internal friction coefficient of the particle. As the shear rate increases the friction coefficient becomes dependent on the shear rate.

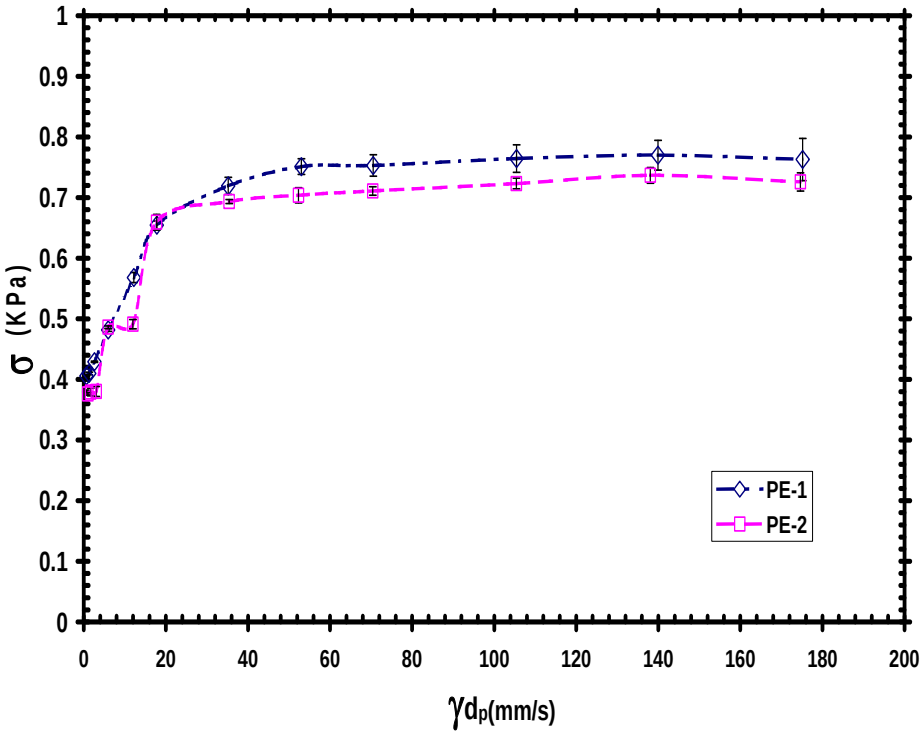

Figure 50: Normal stress vs. shear rate for polyethylene powders in Couette experiment

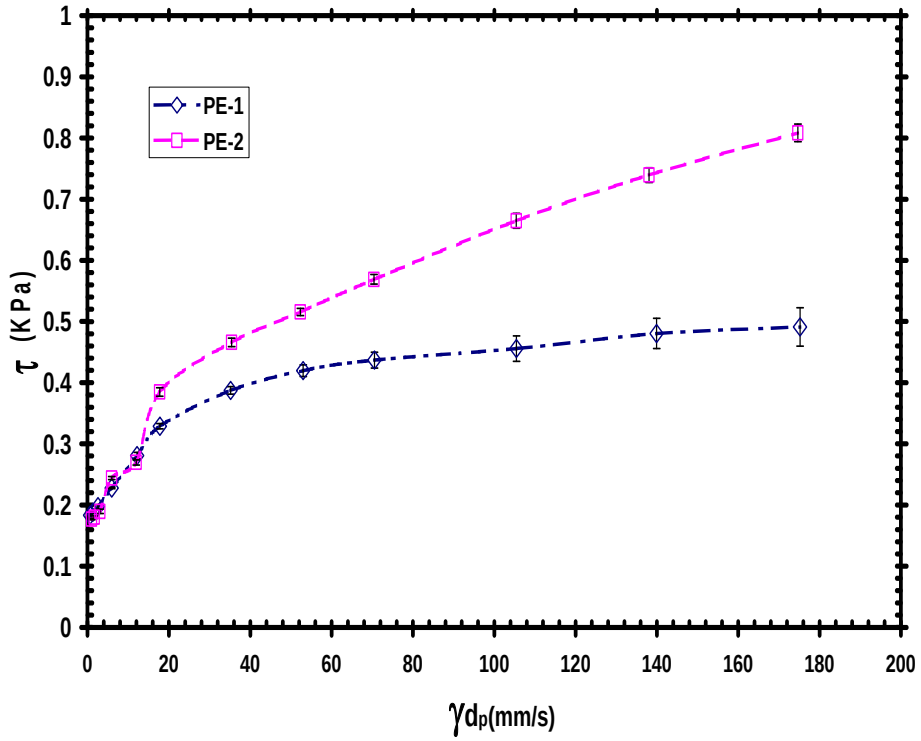

Figure 51: Shear stresses (calculated from torque) vs. shear rate for polyethylene powders in Couette experiment

As discussed earlier, in Chapter 4, this behavior is mainly due to the superposition of collisions between particles on the sliding friction of surfaces.

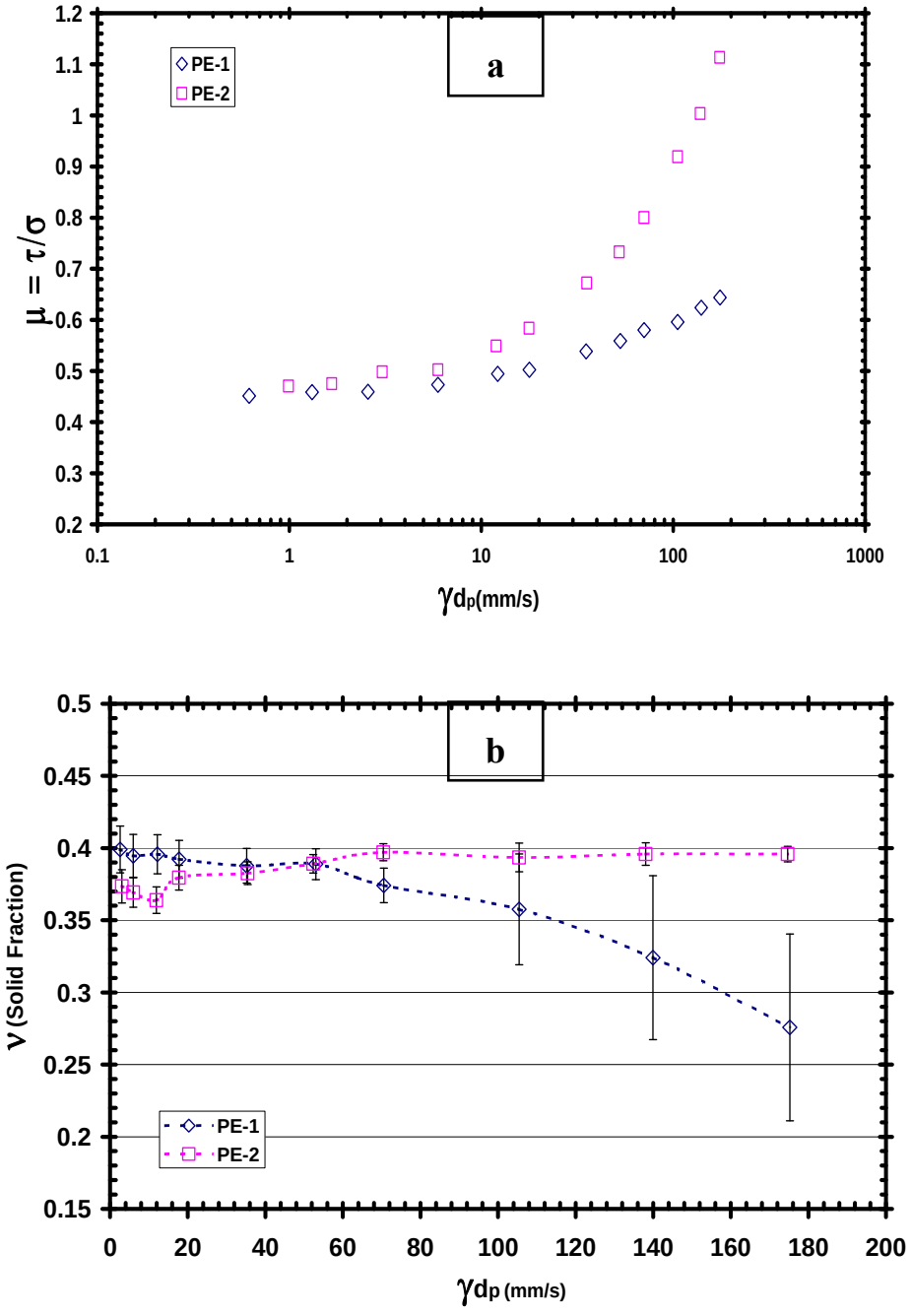

Figure 52: (a) Apparent friction coefficient at different shearing rate for polyethylene powders (b) Solid volume fraction vs. shear rate inside the shear band for the two polyethylene powders

The equations fitted to the experimental data are shown in Table 7 and indicate that the power-law index of the dependency of the apparent friction coefficient on shear rate is higher for PE-2 as compared to PE-1 (as also shown in Table 2, Chapter 4).

Table 7: Rheological models fitted on Figure 52a

Material	Model
PE-1	$\mu = 0.43 + 0.0125\dot{\gamma}^{0.45}$
PE-2	$\mu = 0.45 + 0.0125\dot{\gamma}^{0.68}$

We showed before (Kheiripour Langroudi et. al., 2010a, Chapter 4) that the yield condition obtained from the Couette experiment can be generalized to generate a constitutive equation that holds at both low and higher shear rates. Since the data in Figure 52a are close for the two powders at low shear rates and also close to the tangent of the angle of internal friction, a~tanϕ, one can fit the following equation to the data:

$$\mu = \frac{\tau}{\sigma} = \tan(\phi) + b\left|\dot{\gamma}\right|^{n} \tag{6.1}$$

where τ and σ are the shear and normal stresses and "b" and "n" are coefficients characterized by the experimental curve. To understand the reason for the different rheological behavior of the two polyethylene powders, which are different in their shape and surface texture (see Figure 48), we measured the solid volume fraction close to the inner rotating cylinder. It is well known that in general, powder flows are extremely complicated and the powders studied here are no exception. Furthermore, the present powders are compressible, a property that adds more complication. While the stresses

required by the powder to flow are well represented by the constitutive equation given for all powders in Table 7, porosity or solid fraction also plays an important role. To understand in more detail the rheological model (Table 7) we study the difference in behavior of powders in terms of their capability to change their solid fraction. It is well known that dilation or a decrease in solid fraction is necessary for powders to start flowing. Providing axial flow in the Couette device allows a decrease in solid fraction (Kheiripour Langroudi et. al., 2010c, Chapter 5) and changes the regime of flow from quasi-static to intermediate. The level of stress is higher for the material that has more ability to pack under identical conditions. If the packing of particles becomes looser by increasing the shearing rate, the shear stress-shear rate dependence decreases. In this situation the number of collisions increases by increasing shearing rate but at the same time the bulk density decreases. Furthermore, fluctuations of the solid fraction under high shearing rates can also affect the flowability of powders. We found, for example, that an incompressible, free flowing powder behaves differently outside and inside of the active shearing zone. Increasing shearing rate packs the material outside of the zone and by following the variation of solid fraction of the granular layer from outside to inside, the bulk undergoes dilation. In addition, the solid fraction decreases by increasing shearing rate inside the active shearing zone.

We consider the behavior of the powders inside the active shearing zone where the actual shearing occurs (Figure 52b). In this figure solid fraction data is represented at different shearing rates for the two polyethylene powders PE-1 and PE-2. It can be clearly observed that the higher dependency of shear stress to shear rate (larger power law index, n, see Table 7) is for the particle with less propensity to dilate when the

shearing rate increases. This is due to the fact that large decreases and fluctuations in solid fraction by increasing shear rate results in more stress reduction. On the other hand it is true that faster collisions (that occur at higher shearing rates) require more force but at the same time the system became more dilute and less contacts occur between particles; this reduces the force so that there is always a competition between these two effects. One can see that the powder with the larger power law index "n" (PE-2) shows the least variations in solid fraction and by increasing the shearing rates the system packs to some degree. On the other hand the powder with a smaller power law index "n" (PE-1) dilates the most and the fluctuation of solid fractions for this powder are very high. We can see that dilation and its fluctuation has a very important role in the rheology of powders. The more dilute system requires less shear stress for the entire range of shearing rates.

The behavior outside of the shear band is different, powders generally pack more by increasing shearing rates and the fluctuation of solid fraction is less compared to the behavior inside of the zone (Kheiripour Langroudi et. al., 2010c, Chapter 5). Also the fluctuation of solid fraction at low shear rates is higher than that at high shear rates and finally dilation of material occurs if we move from the outer to the inner shearing zone (this dilation should be more significant for a compressible powder).

6.3 Spinning Disc-Mass Flowability vs. Rheology

In order to find the relationship between rheological properties of the powders and their ability to flow, we designed and tested a spinning disc to extract powder from a hopper. In this experiment, a cylindrical vessel (with a conical feeding hopper on top) is placed

on a flat moving disc with one single orifice located at a certain distance (approximately 10 cm) from the center of the disc. The role of the conical hopper is for continuous feeding and discharge to achieve steady-state flow with constant overburden and zero stress on top of the cylindrical hopper. The capacitance probe was mounted flush to the inner wall of the hopper for the measurement of solid fraction. Figure 53a shows a schematic representation of the device while Figure 53b shows the image of the device.

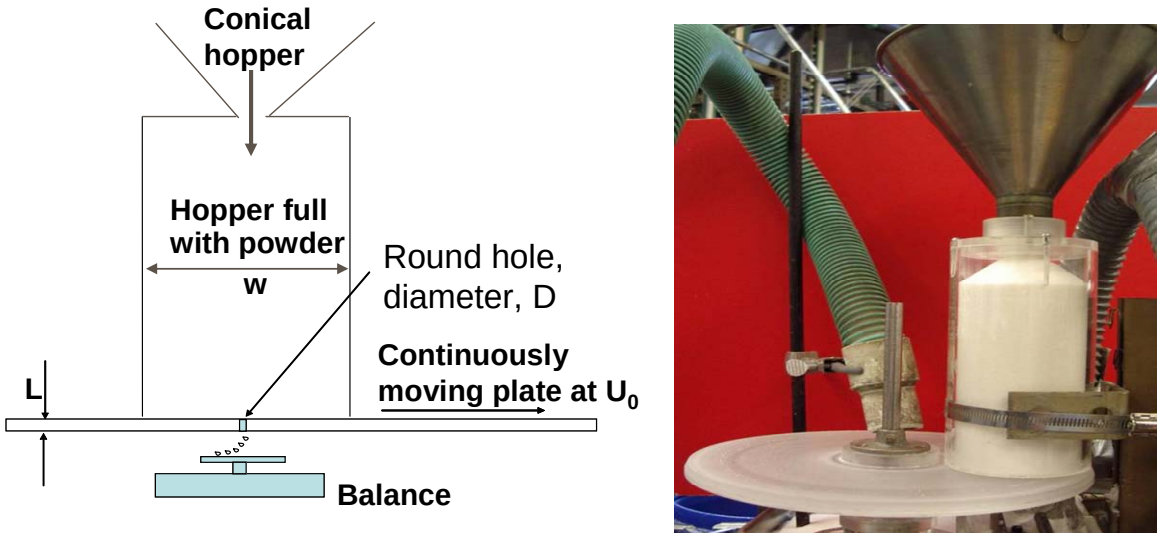

Figure 53: Schematic (a) and picture (b) of the Spinning Disk (Tablet Filling) device

When the orifice of diameter D reaches under the hopper, material fills the orifice and is spilled onto the balance as shown. When the orifice moves out from under the hopper, the flow is interrupted and no material reaches the balance. The disk is put in rotation by a variable speed precision torque-meter so that its speed can be adjusted at will to up to 250 RPM. The shear gap between the hopper and disk is about 300 um (so that in general, the powder cannot escape through the gap). Since slip is always present, the actual velocity of the powder is somewhat lower than the set velocity of the disk. The balance under the spinning disk measures the total mass flow rate through the orifice as

the disk rotates. Having the capacitance probe mounted on the cylindrical hopper (close to the orifice) enables the measurement of the packing or dilation (solid volume fraction) of powders at low and high shearing rates.

Figure 54a shows the mass flow rate (g/s) at different rotational speeds for the two polyethylene powders (PE-1 and PE-2). In order to obtain a meaningful quantity of material that fills the orifice each time it passes under the hopper, the mass flow rate (as a function of time) was divided by the number of times the orifice passes under the hopper (RPM) and the data is given in Figure 54b (the amount of material flowing through the hole at each pass under the hopper) as a function of rotational speed. Figure 54 clearly shows that the best mass flowability through an orifice under high shearing rates is achieved for the powder with highest rheological index "n" which is the one with highest packing (least dilation) during Couette flow.

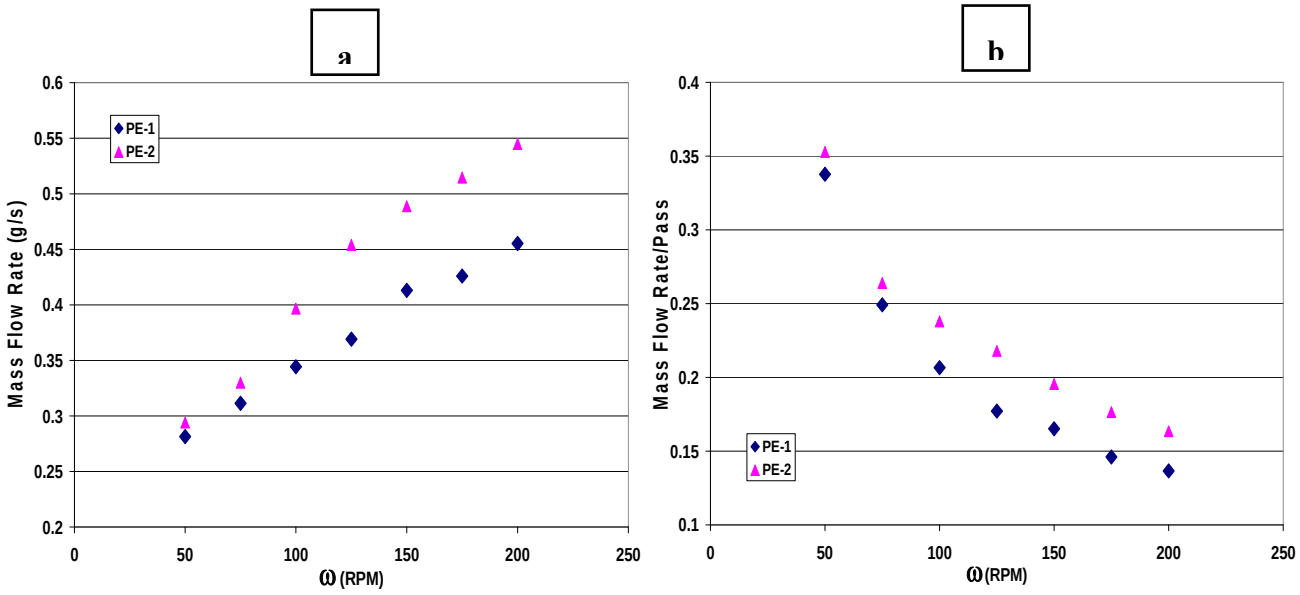

Figure 54: (a) Mass flow rate vs. rotational speed in spinning disk experiment (b) mass flow rate per pass vs. rotational speed in spinning disk experiment for PE-1 and PE-2 powders

One should note that the bulk density for PE-2 is somewhat lower than that of PE-1 so higher flowability should be expected for PE-1 according to the Beverloo equation. In reality however, quite the opposite appears to be true for the case of the moving orifice. Looking at the shape and surface texture of the powders one can see that rough and agglomerate-like (PE-2) powders pack more (stay at higher solid fraction) and flow better than the smooth and crystal-like powders (PE-1) that show more dilation during flow. Both higher stresses (larger index "n") and densities for a powder appear to be favorable in filling the orifice. It can also be seen from Figure 54 that the overall mass flow rate per pass decreases as a function of shear rate as the time that the orifice spends under the hopper also diminishes (at increasing rotation rates). In an industrial application, this diminishing flow rate has a limit below which the orifice does not fill completely with powder and that provides an "upper limit" of the velocity (rotation rate) of the disk (velocity U_0 in our apparatus, see Figure 53). An additional interesting result was obtained by measuring the solid fraction inside the cylindrical hopper as particles are filling the orifice.

Figure 55 shows the results of solid fraction for PE-2 (the powder with the higher mass flow rate) and PE-1 (the powder with lower mass flow rate) for different ranges of the rotational speed. The solid fraction appears constant in the figure (no fluctuations) when the rotation rate is zero (0 RPM). One can also see that for rotational speeds in the range of 50-75 RPM the mass flow rate of the two powders are close and the data for PE-1 fluctuates very little. At higher rotational speeds, the material PE-1 dilates and fluctuates much more than PE-2; this appears to be the reason for its poor mass flowability through the orifice.

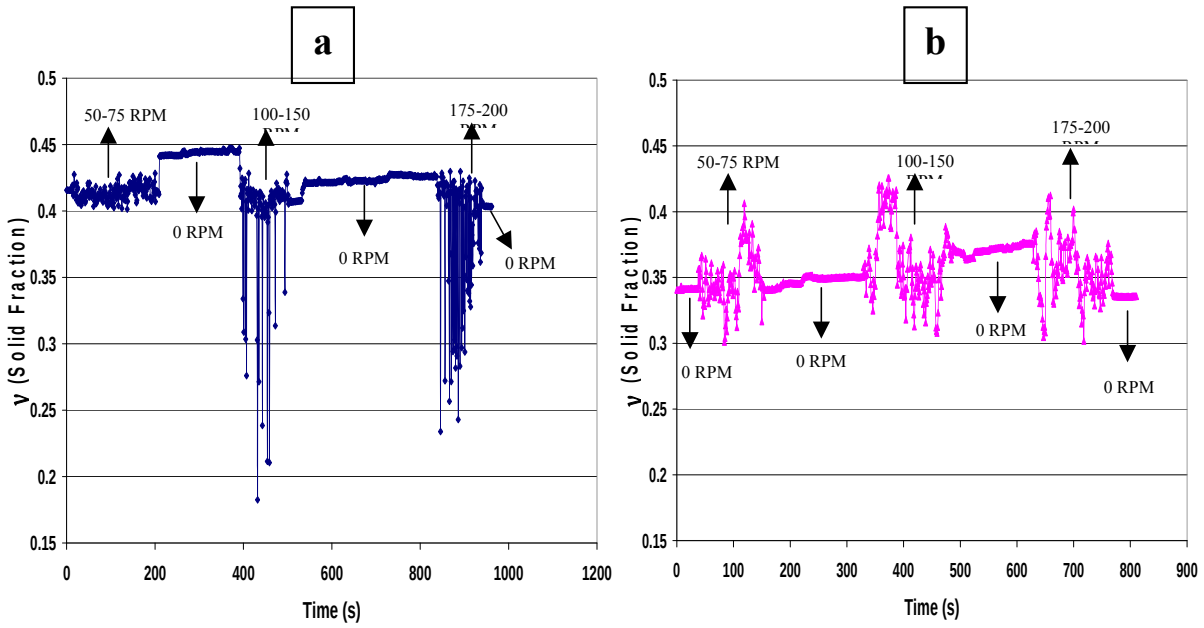

Figure 55: Solid fraction measurements (on the cylindrical hopper wall) at different rotational speeds in the spinning disc experiment for (a) PE-1 (b) PE-2

This finding is similar to what we found in the Couette cell as the powder that shows less dilatancy (with higher amount of stresses at similar shearing rates) can flow better (higher mass flow rate) into an orifice. The high packing (solid fraction), due to surface texture, is responsible for high shear stresses and higher mass flow rate.

6.4 Conclusions

Two compressible powders were tested in our continuous axial flow Couette device as well as in a specially constructed "spinning disk" (or "tablet filling") apparatus to determine their rheology (shear-stress shear-rate dependence) and flowability (flow rate through the moving orifice as it passes under the hopper). The rheological model and physical characteristic of theses powders were shown before in Table 2 of Chapter 4 and here we addressed the reasons for the different behavior of such powders. In both experiments, the solid volume fraction of powders during flow, were measured. Results

of the Couette experiment (rheological model and solid fraction) as well as spinning disc experiment revealed that the powders with higher dependency of shear stress to shearing rate (larger rheological index "n") exhibit higher flowability through an orifice under high shearing rates. These powders require more shear forces to flow and they pack more under shear (higher solid fraction). The powder with a good ability to dilate exhibited a smooth surface texture while the powder with a good ability to pack had a "rough", aggregate-like surface texture. PE-1 shows the highest fluctuation of solid fraction, which results in a decrease in the index "n", makes the system appear "fluffy" and prevents the filling of the orifice at high mass flow rate. Powder PE-2 has the highest index "n" (highest shear stress) and least fluctuation of solid fraction, which results in the system to be more packed and the presence of large stresses which are favorable for filling the moving orifice. The powder that shows more fluctuations in solid fraction at high shearing rates (PE-1) can dilate more and pack less under identical condition. This behavior explains why these powders are very different in terms of rheology. The decrease in solid fraction and its fluctuations at high shearing rates decreases the dependency of shear stress to shear-rate as a more dilute system requires less torque (shear stress).

The main reason why a powder packs or dilates during flow is likely to be its surface texture and shape. Aggregate-like particles (PE-2) generate higher shear stresses at the same shearing rate when flowing (larger value of "n") but pack better (show higher solid fraction and lower porosities) when sheared. This high stress favors packing so that they can fill the orifices better. Quite the opposite is true for a crystalline and ordered surface texture particle (such as PE-1) with low flowability and a smaller rheological index "n".

The flow is more erratic with higher porosity (lower solid fraction) due to its smoother surface texture and lower shear forces. These result in different mass-flow rates and different flow behavior in industrial equipment. The above findings also stress the importance of measuring the solid fraction in addition to the powder's constitutive equation to better characterize its behavior. We also found that when PE-1 does not dilate and the fluctuations in solid fraction are small at low shear rates, it flows in a similar way as PE-2 confirming that packing ability is a key addition to the rheology.

7 A Computational Fluid Dynamics (CFD) Approach to Model Dry Particulate Flows with a Free Surface

7.1 Introduction

The continuum model derived in Chapter 4 based on experiments in the Couette geometry is validated in this chapter in a more complicated geometry to demonstrate its capability of predicting flow and stress fields in granular flows. We chose for this purpose a spheronizer or centripetal flow consisting of a fixed cylinder and a rapidly rotated bottom surface. The spheronization process by which small non-spherical particles produced for example by extrusion, are eroded into a spherical shape, is well known and widely used in the pharmaceutical industry. The size of the spherical particles produced during the process is determined by the diameter of the extruder used in the spheronization process. For example, in order to obtain spheres with a diameter of 1 mm, a 1 mm screen is used on the extruder, although spheres with a slightly smaller diameter will sometimes be obtained. The bottom disc is a rotating, rough, friction disk, designed to increase to entrain the product, which spins at high speed at the bottom of a cylindrical, stationary bowl. The spinning friction disc has a carefully designed grooved pattern on the processing surface. Centrifugal forces send the material to the outside of the disc and up the wall of the stationary wall. The cylindrical extrudates are gradually rounded by collisions with the stationary wall, the rotating plate and each other. The ongoing action of particles colliding with the wall and being thrown back to the inside of the plate creates a "rope-like" movement of product along the wall. The continuous collision of particles with the wall and with the friction plate gradually turn the cylindrical segments

into spheres, provided that the granules are plastic enough to allow the deformation without being destroyed. It is essential that the "rope motion" is present for optimal spheronization.

Granular materials flow only if a continuous input of energy is applied due to their dissipative nature. In the spheronizer geometry inertial effects become important when the centripetal force on a grain due to rotation of the disc becomes comparable to the gravitational (hydrostatic) force on it. This way the kinetic energy of a particle increases to move it past its neighbors as the flow is still dense and many-body interactions exist. There is extensive research in the literature in regard to flow of water in a rotating bucket where both the bottom disc and the sidewalls rotate with the same speed. Newton solved this problem by looking at the motion of fluid when it comes to rest with the rotating frame. Suzuki et. al. (2006) modified the bucket in such a way that only the bottom disc can rotate so that the fluid cannot come to rest with respect to the rotating frame. These authors observed that as the rotation rate reaches higher values the topology of the water changes. In the same experiment by Jansson et. al. (2006), at high rotation rates, a void forms in the center of the disc and it becomes deeper by increasing the rotation rate. In terms of granular matter, Vavrek and Baxter (1994) studied the shape of the free surface of a bucket (same as the one used by Newton) of sand rotating about its cylindrical axis. In contrast to water and due to its frictional nature, granular matter can support a nonzero shearing force before deformation occurs. These authors assumed that sand is rigid when the stress is below yielding and is perfectly plastic after yielding, hence obeying Coulomb yield condition. Furthermore they assumed that the surface is everywhere at the rigid-plastic transition (critical state of yielding) and the density is uniform and constant. In

their experiments they found that at large rotational speeds, the surface is linear and its slope changes slowly with increasing rotation rate, which is in good agreement with their theoretical prediction that at large values of rotational speed the surface slope approaches a constant value (close to the internal angle of friction for sand). This means that the shape of the granular material in a rotating bucket depends on the material's internal angle of friction so in an indirect way one is able to find the internal angle of friction by measuring the slope of a free forming pile. Their theory matches the experiments only if the rotational speed is not too high and the measurements are made quickly before any convection can occur. In other word their theory does not apply for a system in which convection terms are not negligible and/or the density is changing (this being the case most of the time in reality). In a similar experiment, Ngadi and Rajchenbach (1998) observed a dense region near the sidewalls and a loose region close to the center of the bucket. The dynamic of granular materials in a spinning bucket is more complex than the one in rapid granular flows, where the short-lived and binary collisions between particles determines the flow dynamics, even at high shearing rates. The nonlinear elasticity in a rotating bucket of grains may result in an anisotropic stress (Ngadi and Rajchenbach, 1998). In this case granular convection (which was neglected by Vavrek and Baxter, 1994) might form, indicating the existence of complex flow dynamics where the boundaries, but especially the bottom-rotating wall, play an important role in initiating and sustaining relative particle movement. Zamankhan et. al. (2004) numerically examined the flow of grains in a spinning bucket at frequencies higher that 50 1/s. Although they could capture the evolution near the axis of rotation observed before by Vavrek and Baxter (1994), the boundary conditions on the wall were not addressed.

Moreover there is no experiment to validate the stress field that can be obtained with their simulations. In the work of Yeung (1998), heaps of powder exist in the center of the bucket from the beginning and then the rotation started. As the heaps evolved toward the center (as seen by Vavrek and Baxter (1994)) a meta-stable state was found. Using a tilted rotating bucket Yoon et. al. (1999) found the formation of kinks at the boundary between the stable (solid-like) and unstable (fluid-like) regions.

Corwin (2008) modified the split bottom couette geometry in such a way that in his system there is no central wall. The geometry used by Corwin (2008) is similar to the spheronizer geometry (used in this study) and ensures the presence of continuous shear at high rotational rates and can be used for different fill heights if the engine used for the rotation is powerful enough. In his geometry (outer cylinder is fixed and the entire bottom is rotating) the rotation of the bottom disc drives the particles toward the source of shear at the interface of the rotating disc and stationary walls. The surface velocity was measured by high-speed digital video recordings and through particle imaging velocimetry (PIV). Furthermore, because the experiments do not reveal the flow inside the granular material and they only give information about the movement of the surface, Corwin (2008) modified the Large-scale Atomic/Molecular Massively Parallel Simulator (LAMMPS) to reproduce the shearing geometry of the experiments and simulate the system. In this model the spherical particles interact through Hertzian contact forces and tangential frictional forces. He measured the surface height profile and velocities in the azimuthal, radial and axial directions *on the surface,* both experimentally and numerically and in the bulk, for different bead sizes. He found the minimum rotation speed required for a change in topology (evolution that results in an empty hole in the center) as a

function of initial height of particles as well as the final steady state height of materials at different speeds. In his experiments and simulations there exists a region where the azimuthal velocity becomes constant and rate independent (independent of driving frequency). He also showed that this rate-independent flow must be necessarily in the fast (collisional) dense flow regime. Moreover he found that the velocity profile is independent of grain and container size, indicating a universal and scale-invariant flow field. Although the work by Corwin (2008) is a good starting point for studying the granular flow in a rotating system with stationary sidewalls such as the spheronizer flow, he did not address the change in density in such a system, which likely governs the dynamics of flow at high rotation rates. Measurements and computations of forces to find the stress field is another unanswered question.

In this chapter we use a similar geometry as the one used by Corwin (2008) and measure solid volume fraction and wall normal stresses as well as the final rise-up height of granular materials on the stationary walls due to rotation. The numerical study in this chapter includes the use of the constitutive relation obtained for the same granules in Chapter 4 (3 mm in diameter glass beads) to define the frictional "viscosity" in the FLUENT software and to compute the experimentally measured quantities. This geometry has the advantage that there are no static zones in the material and shear is present everywhere i.e.,all particles interact with each other, moreover it is complex enough (existence of a free surface) to show that the visco-plastic model is general and is able to predict stress and flow fields in complex geometries.

7.2 Experimental

A schematic (side view) and picture (from top) of the experimental apparatus (spheronizer) used in this study is shown in Figure 56. The spheronizer consists of a rotating disc (radius, R~15 cm) situated at the bottom (rough sand paper is glued to its surface in such a way that the internal angle of friction of granules is close to the wall angle of friction) and a stationary wall (height, H~30 cm) that can be rough or smooth. The drive shaft (1/2-in.-diam) is activated by a ½ HP motor and the maximum rotational speed is 250 RPM, The rotating disc is the main driving force for the overall circular movement and for particle collisions and the formation of the rope-like motion.

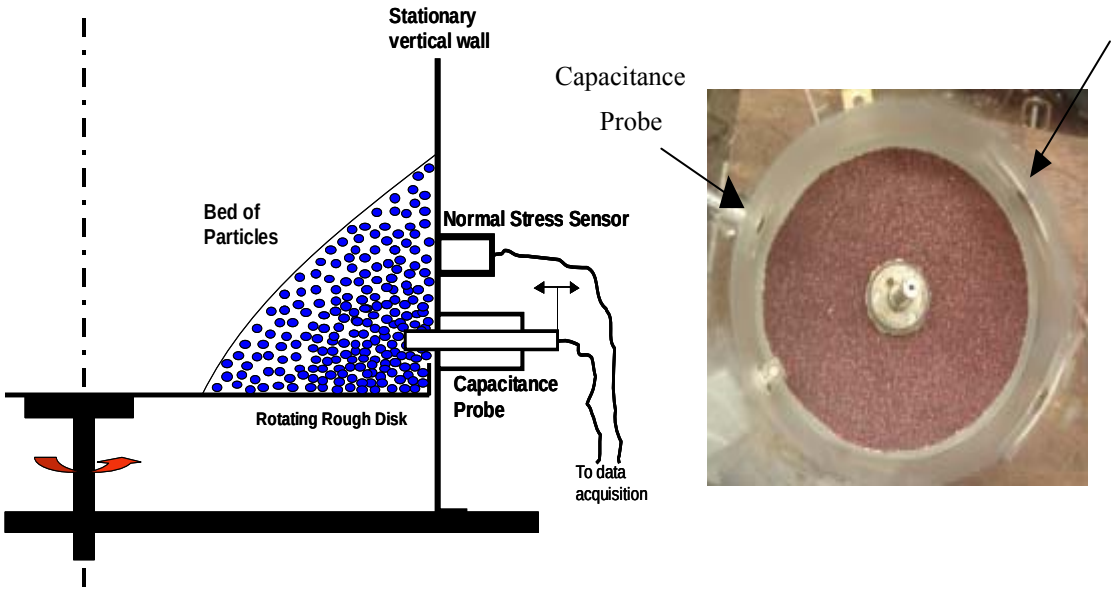

Figure 56: Schematic (left) and picture (right) of the spheronizer used in this study

Due to geometric limitations and the maximum rotational speed of the driving engine, one cannot fill the device to more than approximately 6 cm in height to obtain the rope-like motion for a wide range of speeds. To ensure that the glass beads do not get trapped in the gap between the stationary cylinder and the rotating disc, there is a clearance of approximately 1mm between them. Since the particles need to be larger then the gap so

as to be contained in the device, we use in this study 3 mm spherical glass particles (their rheological properties were measured before in the simple geometry of the Couette device in Chapter 4). We used two initial fill heights of glass beads in this study of 3 cm and 6 cm, respectively. We measure the surface height profile of particles at different speeds. Also, using the same remote normal stress sensor described in Chapters 3 and 4 and the capacitance probe (to measure density) described in Chapters 5 and 6, we recorded the normal stress on the stationary wall and the solid volume fraction on the stationary wall and inside the bed at different speeds.

7.3 Computational

In order to validate the experiments and to generalize the constitutive equation obtained in Chapter 4, we had to solve the equations of motion and continuity for the entire system of the spheronizer. In contrast to the Couette geometry, none of the velocities (radial, axial and swirl) can be neglected. Moreover the inertial term in the momentum equation is non-linear (presence of shear rate term in the denominator) and the presence of the free surface requires the solution of the equations of motion simultaneously for both phases (particles and air). The equation of continuity for each phase takes the form:

$$\frac{\partial}{\partial t}(\alpha\rho) + \nabla.(\alpha\rho\vec{v}) = 0 \tag{7.1}$$

where α is the volume fraction for each phase. We showed earlier that using the yield condition obtained in the Couette geometry for the same granular material, one is able to derive a generalized form of the Cauchy equation for the conservation of momentum in which the viscosity term is a function of pressure, shear rate and two rheological constants “b” and “n”. This can be shown in Equation 7.2:

$$\frac{D(\rho u)}{Dt} = -\nabla P + \sqrt{2}\sin(\phi)\nabla.((\frac{P}{\left|\dot{\gamma}_{ij}\right|} + b\cot(\phi)\left|\dot{\gamma}_{ij}\right|^{n})\dot{\gamma}_{ij}) + \rho g \tag{7.2}$$

For the case of 3 mm spherical glass the constants take the values b=0.13 and n=0.75 (from Couette experiment). All shearing rates have to be taken into account and equations 7.3 and 7.4 contain two deformation tensors:

$$\dot{\gamma}_{\theta r} = \frac{v_\theta}{r} - \frac{dv_\theta}{dr} \tag{7.3}$$

$$\dot{\gamma}_{\theta z} = -\frac{dv_\theta}{dz} \tag{7.4}$$

One can see the complexity of the equations obtained for such geometry when none of the velocities are negligible, by looking at the conservation of momentum in the swirl direction (Equation 7.5):

$$\frac{\partial}{\partial t}(\rho v_\theta) + \frac{1}{r}\frac{\partial}{\partial z}(r\rho v_r v_\theta) + \frac{1}{r}\frac{\partial}{\partial r}(r\rho v_r v_\theta) = \frac{1}{r}\frac{\partial}{\partial z}\left[r\eta(\dot{\gamma}_{II}, P)\frac{\partial v_\theta}{\partial z}\right] + \frac{1}{r^2}\frac{\partial}{\partial r}\left[r^3\eta(\dot{\gamma}_{II}, P)\frac{\partial}{\partial r}(\frac{v_\theta}{r})\right] - \frac{\rho v_r v_\theta}{r} \tag{7.5}$$

While the viscosity ($\eta(\dot{\gamma}_{II}, P)$) itself has the form:

$$\eta(\dot{\gamma}_{II}, P) = \sqrt{2}\sin(\phi)(\frac{P}{\left|\dot{\gamma}_{ij}\right|} + b\cot(\phi)\left|\dot{\gamma}_{ij}\right|^{n}) \tag{7.6}$$

It is obvious that an analytical solution is not possible so a CFD (Computational Fluid Dynamics) approach is required to model the centripetal flow of granules in the spheronizer. We use in the present work ANSYS Fluent 12.1 software, which is capable of solving non-linear inertial terms in the momentum equation. To achieve this we use the 2-phase flow (phase I: air, phase II: granules) toolbox. This numerical scheme allows for the modeling of multiple separate, yet interacting phases and solves for each phase the

momentum and continuity equations. It should also be noted that although both glass beads and air are assumed to be incompressible, the granular and air phases are compressible so that void fraction between particles increases when they penetrate to the air phase at the interface. This is a 2-D axisymmetric problem where material properties such as size and internal angle of friction are inserted into the program. The boundary condition on the stationary wall is determined from its roughness, as we can never reach a no-slip condition. Furthermore the constitutive relation for this material is furnished to the program by writing a user defined function (UDF) with C++ code (written by Dr. M. Shahnam) for the frictional viscosity. The goal is to simulate the system for different speeds and initial heights and then to compare the results of the computations with experiments. The quantities for comparison are surface height (final shape of the free surface), wall normal stress and solid fraction at different speeds. We performed calculations for two initial surface heights (3 and 6 cm), the same as in the experiments. Also the velocity profiles, their vectors and the direction of flow is shown and discussed and compared with other simulations and experiments from the literature.

7.4 Results and Discussions

A. Height Profile and Shape

In both experiments and simulations the particles are first at rest and then the rotational speed is increased resulting in a change from a solid body rotation (at low speeds) to a rope-like motion (at high speeds). In order to check the shape of the free surface one measures the height (distance from the rotating bottom) to the highest particle located on the stationary rough wall, at each rotational speed. As mentioned before two initial

heights tested in this study were 3 and 6 cm and we compare the increase in height at each rotational speed as particles climb up the stationary wall due to centrifugal forces. Both experiments and simulations show that there is a threshold (minimum) speed below which a solid body rotation is observed and after which the rope-like motion starts to form as the rotational speed is increased. At the threshold speed the height of particles at the center of the spheronizer (axis of symmetry) becomes zero and a hole starts to form in the center of the system. Figure 57 shows the evolution from solid body rotation to rope-like flow by increasing the rotational speed for a system of 3 mm beads of initially 3 cm height.

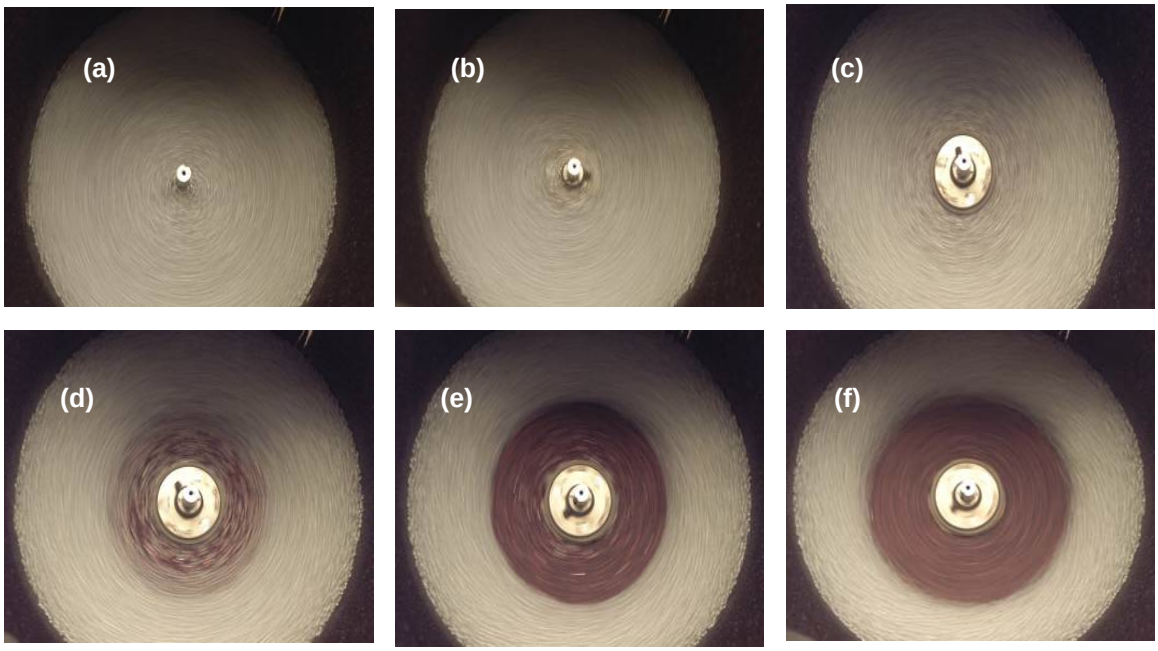

Figure 57: Shape of free surface flow of 3 mm glass beads (initially at 3 cm height) at different rotational speeds: (a) 50 RPM (solid body rotation) (b) 78 RPM: threshold speed (c) 85 RPM (d) 100 RPM (e) 125 RPM (f) 250 RPM

One can see from Figure 57b that several particles start to leave the center at this speed (78 RPM, threshold) and by increasing the rotational speed from this point; the empty hole in the center of spheronizer grows. We can measure the diameter of the empty space as well as the height of the last layer of granules attached to the rough stationary wall and

we can compare this height obtained from simulation at each rotational speed. Figure 58 shows the computed shape of the granular flow in the spheronizer geometry at two different rotational speeds of 50 (before formation of empty hole) and 85 (after formation of empty hole). The variable in the Figure is the density of granular phase (blue color is for air and dark red color is for the densest part).

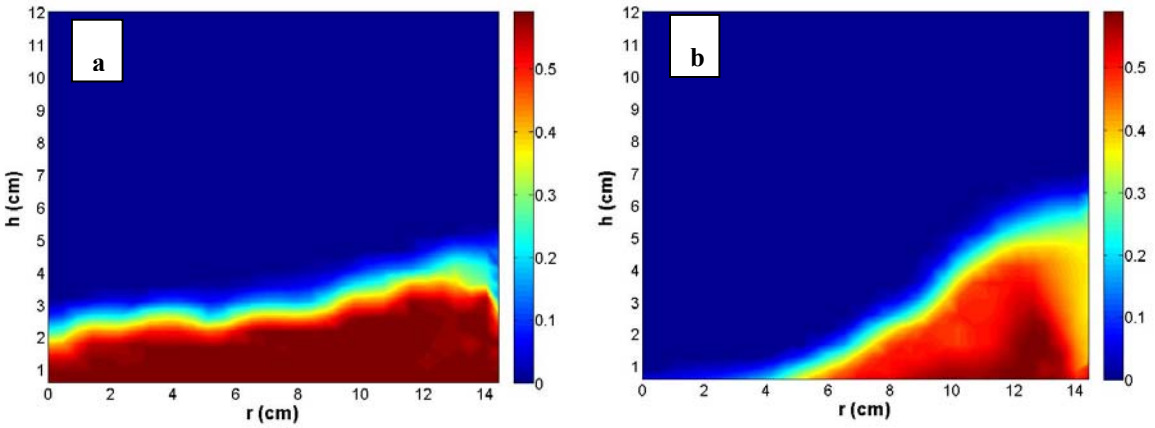

Figure 58: Shape of 3 mm glass particles rotating with (a) 50 RPM (b) 85 RPM obtained from simulation for half of the device (axisymmetric). The y-axis is the axis of symmetry

Figure 59 shows the comparison of simulations with experiments for change in the height by changing the rotational speed for 3 mm glass particles initially at 6 cm height. In the simulation, this height can be calculated by looking at the solid volume fraction data on the stationary wall, and the final height of granules is recorded on the gas-solid interface where the solid volume fraction becomes meaningful (>0.1). In Figure 60 we did this comparison for the same glass particles initially at 3 cm height and, since in the computations we do not have any limitation for increasing the speed, we could find the final height for rotational speeds as high as 1000 RPM. It can be seen from both Figures that the shape of granular flow matches well with results obtained from experiments.

Also by running the simulations at higher rotational speeds, 500 and 1000 RPM, (Figure 60) we can see that the particles continue to move away from the center of the device, i.e., increasing the diameter of the hole and rise up more on the stationary wall.

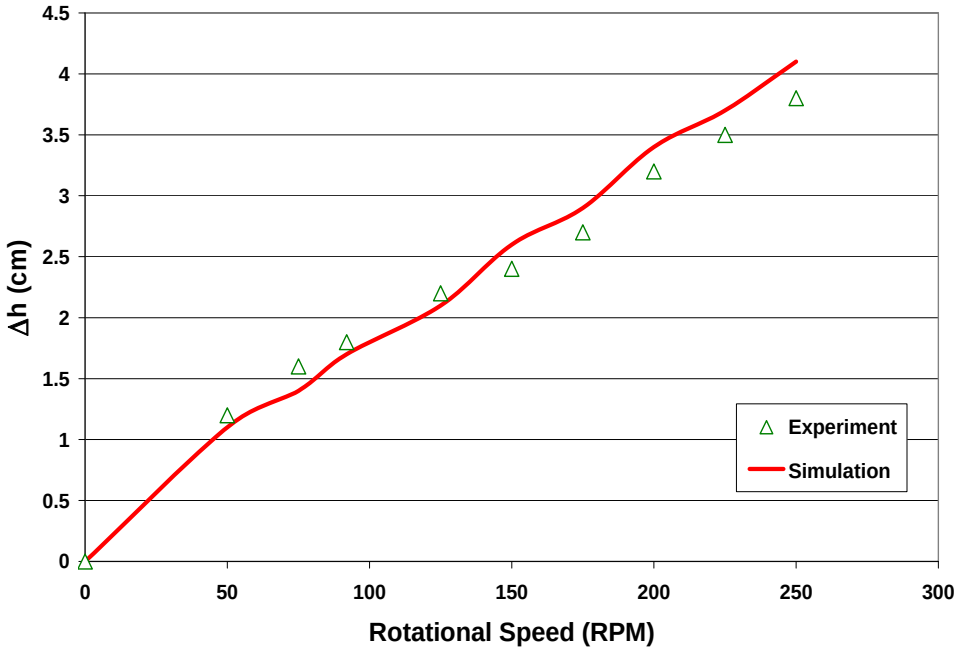

Figure 59: Experimental and computational results of height difference vs. rotational speed for 3mm glass beads initially at 6 cm height

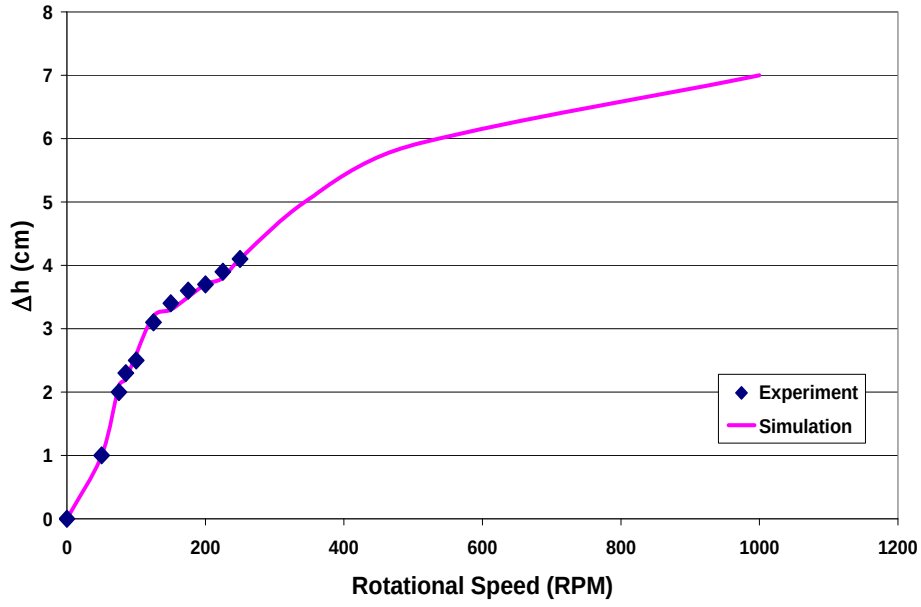

Figure 60: Experimental and computational results of height difference vs. rotational speed for 3mm glass beads initially at 3 cm height: 500 RPM and 1000 RPM were tested in simulation only

It can be seen that by increasing the rotational speed by a factor of 4 (from 250 RPM to 1000 RPM), the height for the 3 cm bed increases by less than a factor of two. Another interesting result comes from comparing the threshold (minimum) rotational speed from simulations and experiments, respectively. This threshold speed is, from experiments, 78 RPM for the initially 3 cm height bed and 92 for the initially 6 cm bed. Computations for the first case (initially 3 cm height bed) yield a threshold speed by iteration to be very close to 78 RPM. The iterations were numerical runs, first at 75 RPM when we saw the existence of particles in the center space and then at 85 RPM where an empty hole has been clearly identified. The computation at 78 RPM yielded a few particles in the middle and the empty hole was just created. The same observation was made for simulation with 3 mm glass beads initially in the 6 cm bed, as at 85 RPM there is no hole in the middle but at 100 RPM the hole has been clearly formed.

B. Solid Volume Fraction

The key parameter for this free surface flow is the change in density of the granular bed. We showed previously that if the solid volume fraction does not change, granular matter only shows solid-like behavior (Kheiripour Langroudi et. al., 2010a) that, in this case, is a solid body rotation. In order for particles to empty the hole at the center of the device and rise up on the stationary wall, they have to "flow" and a certain decrease in solid volume fraction is required. Results in Figure 58 clearly show that a density distribution exists in the system and this variation can be compared with experiments. A first important result is the change in solid fraction on the stationary wall by increasing the rotational speed. As shown in Figures 59 and 60, by increasing the rotational speed,

the height of particles on the stationary wall increases and hence we expect a density distribution if the position of the probe is constant (3.5 cm above the rotating wall and flush with the stationary wall). Figure 61 shows the results of experiments and simulations for solid fraction at different rotational speeds for particles, which are initially in a 3 cm high bed. As seen in the Figure, experiments and computations are in a very good agreement. For the case of a low speed of 50 RPM the volume measured "seen" by the probe is partially filled with particles and that is why we measure a very small solid volume fraction. By increasing the shearing rate, the solid fraction increases until it reaches the maximum packing (~ 0.55-0.59) because particles are situated further from the top (air) and have a better chance to be in close contact.

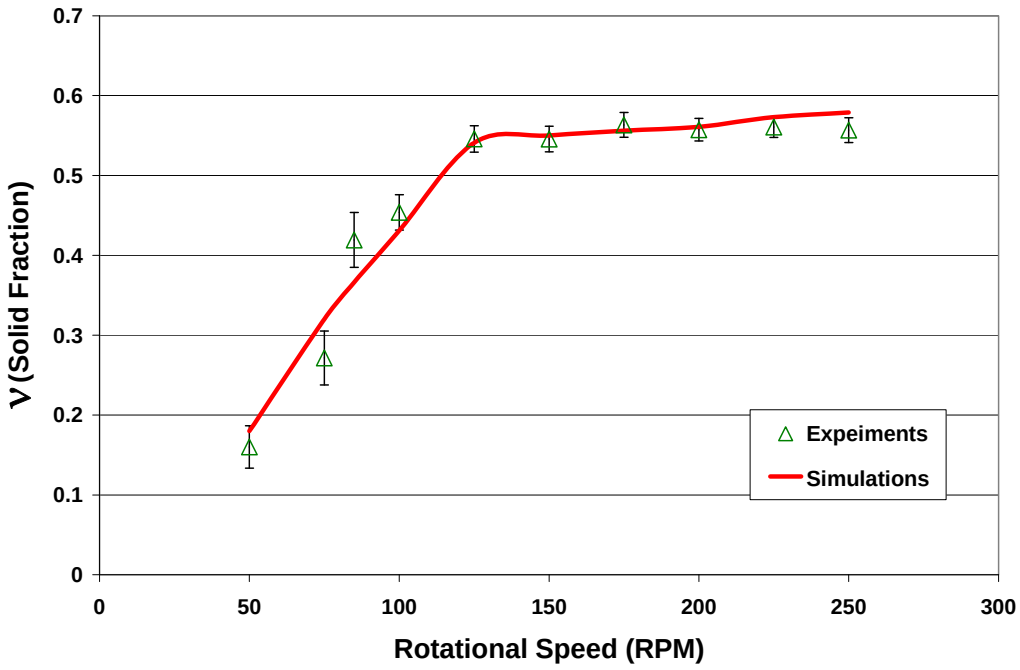

Figure 61: Measurements and computations of solid volume fractions at different rotational speeds (RPM) for a system of 3 mm spherical glass initially at 3 cm obtained 3.5 cm above the bottom disc on the stationary wall.

One can see from Figure 61 that fluctuations of solid fraction are higher for lower rotational speeds: at lower speeds the height of material is also low and the solid fraction is measured closer to the free surface. In those loose regions, the probability of random collisions increases so that the solid fraction cannot be constant and it has more variations. Results of Figures 58, 59 and 60 clearly show that there exists a dense region in the rotating bed close to the bottom. For example in Figure 61 where the position of the sensor is fixed, higher rotational speeds enable the probe to "see" regions further from the free surface and thus the dense region was captured on the stationary wall. The existence of dense regions in the rotating bed that has been proven experimentally and computationally brings up the question: what will happen if the rotational speed is further increased? Looking at simulations for 500 RPM and 1000 RPM we found that such regions becomes smaller by increasing the speed but never disappear. To better understand the flow field in such a granular system we look at the density and velocity profiles simultaneously (Figure 62). Figure 62a shows the density profile and Figure 62b shows the velocity vectors in r and z directions. The vectors show the direction of the flowing particles and the intensity is given by the magnitude of the convective velocity ($\sqrt{v_z^2 + v_r^2}$; both are for 3 mm spherical glass rotating at 350 RPM and initially at 3 cm height. We can easily see from Figure 62 that for the dense region a solid body rotation exists where the axial and radial velocities are negligible (shown by dots in lower right hand corner) while for the remainder of the bed, in regions where the solid fraction decreases and particles are free to move, a rope-like motion is observed.

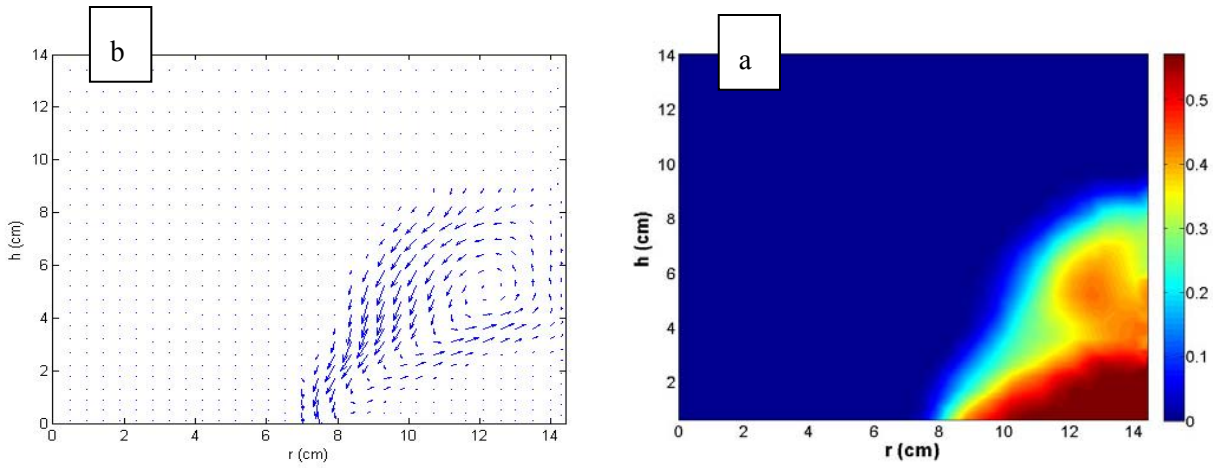

Figure 62: Simulation of free surface flow of 3 mm spherical glass particles initially at 3 cm rotating at 350 RPM (a) density profile (b) vector of velocity (r-z)

It should be noted that the magnitude of the total velocity in those regions (dotted) are highest as the dominant velocity (swirl) is at its maximum value while Figure 62 only shows the axial and radial velocities (not the swirl) as the purpose here is to show the direction of flow in the r-z plane. Higher in the flow, i.e., further up from the rotating bottom, the main velocity (swirl) decomposes to axial and radial and swirl due to gravity and to the centrifugal forces that push the particles to the stationary wall and outward, away from the center (axis of symmetry). Results in Figure 64b explain why such a dense region exists. This is due to the fact that the flow in the swirl direction generates a solid body rotation and therefore a dense system. This is an interesting finding if we couple this idea with what has been observed before for the quasi-static and intermediate regimes of flow. The dense region with no change in solid fraction and with solid body rotation represents the quasi-static regime of flow while the domain in which the rope-like motion can be identified is the intermediate regime of flow. Furthermore, we observe a "rapid flow regime" in this system at the interface with air where the solid fraction is

less than 0.2. As a consequence, this geometry shows a complete map for all regimes of flow and this is captured both experimentally and by simulations.

C. Normal Stresses

Validation of the constitutive equation inserted into Equation 7.2 (Navier-Stokes) and Equation 7.5 for the "viscosity" of the granular flow also requires measurement and computation of forces in the system. The normal stress sensor was mounted on the rough stationary wall 2.5 cm away from the rotating bottom. The spheronizer was filled with the same 3 mm round glass particles to the initial height of 6 cm. Normal stresses are measured at increasing rotational speeds during the experiment and then compared to the computed normal stress at the same point of the stationary wall as shown in Figure 63.

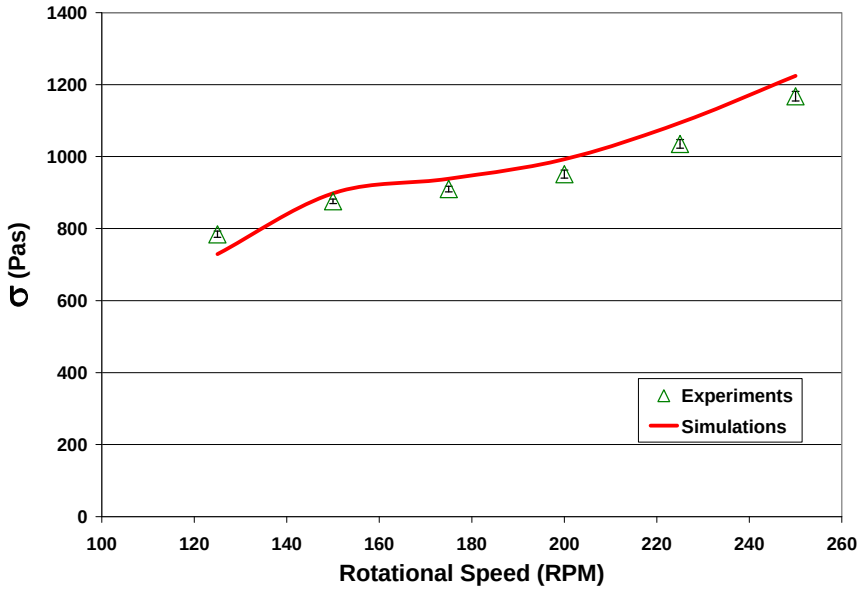

Figure 63: Experimental and computational values of the wall normal stress at different rotational speeds. The spheronizer is filled with 3 mm spherical glass initially at 6 cm height from rotating disc.

It can be seen from the figure that the wall normal stress depends on rotational speed somewhat linearly and its fluctuations increase at increasing speeds. The results of the

simulation match the experimental results, again demonstrating that using a unified constitutive equation, valid for both frictional and collisional behavior of granular matter and obtained in a simple geometry of the Couette device, allow to match both flow and stress fields even in this more complicated geometry of the spheronizer where free surfaces exist.

7.5 Conclusions

We studied a free surface flow of dry granular matter through experiments and simulations. We designed a laboratory scale spheronizer filled with particles 3 mm in diameter and rotated at spinning rates as high as 250 RPM. In the computations, a continuum modeling approach with a Visco-plastic constitutive equation, previously developed in the Couette geometry for the same material, was used. We presented comprehensive measurements of surface height and shape, solid volume fraction and wall normal stress as a function of rotational speed. We found that the simulations are reasonably accurate in predicting the final height and shape of the granular flow at different rotational speed. Solid volume fraction on the stationary wall was also captured experimentally and computationally and the results match quite well. We found that there always exists a dense region (3-5 % looser than random packing) in both experiments and simulations no matter how fast the bottom disc rotates (up to 1000 RPM). Interestingly, in this dense region the z and r components of the velocity diminish and the particles undergo a solid body rotation with a high velocity in the swirl direction. This appears to be a fundamental property of granular matter in this geometry and all three regimes of flow (quasi-static, intermediate and rapid flow) exist at the same time. Finally the constitutive equation was validated by comparing the wall normal stress obtained from

simulations and experiments. The normal stress on the wall increases by increasing the rotational speed, as faster rotation (larger centrifugal force) imparts more energy to colliding particles.

Appendix: Numerical solution of the flow in the Couette device

1. Finite element method

The underlying finite element technique, which is the basis for the developed software package FeatFlow, is described in detail in Ouazzi et al. (2005). The essence of the special techniques for this kind of flow problems is the introduction of a stabilization term in the denominator that contains the magnitude of the shear stress and a modified multigrid solver. The method was used successfully to solve for incompressible granular flow in a two dimensional hopper using Equation 4.12-3. In the present work we use the same method to solve the modified Navier–Stokes equations (Equation 4.11) with the new closure that applies to the quasi-static and the intermediate regime i.e., Equation 4.12-5 in the Couette geometry and also compare this solution to results obtained for all other closures (Equations 4.12-1, 4.12-2, 4.12-3, 4.12-4 and 4.12-5).

The numerical method yields as a first result the velocity and pressure distribution in the gap of the Couette device. Stresses are then computed from the velocity gradients using the constitutive laws (Equations 4.12-1, 4.12-2, 4.12-3, 4.12-4 and 4.12-5) for the respective material. From these results, and $T_{ij} = \tau_{ij} - pI$, the force (F) and torque (M) on the inner, rotating cylinder are calculated as follows:

$$F = -\oint_S T_{ij} \vec{n} ds \; and \; M = -\oint_S (X - X_0) T_{ij} \vec{n} ds) \tag{4.13}$$

In the above equation, S and X_0 are the surface and the centre of the inner cylinder and $\vec{n}$, is the direction vector.

2. Computer simulations

This section is intended to validate the proposed model via the FEM code *FeatFlow* for complex flow problems (Ouazzi et. al., 2005). The 2D simulation was done for two concentric cylinders. The outer cylinder was kept fixed while the inner cylinder was rotating. The torque was calculated for a section of the cylinders with length unity. Figure 66 depicts a sample calculation with the numerical method, for four continua including a Newtonian liquid, Bingham plastic (solid) and powder in the quasi-static regime (Schaeffer solid) compared with the proposed new constitutive equation, (Equation 4.11) that contains the viscous term as in Equation 4.12-5. The torque on the inner rotating cylinder is given as a function of the rotational speed of the inner cylinder (in RPM). The powder in the quasi-static regime (Schaeffer solid) yields a constant torque as a function of rotation (or shear) rate, as expected. The Bingham plastic also yields a constant torque at low shear rates but then behaves like the Newtonian fluid and, above a rotational speed of about 10 RPM, the data become indistinguishable.

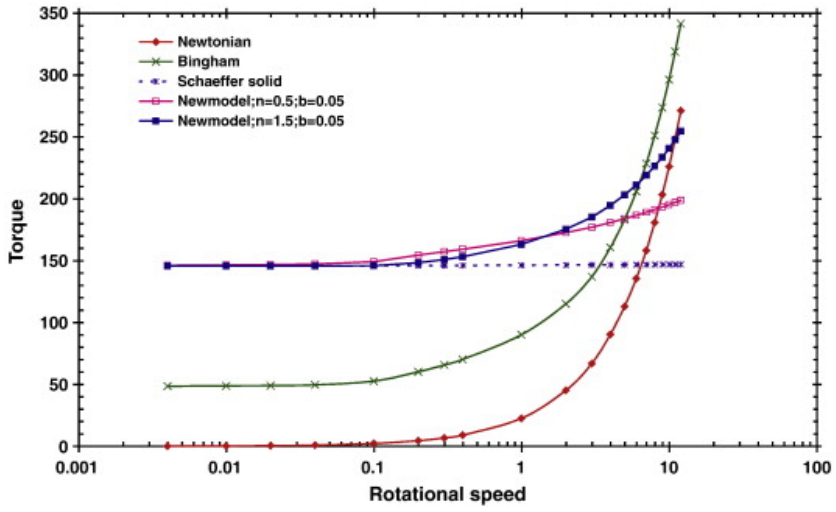

Figure 64: Numerical solution of the generalized Navier–Stokes equations for concentric cylinders for (a) Newtonian fluid, (b) Bingham plastic, (c) powder in the quasi-static regime (Schaeffer solid), and (d) powder in the intermediate regime (new constitutive equation, Equation 2.36).

Two curves are presented in Figure 64 for the powder in the intermediate regime ("New model" in the figure, Kheiripour Langroudi et. al., 2010a) for a power-law index of $n = 0.5$ and $n = 1.5$, respectively. One can see that the viscous term has a significant influence and the torque and shear stress are shear-rate-dependent at higher shear rates as was found experimentally in Figure 28 (the shear stress and torque are related linearly as in Equation 4.2).

Figure 65 gives the torque on a slice of the Couette of height "unity" for all four continua as a function of the rotational speed of the inner cylinder. Different simulations were performed for the concentric cylinder (taken partially from Figure 64) and for the case when the inner cylinder is moved off-center by one quarter of the gap (0.25 in.) and half of the size of the shear gap (0.5 in.). An important conclusion from these simulations is that the torque is not influenced in a significant way by the eccentricity for any continua considered herein. Of course, this is true only as long as the eccentricity is kept to less or equal to half of the shearing gap as shown in the figure. This conclusion is relevant from an experimental point of view since small eccentricities and "wobbles" of rotating parts are very difficult to avoid in practice. Note that the torque generated by the Schaeffer solid is constant for all shear rates since the pressure is constant (constant stress experiment); this is to be expected for a solid powder moving in the quasi-static regime. The appropriate change in solid fraction (or bulk density) to achieve this is not captured by the model since it is assumed that the powder is incompressible. Experiments performed with an off-center cylinder (situated 0.25 in. off-center) actually proved that there is no difference in the behavior of the powder and the overall torque is practically the same.

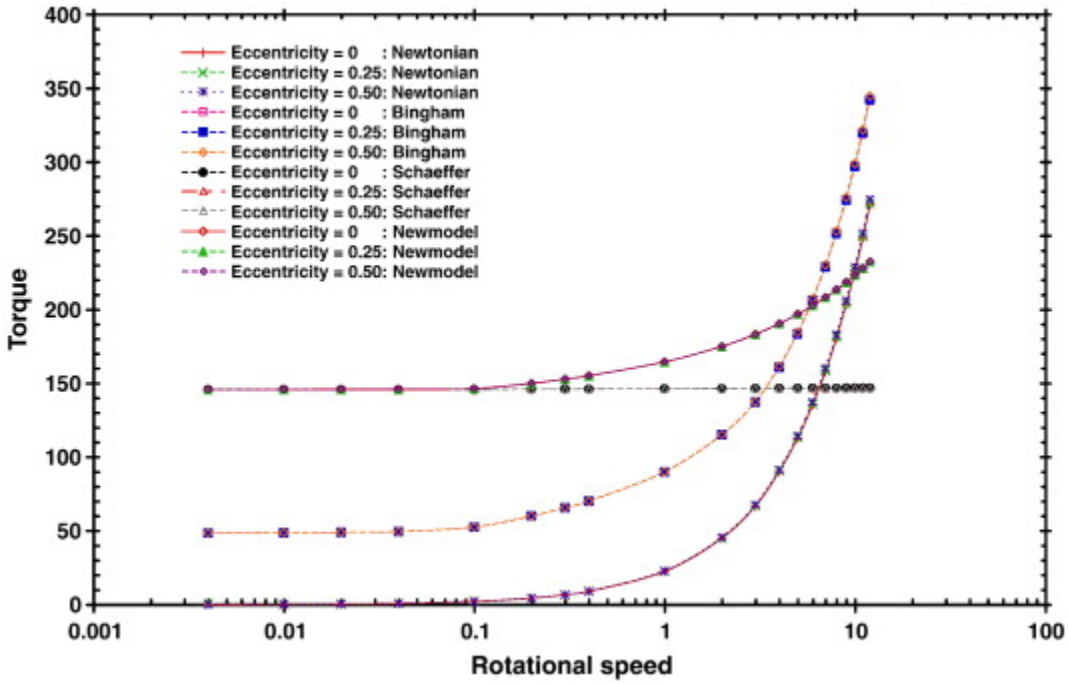

Figure 65: Comparison of concentric and two eccentric cylinders. Numerical solution of the generalized Navier–Stokes equations for (a) Newtonian fluid, (b) Bingham plastic, (c) powder in the quasi-static regime, (Schaeffer solid), and (d) powder in the intermediate regime (new constitutive equation, Equation 4.7).

Figure 66 gives similar results for the four continua for the concentric case where an additional stationary cylinder is introduced in the middle of the gap. This cylinder is denoted “obstacle” in the figure and occupies a quarter of the gap (at 0.25) and half of the gap (at 0.5). The Newtonian fluid and the Bingham plastic with the same viscosity appear to be quite sensitive to the presence of the obstacle, as expected, while the Schaeffer solid seems to be quite insensitive. This last result is again to be expected since previous studies (Tardos et. al., 2003) showed that the shearing zone in the quasi-static regime is actually very close to the moving surface and decreases exponentially from the boundary. For this reason, the presence of an obstacle in the middle of the shearing gap, even if it occupies one half of the distance, does not affect the torque on the rotating cylinder to a significant degree.

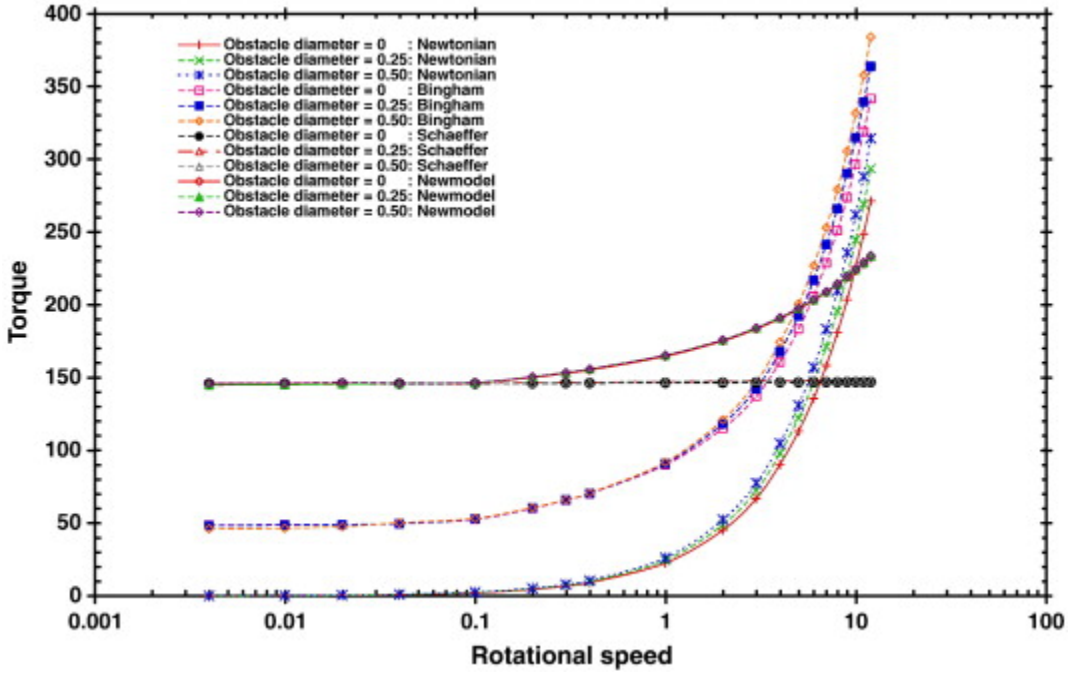

Figure 66: Numerical solution of the generalized Navier–Stokes equations for concentric Couette with a cylindrical obstacle in the center of the shearing gap for (a) Newtonian fluid, (b) Bingham plastic, (c) powder in the quasi-static regime (Schaeffer solid), and (d) powder in the intermediate regime (new constitutive equation, Equation 4.7)

The behavior of the modified Schaeffer solid i.e., using the constitutive law in Equation 2.37-5 is intermediate between the viscosity containing continua and the Schaeffer solid. The larger obstacle generates a somewhat higher torque but experiments performed so far with a similar system (in which the "obstacle" occupies half the shear gap) yielded results that are inconclusive in the sense that the fluctuation of the experimental torque is larger than the difference in torque between the absence and presence of the obstacle.

3. Conclusions

A new finite element solver FeatFlow of the generalized Navier–Stokes equations that uses, in addition to the yield condition determined experimentally for a relatively free flowing powder, a generalized viscosity that describes a Newtonian fluid, a Bingham

Plastic, an incompressible frictional powder (Schaeffer solid) and a power-law fluid was described. The numerical method was used to validate some experimental measurements and calculate the torque in the Couette device in three different geometries: a concentric, two cylinder, arrangement and two new geometries in which the cylinder is positioned eccentric in the Couette and one where an additional cylindrical object is placed into the shearing gap and obstructs parts of it. This also shows some of the capabilities of the model to predict the more important parameters of the experiment for the most complicated geometry that of the “obstacle” occupying 1/2 of the shearing zone.

References

Ancey, C., Coussot, P. & Evesque, P. (1999), 'A theoretical framework for granular suspension in a steady simple shear flow', *J. Rheol.* 43, 1673–1699.

Ancey, C. (2001), 'Dry granular flows down an inclined channel: Experimental investigations on the frictional-collisional regime', *Phys. Rev. E*. 65, 011304.

Bagnold, R.A. (1954), 'Experiments on a gravity-free dispersion of large solid particles in a Newtonian fluid under shear', *Proc. R. Soc. Lond. A* 225, 49–63.

Bazant, M. Z. (2006), 'The Spot Model for random-packing dynamics', *Mech. Mater.* 38, 717-731.

Behringer, R. P., Howell, D., Kondic, L., Tennakoon, S. & Veje, C. (1999), 'PredictabiIity and granular materials', *Physica* D 133, 1 - 17.

Blinowski, A. (1978), 'On the dynamic flow of granular media', *Arch. Mech.* 30, 27-34.

Bocquet, L., Losert, W., Schalk, D., Lubensky, TC. & Gollub, JP. (2002), 'Granular shear flow dynamics and forces: experiments and continuum theory', *Phys. Rev. E* 65, 011307.

Brennen, C. & Pearce, J.C. (1978), 'Granular material flow in two-dimensional hoppers', *J. Appl. Mech.* 45, 43–50.

Brown, R. C. and Richards, J. C. (1970), 'Principles of powder mechanics', *London Pergamon Press*.

Bulícek, M., Malék, J., and Prazák, D. (2005), 'On the dimension of the attractor for a class of fluids with pressure dependent viscosities, *Comm. Pure Appl. Anal.* 4, 805-822.

Bulícek, M., and Kaplický, P. (2008), 'Incompressible Fluids with Shear Rate and Pressure Dependent Viscosity: Regularity of Steady Planar Flows', *Discrete and Continuous Dynamical Systems Series S.* 1, 41-50.

Campbell, C.S. and Brennen, C.E. (1985), 'Computer simulation of granular shear flows', *J. Fluid Mech.* 151, 167–188.

Campbell, C. S. (1990), 'Rapid granular flows', *Annu. Rev. Fluid Mech.* 22, 57–92.

Campbell, C.S. (1993) 'Boundary interactions for two-dimensional granular flows: Part I. Flat boundaries, asymmetric stresses and couple stresses, *J. Fluid Mech.* 247, 111–136.

Campbell, C.S., Cleary, P. W., and Hopkins, M. (1995), 'Large-scale landslide simulations: Global deformation, velocities and basal friction', *J. Geophys. Res.* 100, 8267-8283.

Campbell, C.S. (2002), 'Granular shear flows at the elastic limit', *J. Fluid Mech.* 465**,** 261–291.

Campbell, C. S. (2006), 'Granular material flows – An overview', *Powder Technol.,* 162, 208-229.

Corwin, E.I., Hoke, E.T., Jaeger, H.M., and Nagel, S.R. (2008), 'Temporal force fluctuations measured by tracking individual particles in granular materials under shear', *Physical Review E* 77, 061308-6.

Corwin, E. I. (2008), 'Granular flow in a rapidly rotated system with fixed walls', *Phys. Rev. E* 77, 031308.

Coulomb, C.A. (1773), 'Essai sur un application de règles de maximis et minimis à quelques problèmes de staique relatifs à l'architecture', *Mém. Math. Phys. Acad. R. Sci., Paris* **7**, 343–382.

Da Cruz, F., Chevoir, F., Bonn, D., Coussot, P. (2002). 'Viscosity bifurcation in granular materials, foams, and emulsions', *Phys. Rev. E.* 66, 051305.

Da Cruz, F., Emam, S., Prochnow, M., Roux, JN., Chevoir, F. (2005), 'Rheophysics of dense granular materials: discrete simulation of plane shear flows', *Phys. Rev. E.* 72, 021309.

Daerr, A., Douady, S. (1999), 'Sensitivity of granular surface flows to preparation' *Europhys. Lett.* 47, 324–30.

Daniel, R.C., Poloski, A.P. & Sáez, A.E. (2007), 'A Continuum Constitutive Model for Cohesionless Granular Flows', *Chem. Eng. Sci*. 62, 1343-1350.

Depken, M., Hecke, M. & Saarloos, W. (2006), 'Continuum approach to wide shear zones in quasistatic granular matter', *Phys. Rev. E*. 73, 031302.

Fenistein D., van de Meent JW., van Hecke M. (2004), Universal and wide shear zones in granular bulk flow, *Phys. Rev. Lett.* 92:094301.

Forterre Y., and Pouliquen O. (2008), Flows of dense granular media, *Annu. Rev. Fluid Mech.* 40 , 1-24.

GDR MiDi (2004), 'On dense granular flows', *Eur. Phys. J. E* 14, 341–65.

Goldhirsch, I., and Zanetti, G. (1993), 'Clustering instability in dissipative gases', *Phys. Rev. Lett.* 70, 1619–1622.

Goldhirsch, I. (1999),' Scales and kinetics of granular flows', *Chaos.* 9, 659–672.

Haff, P.K. (1983), 'Grain flow as a fluid-mechanical phenomenon', *J. Fluid Mech.* 134, 401–430.

Hermann, H. J. & Luding, S. (1998), 'Modeling of granular media in the computer'. *Continuum Mech. Thermodyn*. 10, 189-231.

Howell, D.W., Behringer, R.P. and Veje, C.T. (1999), 'Fluctuations in granular media', *Chaos* 9**,** 559–572.

Howell, D.W., Behringer, R.P. and Veje, C.T. (1999), 'Stress fluctuations in a 2D granular Couette experiment: a continuous transition', *Phys. Rev. Lett.* 26, 5241–5244.

Hron, J., Malek, J., Necas, J. and Rajagopal, K.R. (2003), 'Numerical simulations and global existence of solutions of two-dimensional flows of fluids with pressure and shear dependent viscosities', *Math. Comput. Simul.* 61, 297–315.

Jackson, R. (1983), 'Some mathematical and physical aspects of continuum models for the motion of granular materials', R.E. Meyer, Editor, *Theory of Dispersed Multiphase Flow*, Academic Press, New York, 291-337.

Jackson, R. (1986), 'Some features of the granular materials and aerated granular materials', *J. Rheol.* 30 (5) 907-930.

Jaeger, HM., Nagel, SR., Behringer, RP. (1996), 'Granular solids, liquids, and gases'. *Rev. Mod. Phys.* 68, 1259-1273.

Janssen, H.A. (1895), Versuche über getreidedruck in silozellen, *Z. Ver. Dtsch. Ing.* 39, 1045–1049.

Jansson, T. R. N., Haspang, M. P., Jensen, K. H., Hersen, P. and Bohr, T. (2006), 'Polygons on a Rotating Fluid Surface', *Phys. Rev. Lett.* 96, 174502.

Jenike, A.W. (1964), 'Storage and flow of solids', *Bulletin of University of Utah, Bulletin No. 123, Vol. 53.*

Jenkins, J. T. and Savage, S. B. (1983), 'A theory for the rapid flow of identical, smooth, nearly elastic, spherical particles', *J. Fluid Mech.* 130, 187-202.

Johnson, P.C., Nott, P., Jackson, R. (1990), 'Frictional–collisional equations of motion for particulate flows and their applications to plane shearing', *J. Fluid Mech.* 210, 501–535.

Jop, P., Forterre, Y., Pouliquen, O. (2005), 'Crucial role of sidewalls in granular surface flows: consequences for the rheology', *J. Fluid Mech.* 541, 167–192.

Jop, P., Forterre, Y., Pouliquen, O. (2006), 'A constitutive law for dense granular flows', *Nature* 441, 727–730.

Kamrin K. and Bazant MZ. (2007), 'A stochastic flow rule for granular materials', *Phys. Rev.E.* 75, 041301.

Kheiripour Langroudi, M., Tardos, G., Michaels, J. and Mort, P., (2009), 'Effect of material properties, boundary conditions and flow fields on the rheology of dense granular matter', *AIP Conference Proceedings*, 1145, 587-590.

Kheiripour Langroudi, M., Turek, S., Ouazzi, A., and Tardos, G., (2010a), "An investigation of frictional and collisional powder flows using a unified constitutive equation", *Powder Technoogy*, 197, 91-101.

Kheiripour Langroudi, M., Sun, J., Sundaresan, S. and Tardos, G., (2010b), "Transmission of normal stresses in un-sheared and sheared granular beds: the influence of particle size, shape, stiffness and cohesion", *Powder Techn*ology, 203, 23-32.

Kheiripour Langroudi, M., Mort, P. and Tardos, G., (2010c), "Study of powder flow patterns in the Couette cell with axial flow using tracers and solid fraction measurements", *Accepted for publication in Granular Matter*.

Kheiripour Langroudi, M., Tardos, G. I., (2010), "Importance of solid fraction and its fluctuations on the rheology and flow characteristics of compressible powders", *Submitted to Mechanics Research Communications.*

Latzel, M., Luding, S., Herrmann H.J., Howell D.W. and Behringer R.P. (2003), 'Comparing simulation and experiment of a 2D granular Couette shear device', *European Physical Journal E* 11 (4) 325-333.

Liu, C.h., Nagel, S.R., Schecter, D.A., Coppersmith, S.N., Majumdar, S., Narayan, O. and Witten, T.A. (1995), 'Force fluctuations in bead packs', *Science,* 269, 513–515.

Lois, G., Lemaitre, A., Carlson, JM. (2006), 'Emergence of multi-contact interactions in contact dynamics simulations of granular shear flows', *Europhys. Lett.* 76, 318–324.

Lois, G., Lemaître, A. & Carlson1, J.M. (2007), ' Spatial force correlations in granular shear flow. I. Numerical evidence', *Phys. Rev. E* 76, 021302.

Lois, G., Lemaître, A. & Carlson1, J.M. (2007), ‘ Spatial force correlations in granular shear flow. II. Theoretical implications’, *Phys. Rev. E* 76, 021303.

Losert, W., Bocquet, L., Lubensky, TC., Gollub, JP. (2000), ‘Particle dynamics in sheared granular matter’, *Phys. Rev. Lett.* 85, 1428–1431.

Louge M. Y. and Keast S. C. (2001), ‘On dense granular flows down flat frictional inclines’, *Physics of Fluid,* 13, 1213-1233.

Louge M. Y., Tuccio M., Lander E., and Connors P. (1996), ‘capacitance measurements of the volume fraction and velocity of dielectric solids near a grounded wall’, *Rev. Sci. Instrum*. 67 (5), 1869-1877

Louge M. and Opie (1990), ‘Measurement of the Effective Dielectric Permittivity of Suspensions’, *Powder Technology*, 62, 85-94.

Luding, S. (2005), ‘Shear flow modeling of cohesive and frictional powders’, *Powder Technol.* 158, 45-50.

Lun, C. K. K., Savage, S. B., Jeffrey, D. J., Chepurniy, N. (1984), ‘Kinetic theories for granular flow; inelastic particles in Couette flow and slightly inelastic particles’. *J. Fluid Mech*., 140, 223-256.

Malék, J., Necãs, J., and Rajagopal, K.R. (2002), ‘Global existence of solutions for flows of fluids with pressure and shear dependent viscosities’, *Appl. Math. Lett.* 15, 961-967.

Massoudi, M., Mehrabadi, M. M. (2000), ‘A continuum model for granular materials: Considering dilatancy and the Mohr Coulomb criterion’, *Acta Mechanica.* 152, 121-138.

Miller, B., O’Hern, C. & Behringer, R. P. (1996), ‘Stress Fluctuations for Continuously Sheared Granular Materials’, *Phys. Rev. Lett*. 77, 3110.

Mills P., Loggia D., Tixier M. (1999), 'Model for a stationary dense granular flow along an inclined wall', *Euro. phys. Lett.* 45:733-738.

Mohan, L. S., Nott, P. R. and Rao, K. K. (1997), 'Fully developed flow of coarse granular materials through a vertical channel', *Chem. Eng. Sci*. 52, 913-933.

Mohan, L. S., Nott, P. R. and Rao, K. K. (1999), 'A frictional Cosserat model for the flow of granular materials through a vertical channel', *Acta Mech.* 138, 75-96.

Mohan, L. S., Rao K. K., and Nott, P. R. (2002), 'A frictional Cosserat model for the slow shearing of granular materials', *J. Fluid Mech.* 457, 377-409.

Moreno-Atanasio, R., Anthony, S.J., and Ghadiri, M. (2005), 'Analysis of flowability of cohesive powders using Discrete Element Methods', *Powder Technol.* 158, 41-57.

Mort, P., Turton, R., Canty, T. (2004), 'Characterization of ordered mixtures on bulk and granular scales', AIChE Annual Meeting, Austin TX.

Mueth, D.M., Jaeger, H.M. and Nagel, S.R. (1998), 'Force distribution in a granular medium', *Physical Review E* 57, 3164–3169.

Mueth, DM., Debregeas, GF., Karczmar, GS., Eng, PJ., Nagel, SR. and Jaeger, HM. (2000), 'Signatures of granular microstructure in dense shear flows'. *Nature* 406, 385–89.

Muguruma, Y., Tanaka, T. and Tsuji, Y. (2000), ' Numerical simulation of particulate flow with liquid bridge between particles' *Powder Technol.* 109, 49-57.

Muhlhaus, H. B. and Vardoulakis, I. (1987), 'The thickness of shear bands in granular materials'. *Geotechnique* 37, 271-283.

Ngadi, A. and Rajchenbach, J. (1998), 'Intermittencies in the compression process of a model granular medium', *Physics Review Letters* 80, 273-276.

Nedderman, R. M. (1992), 'Statics and kinematics of granular materials', Cambridge University Press.

Newton, I. (1689), 'Scholium to the Definitions in Philosophiae Naturalis Principia Mathematica', *Bk. 1* (University of California Press, Berkeley, 1934).

Nixon, S. A. and Chandler, H. W. (1999), 'On the elasticity and plasticity of dilatant granular materials'. *J. Mech. Phys. Solids*. 47, 1397-1408.

Ogawa, S. (1978), 'Mutitemperature theory of granular materials', In *Proc. U.S.-Japan Symp. On Continuum Mechanics and Statistical Approaches in the Mechanics of Granular Materials*, Gakujutsu Bunken Fukyu-kai.

Ouazzi, A., Turek, S., and Hron, J. (2005), 'Finite element methods for the simulation of incompressible powder flows', *Commun. Numer. Methods Eng.* 21, 581-596.

Pouliquen, O. and Chevoir, F. (2002), 'Dense flows of dry granular material', *C. R. Phys.* 3, 163–175.

Pouliquen, O. and Forterre, Y. (2002), 'Friction law for dense granular flows: application to the motion of a mass down a rough inclined plane', *J. Fluid Mech.* 453, 133–151.

Prasad, S. and Rajagopal, K.R. (2006), ' Flow of a fluid with pressure dependent viscosity due to a boundary that is being stretched', *J. Appl. Math. Comput.* 173, 50-68.

Quartier L, Andreotti B, Douady S, Daerr A. (2000), 'Dynamics of a grains on a sandpile model'. *Phys. Rev. E* 62:8299-07.

Radjai, F., Jean, M., Moreau, J. J., Roux, S. (1996), 'Force distributions in dense two-dimensional granular systems', *Phys. Rev. Lett*. 77, 274.

Radjai, F. and Roux, S. (2002), 'Turbulentlike behavior in quasi-static flow of granular media', *Phys. Rev. Lett.* 89, 064302.

Renardy, M. (2003), 'Parallel shear flows of fluids with a pressure-dependent viscosity', *J. Non-Newton. Fluid Mech.* 114, 229-236.

Reynolds, O. (1885), 'On the dilatancy of media composed of rigid particles in contact with experimental illustrations', *Phil. Mag. S*. 5 20, 469-481.

Roux, S. & Radjai, F. (1998), 'Texture-dependent rigid-plastic behavior', In *Physics of Dry Granular Media*, Dordrecht: Kluwer Acad, 229–36.

Roux, J-N & Combes, G. (2002), 'Quasistatic rheology and the origin of strain', *C. R. Phys.* 3, 131–40.

Rycroft, C. H., Grest G. S., Bazant, M. Z. and Landry, J. (2006), 'Analysis of granular flow in a pebble-bed nuclear reactor, *Phys. Rev. E* 74 , 021306.

Sakaie, K., Fenistein, D., Carroll, T.J., Hecke, M., & Umbanhowar, P. (2008), 'MR Imaging of Reynolds dilatancy in the bulk of smooth granular flows', *Phys. Rev. Lett.* 81, 123–126.

Savage, SB. (1984), 'The mechanics of rapid granular flows', *Adv. Appl. Mech.* 24, 28966.

Savage, S.B. and Sayed, M. (1984), 'Stresses developed by dry cohesionless granular materials in an annular shear cell', *J. Fluid Mech.* 142, 391–430.

Savage, SB. and Hutter, K. (1989), 'The motion of a finite mass of granular material down a rough incline', *J. Fluid Mech.* 199, 177–215.

Savage, SB. (1998), 'Analyses of slow high-concentration flows of granular materials'. *J. Fluid Mech.* 377, 1–26.

Schaeffer, DG. (1987), 'Instability in the evolution equations describing incompressible granular flow', *J. Differ. Equat.* 66, 19-50.

Schaeffer, D.G. (1990), 'Mathematical issues in the continuum formulation of slow granular flow. In: D.G. Joseph and D.G. Schaeffer, Editors, *Two Phase Flows and Waves*, Springer Verlag, 118–129.

Schöllmann, S. (1999), 'Erratum: Simulation of a two-dimensional shear cell', *Phys. Rev. E.* 59, 889.

Shen, HH. and Sankaran, B. (2004), 'Internal time scales in a simple shear granular flow', *Phys. Rev. E.* 70, 051308.

Silbert, LE., Ertas, D., Grest, GS., Halsey, TC., Levine, D. & Plimpton, SJ. (2001), ' Granular flow down an inclined plane: Bagnold scaling and rheology', *Phys. Rev. E.* 64, 051302.

Srivastava, A. and Sundaresan, S. (2003), 'Analysis of a frictional kinetic model for gas particle flow', *Powder Technol.* 129, 72–85.

Suzuki, T., Iima, M. and Hayase, Y. (2006), 'Surface switching of rotating fluid in a cylinder', *Phys. Fluids* 18, 101701.

Tardos, G.I. (1997), 'A fluid mechanics approach to slow, frictional powder flows', *Powder Technol.* 92, 61–74.

Tardos, G.I., Khan, M.I. and Schaeffer, D.G. (1998), 'Forces on a slowly rotating, rough cylinder in a Couette device containing a dry, frictional powder', *Phys. Fluids* 10, 335-341.

Tardos, G. I., McNamara, S. and Talu, I. (2003), 'Slow and intermediate flow of a frictional bulk powder in the Couette geometry', *Powder Technol.* 131 , 23-39.

Tardos, G.I., and Mort, P.J. (2005), 'Dry powder flows', Chapter 9. In: C. Crowe, Editor, *Multiphase Flow Handbook*, CRC Press, Boca Raton, Florida.

Tejchman, J. and Gudehus, G. (1993), 'Silo-music and silo-quake experiments and a numerical Cosserat approach', *Powder Technol.* 76, 201-212.

Tejchman, J. and Wu, W. (1993), ' Numerical study of patterning of shear bands in a Cosserat continuum', *Acta Mech.* 99, 61-74.

Turek, S. (1998), 'Efficient Solvers for Incompressible Flow Problems: An Algorithmic Computational Approach', *LNCSE* vol. 6, Springer.

Turek, S. and Ouazzi, A. (2007), 'Unified edge-oriented stabilization of nonconforming FEM for incompressible flow problems: numerical investigations', *J. Numer. Math.* 15, 299-322.

Turek, S., Quazzi, A. and Schmachtel, R. (2002), 'Multi-grid methods for stabilized nonconforming finite elements for incompressible flow involving the deformation tensor formulation', *Journal of Numerical Mathematics* 10, 235–248.

Vavrek, M.E. and Baxter, G.W. (1994), 'Surface shape of a spinning bucket of sand', *Physics Review E* 50, R3353.

Yeung, C. (1998), 'Metastability of a granular surface in a spinning bucket', *Physics Review E* 57, 4528-4534.

Yoon, S., Eom, B., Lee, J. and Yu, I. (1999), 'Circular kinks on the surface of granular material rotated in a tilted spinning bucket', *Physics Review Letters* 82, 4639-4642.

Yu, C-M., Craig, K., and Tichy, J. (1994), 'Granular collisional lubrication', *Journal of Rheology* 38 (4) , 921–936.

Yu, C-M., and Tichy, J. (1996), 'Granular collisional lubrication: effect of surface roughness, particle size and solid fraction', *Tribology Transactions* 39 (3), 537-546.

Zamankhan, P., Soleymani, A., Polashenski, W., and Zamankhan, P. (2004), 'Flow dynamics of grains in spinning bucket at high frequencies', *Chem. Eng. Sci.* 59, 235-246.

Zhang, Y. and Campbell, C.S. (1992), 'The interface between fluid-like and solid-like behavior in two-dimensional granular flows', *J. Fluid Mech.* 237, 541–568.